UNIVERSITY OF OKLAHOMA

GRADUATE COLLEGE

# APPLICATION OF TRAFFIC SPEED DEFLECTOMETER AND AI-BASED MODELS FOR STRUCTURAL CALIBRATION AND PAVEMENT MANAGEMENT ENHANCEMENT

A DISSERTATION

SUBMITTED TO THE GRADUATE FACULTY

in partial fulfillment of the requirements for the

Degree of

DOCTOR OF PHILOSOPHY

By

MATIAS M. MENDEZ LARRAIN
Norman, Oklahoma
2023

# APPLICATION OF TRAFFIC SPEED DEFLECTOMETER AND AI-BASED MODELS FOR STRUCTURAL CALIBRATION AND PAVEMENT MANAGEMENT ENHANCEMENT

A DISSERTATION APPROVED FOR THE
SCHOOL OF CIVIL ENGINEERING AND ENVIRONMENTAL SCIENCE

BY THE COMMITTEE CONSISTING OF

Dr. Musharraf Zaman, Chair

Dr. Talayeh Razzaghi

Dr. Gerald A. Miller

Dr. Kanthasamy Muraleetharan

Dedicated

to

My Wife, Parents, and Sisters

## Acknowledgements

First, I would like to express my sincere gratitude to God for all my blessings throughout my career and life. I would like to thank my beloved wife Vania Carvajal Sejas, who has supported me in every step with love, patience, and energy. Then, I would like to thank my mom, dad, and sisters, who always supported me in every decision in my life. I would not have made it without them. I want to express my sincere thanks and gratitude to my advisor, Prof. Musharraf Zaman, for his continuous support of my Ph.D. study and related research and for his patience, motivation, energy, humbleness, and immense knowledge. His guidance helped me throughout the research and in writing of this thesis. I also would like to thank the members of my committee, Dr. Razzaghi, Dr. Miller, and Dr. Muraleetharan for their valuable time and support.

I would like to acknowledge Dr. Syed Ashik Ali for his assistance, mentorship, guidance, and most of all his friendship. Also, I would like to thank Kenneth Hobson, Sagar Ghos, Paul Cancino, Linda Nowlan, and Luis Urbina for their help and support throughout my studies. I also want to thank all of my research group members for their inspiration and friendship.

I would like to express my sincere gratitude to the staff of the School of Civil Engineering and Environmental Science, the Southern Plains Transportation Center (SPTC), and the Oklahoma Department of Transportation (ODOT) for their assistance and support. I also want to acknowledge the financial support provided by ODOT, SPTC, Oklahoma Center for the Advancement of Science and Technology (OCAST), and Dolese during my study. Last but not the least, I want to thank the Villarroel family, my grandparents, my godson Augusto, the Pozadas Family, Bryce Hanlon, Sebastien

Perrier, Roca Engineering, EST, Inc., and my family and friends for supporting me in all the different stages of my Ph.D. studies.

## Table of Contents

## List of Tables

## List of Figures

## Abstract

Currently, different methods are used for the evaluation of pavement conditions including the surface, base, subbase, and subgrade. Among these, Falling Weight Deflectometer (FWD) and/or Fast Falling Weight Deflectometer (FFWD), a non-destructive method, is widely used for pavement condition monitoring and forensic studies. Its ability to back-calculate the elastic moduli or stiffness of different layers can be a useful tool for estimating the remaining life of the pavement based on the rutting and cracking criteria. Currently, several state Departments of Transportation (DOTs) use FWD in their preventive maintenance program at both project level and network level. Collection of FWD and FFWD data requires traffic control and disruptions to traffic flow. The Traffic Speed Deflectometer (TSD) is an instrumented vehicle that is capable of measuring deflection, International Roughness Index (IRI), rut depths and other distresses at traffic speed without requiring any traffic control.

Reflection cracking, edge cracking, rut and longitudinal edge depressions are some of the major problems in asphalt pavements near the intersection of Interstate 35 (I-35) and State Highway 7 (SH-7) in Oklahoma. In this study, over forty (40) miles of FFWD and TSD test data were collected from SH-7 and I-35. More than 380 FFWD tests were conducted at different locations throughout the studied sections. Deflections at different sensors and temperatures during testing were recorded. Also, TSD data were collected from the same pavement sections, as part of a nationwide pool fund study involving the Oklahoma Department of Transportation (ODOT). Specifically, deflections, rut depths, roughness, temperatures, loading and distress data were collected. Thicknesses of different layers were determined from the Ground Penetration

Radar (GPR) and from coring. From these data, two different types of pavements were identified under the Asphalt Concrete (AC) layer in the studied section of I-35, namely Jointed Concrete Pavement (JCP) and Continuously Reinforced Concrete Pavement (CRCP). The pavement structure in SH-7, on the other hand, consisted of only AC layers over native subgrade soil. The following laboratory performance tests were conducted on the extracted asphalt cores: Semi-Circular Bend (SCB), Texas Overlay (TO), Tensile Strength Ratio (TSR), Indirect Tensile Asphalt Cracking (IDEAL-CT), and Hamburg Wheel Tracking (HWT). Also, roughness and rut data were collected by Pave3D 8k, in collaboration with the Oklahoma State University team, and compared with the corresponding TSD data. In addition, elastic moduli obtained from the FWD and TSD data were compared in this study. For this purpose, FWD data were used in Modulus 7.0 Software to back-calculate elastic modulus. The deflection values from the TSD data were reformatted and used in Modulus 7.0 to determine the corresponding elastic moduli. A linear elastic model option in KENLAYER was used to determine strains at the bottom of the AC layer. These strains were then used to calibrate the coefficients of the model that are currently used to calculate strains at the bottom of the AC layer from the TSD deflection data. Further, the coefficients used in models by Rhode (1994) and by AASHTO 93 to determine Effective Structural Number ($SN_{eff}$) were calibrated for both studied sections. Temperature corrections and matching of deflection data obtained from the FWD and TSD testing were needed for these calibrations and their comparison (i.e., FWD vs TSD). Recent developments in Artificial Intelligence (AI)-based models were employed in this study in developing the aforementioned correlations. For comparison purposes, both regression and AI-based models were used to predict the back-calculated elastic moduli values from the TSD data using a Python code. Finally, the predicted elastic moduli (based on the FWD deflections) by linear regressions and Random Forest (RF) models were compared and relative strengths of the AI models discussed.

CHAPTER

# 1

# INTRODUCTION

## 1.1 BACKGROUND

Transportation agencies invest billions of dollars each year to construct, assess, preserve, and maintain transportation infrastructure. Pavements are the largest transportation infrastructures nationwide, with high costs of rehabilitation and maintenance. Currently, sixty-eight (68) percent of roadway pavements in the United States of America (USA) are in poor condition (1). Pavement maintenance costs have an exponential trend with time; maintenance costs increase exponentially, and the remaining service life of pavement goes down significantly with time.

A Pavement Management System (PMS) is a key component of an overall Transportation Asset Management Plan (TAMP). The American Association of State Highway and Transportation Officials (AASHTO) defines PMS as “a set of tools or methods that assist decision-makers in finding optimum strategies for providing, evaluating, and maintaining pavements in a serviceable condition over a period of time (2).” A PMS helps with decision-making for long-term and "needs-based" budgeting at the network level to handle the overall state of the network. At project level, PMS covers the most economical methods of maintenance and rehabilitation for each road segment. Allocating limited resources in the most effective way possible to maximize benefits during the asset life cycle is a crucial component of asset management. When using PMS, transportation agencies generally set asset condition targets, and implement management systems to estimate performance at expected funding levels.

The most critical components of a PMS, as shown in Figure 1.1, include the following:

- **Inputs:** which include inventory, pavement condition information (both current and historical), and additional data such as traffic and construction and maintenance history.
- **Database:** which stores, sorts, and retrieves the inventory and condition information at project and network levels.
- **Analysis Parameters:** which are used to generate pavement project and treatment recommendations, including deterioration models, treatment rules, and impact rules.
- **Analysis Module:** which assists agencies in evaluating the consequences of applying different investment levels and treatment strategies.
- **Reporting Module:** which generates standard and Ad Hoc reports in different formats.
- **Maintenance and Improvement Plan:** which provides information relative to the selected treatments, and implementation.

The overall objective of PMS is to evaluate, redefine, and validate the analysis parameters that are commonly used by the agency. For project and/or network level PMS, after pavement condition data has been collected and verified, the data are utilized for the evaluation and refinement of the deterioration models, realistic benefit/cost analysis for various treatment options, and validation of treatment triggers and their reset values. Pavement deterioration models provide the basis for predicting future changes in network conditions, estimating future funding needs, and determining the effectiveness and timing of maintenance and rehabilitation activities. The evaluation of pavements (project and network level) come from a detailed database and data collection that includes inventory data by manual and automated methods, design data, condition data (structural and functional) by manual, semi-automated, automated, and cost-effective methods.

Generally, roadway condition data involves structural condition, roughness, rut, and distresses that are used to determine the overall condition of the pavements. Structural condition (e.g., structural number, layer modulus, drainage) as well as surface condition (e.g., roughness, rut, crack, patch) and other factors (e.g., safety, traffic, accidents) are used to determine the condition or rating of the pavement. Structural condition and capacity data are generally used at the project level. However, some agencies are seeing benefits of including these indicators at the network level (3). Different tools and techniques are currently available for these evaluations and used by transportation agencies. However, concerns, such as slow rate of data collection and possibility of traffic congestion and safety hazards have limited their use. Recently, Traffic Speed Deflectometer (TSD) has emerged as a useful tool for measuring surface deflections of pavements at close intervals as well as roughness, texture, and rut at traffic speed. Because data are collected at traffic speed, no traffic control is needed. This device is gaining popularity within the transportation agencies for pavement condition assessment and management at network level. Despite its advantages in quantifying both surface condition and structural condition of roadway pavements, there are issues pertaining to using deflection data in determining tensile strain at the bottom of asphalt layer and assessment of structural capacity or remaining service life of the pavement. Also, the usefulness of TSD in assessing structural conditions of composite pavements has not been addressed yet. Several previous studies have shown high correlations between pavement conditions assessed using the TSD data and with other traditional methods such as Falling Weight Deflectometer (FWD) and fast FWD (FFWD) used by Department of Transportations (DOTs) (4,5). As discussed subsequently in this dissertation, there is a need to closely review the input parameters (indices and variables) and models being used by TSD and to develop calibration tools for enhancing applications of these correlations or models, and to calibrate the model parameters or coefficients for both Asphalt Concrete (AC) and composite pavements. The present study considers a broader set of parameters including temperature, materials, pavement thickness, load level, and load type, among others, in calibrating the model parameters or coefficients.

## 1.2 OBJECTIVES

In this study, both destructive and non-destructive tests were conducted on a state highway and an interstate section in Oklahoma. Specifically, a 14.5-mile section of Interstate 35 (I-35) and a 5-mile section of State Highway 7 (SH-7) were studied to assess the condition of the associated pavement and to calibrate the coefficients or parameters of common models used to process TSD data. The selected sections have exhibited distresses in the form of reflection cracking, edge cracking, rutting, and longitudinal edge depressions. The non-destructive test methods used in this study included Falling Weight Deflectometer and/or FFWD, Ground Penetration Radar

(GPR), Pave3D 8k and TSD. The destructive method included coring and associated laboratory testing, namely Semi-Circular Bend (SCB), Texas Overlay (TO), Tensile Strength Ratio (TSR), Indirect Tensile Asphalt Cracking (IDEAL-CT), and Hamburg Wheel Tracking (HWT), as well as in-situ tests. Finally, Artificial Intelligence (AI)-based models were developed and used for the calibration of model parameters and assessment of pavement conditions based on the TSD, FWD, and other data. The specific objectives of this study are as follows:

i. Collect project information and conduct a subsurface investigation using non-destructive (FWD, TSD, GPR, Pave3D 8k) and destructive (selective coring and laboratory tests on cores) testing.
ii. Collect and analyze TSD, Pave3D 8k and FWD deflections, rutting, and roughness. Also, compare deflections, basin parameters, and back-calculated elastic moduli obtained from the FWD and TSD data and evaluate relevance of these parameters on the structural condition assessment.
iii. Use linear elastic model in KENLAYER (6) to determine tensile strain at the bottom of the AC layer. Also, calibrate the model parameters used to determine the tensile strains at the bottom of the AC layer from the TSD data.
iv. Calibrate the model parameters or coefficients used to determine Effective Structural Number ($SN_{eff}$) based on the type of pavement structure (asphalt and composite) using Rhode and AASHTO methods (7,8).
v. Develop linear regressions and AI-based model, namely Random Forest (RF) model to predict FWD elastic modulus and deflections from TSD data.

## 1.3 LITERATURE REVIEW

### 1.3.1 Falling Weight Deflectometer and Traffic Speed Deflectometer

Since the 1980's, FWD has been the most used device for assessment of pavement condition by the transportation agencies in the United States as well as other countries. This test aims to measure deflection under impact loads that simulate traffic. The device consists of an impulse loading device mounted with geophones to measure surface deflection at several radial distances due to the application of half of Equivalent Single Axle Load (ESAL) on a 12 in. (300 mm) diameter circular plate on the pavement surface. Transportation agencies generally use these deflection readings and pavement thicknesses to determine the layer stiffness or elastic moduli of the underneath materials (9–13) . Likewise, subgrade properties can be calculated from the data obtained from this device (14).

On the other hand, TSD is a load-mounted truck that applies a rear axle load from 13 to 28 kips (57 to 124 kN) on the pavement surface. It commonly has seven to nine Doppler lasers that are generally positioned in front of the loaded axle and single laser located outside the bowl that serves as the reference sensor (15). TSD can operate at different speeds, however, a speed of 60 mph (96.5 km/h) with a data collection rate of 1 KHz is commonly used (15). TSD measures the deflection slope from the vertical pavement deflection velocity and the vehicle horizontal velocity for each laser location. Using these data, a deflection basin is generated which represents the profile of the deflected pavement due to axle load. Deflections at different points of the pavement can be obtained by integrating the slope of the deflection basin.

The main difference between FWD and TSD is the application of load. While FWD applies a static impact load, TSD applies dynamic load on the pavement surface using rare axle. Also, deflections in the FWD are measured by geophones, whereas TSD uses lasers for deflection measurements at highway speed. Furthermore, some of the accuracy in TSD measurements are lost due to the averaging process. There are several factors that can vary the readings in TSD. Damping plays a role in the form of time difference between the loaded tire and the deflection response. Also, tire pressure should be accounted for while measuring deflection using TSD. The tire pressure should be monitored during operation, and in the long term, appropriate instruments that measures the magnitude of the applied load should be enforced (16).

### 1.3.2 Deflection Basin Indices

Over time, several studies have proposed deflection basin-related indices or deflection bowl parameters to analyze deflection data from deflectometers (8,17–19). These parameters tend to focus mainly on the deflection under the center of the load (maximum deflection) and differences in deflection among the sensors as an indicator of stiffness of different layers within the pavement structure, including the stiffness of the subgrade, and the remaining life. The maximum deflection can be considered as an indicator of the structural layers, Base Layer Index (BLI) or Surface Curvature Index (SCI) which is being used lately to classify the structural conditions of the pavements by several researchers (15). Similarly, Deflection Slope Index (DSI), that characterizes the structural condition, can separate structurally good from structurally fair pavements (Shrestha, 2017). Also, the Area Under Pavement Profile (AUPP) and Area Indices (AI) are commonly used to characterize the upper layers of the pavements (8).

### 1.3.3 Tensile Strains at the Bottom of Asphalt Concrete

The tensile strain at the bottom of AC layer and its relationship with deflection curvature indices are good indicators of the pavement condition as it can indicate how deteriorated or distressed the pavement is. Similarly, the compression strain at the top of the subgrade can indicate the condition of the subgrade soil. These horizontal and vertical strains are critical load-induced pavement response in the mechanistic-empirical design of pavement. Previous studies have shown that vertical and horizontal strains can be estimated from vertical deflection indices (9,19–21).

A recent study (22) proposed deflections and slope indices, such as $DSI_{8-12}$ ($D_8$–$D_{12}$) and $DSI_{12-36}$ ($D_{12}$–$D_{36}$) as indicators of asphalt fatigue and subgrade rutting strains, respectively, for AC layer thicknesses at 1 in. (25 mm) intervals using TSD data. Several existing software, namely WESLEA, JULEA, 3D MOVE and KENPAVE can accurately estimate strains based on numerical and/or analytical methods. Based on Katicha et al. (2020), the $SCI_{12}$ has some advantages as it does not require pavement thickness information, and it is mechanistically related to the tensile strain at the bottom of the asphalt layer (5). According to these researchers, using $D_{max}$ instead of $D_0$ to calculate $SCI_{12}$ does not significantly improve the correlation since TSD does not have any sensor immediately behind the wheel to capture the maximum deflection (22). In that study, the 3D Move software was used to simulate strain at the bottom of AC. Previous studies have shown that the 3D Move software is quite versatile to model strains (8,23,24). A study conducted by Nasimifar et al. (2017) reported good correlation when comparing deflection velocities between TSD and 3D Move results (24). About 67 indices were evaluated with fatigue and rutting strains by Nasimifar, et al (2016). The $DSI_{8-12}$ ($D_8$–$D_{12}$) and $DSI_{12-36}$ ($D_{12}$–$D_{36}$) were found to exhibit good correlations with critical pavement responses for different pavement categories, based on thickness (22).

### 1.3.4 Structural Number

American Association of State Highway Officials (AASHO) has introduced the use of a structural indicator of pavements, first known as "thickness index" and then as "Structural Number (SN)". It is mainly used to determine the structural capacity or traffic load carrying capacity of a given pavement structure with known materials at a given location. In this method contributions of all layers within the pavement structure are added to obtain the overall capacity of the pavement (17). The SN determines the total number of ESAL a given pavement can support during its service life. The most used equivalent load is 18 kips or 80 kN. Equation 1.1 describes the SN based on layer coefficients, drainage coefficients, and layer thicknesses.

$$SN = a_1 D_1 + a_2 D_2 m_2 + a_3 D_3 m_3 + \cdots \qquad \text{Equation 1.1}$$

where,

$a_i$ = $i^{th}$ layer coefficient

$D_i$ = $i^{th}$ layer thickness

$m_i$ = $i^{th}$ layer drainage coefficient

The layer coefficients $a_i$ can be determined by equations that are based on the 1993 AASHTO Guide (25). Rhode proposed Equation 1.2 to calculate $SN_{eff}$ from FWD measurements (7).

$$SN_{eff} = k_1 SIP^{k_2} Hp^{k_3} \qquad \text{Equation 1.2}$$

where,

Hp = total thickness (mm)

SIP = Structural Index of Pavement = $D_0$-$D_{1.5HP}$

For an asphalt pavement, Rhode (1994) proposed 0.4728, -0.4810, and 0.7581 as values for constants $k_1$, $k_2$, and $k_3$, respectively. Nasimifar et al. (2019) updated the $k_1$, $k_2$, and $k_3$ constants for TSD data and proposed as 0.4369, -0.4768, and 0.8182, respectively (26).

The moduli of pavement layers can be back-calculated from the FWD data. Several analysis tools have been developed over time to determine back-calculated elastic moduli from measured deflection basins using numerical and analytical methods. Examples of these tools include MODCOMP®, ELMOD®, MODULUS, and BACKCALC. Not much work has been done yet on back calculation of layer elastic moduli from TSD data. A recent study reported that TSD data can be used to back-calculate pavement layer elastic moduli using two different approaches, namely 3D-Move and a linear elastic analysis (27). Also, effective structural numbers calculated from the TSD measurements were found to be similar to that obtained from the FWD measurements for interstate pavements.

### 1.3.5 Temperature Correction

Currently, there is no proven method to correct TSD measurements for temperature. Researchers have proposed a method to adjust strains at the bottom of AC based on the temperature correction. It essentially measures the elastic moduli ($E_f$)

based on the strain at the time of the test. The elastic moduli can be calculated as $E_f = c * \varepsilon^d$, where, c and d are coefficients given by Rada et al. (8). The temperature correction for $SCI_{12}$ was performed using the approach developed by Nasimifar et al. (2018) (28). The approach is inspired by the Lukanen method for FWD measurements and considers the loading specific to a moving device and the viscoelastic effects (29). A similar approach was used by Katicha et al. (2020) (5). In these approaches, BELLS equation is commonly used to calculate the pavement temperature at mid-layer of the pavement (29). Also, temperature correction using a model known as VEA was proposed by Nasimifar et al. (2018) (28). The VEA model accounts for all the sensitive parameters including thicknesses, temperatures, modulus, and binder types.

### 1.3.6 Roughness and Rutting

Roughness and rut are commonly used by DOTs as indicators of surface conditions of pavements. Different methods are used to determine the roughness (commonly known as International Roughness Index (IRI)) and rut. Researchers and practitioners have developed handheld to vehicle-based technologies for data collection. However, relationships between FWD and other deflection devices remain uncertain. Previous studies have shown that IRI has a significant relation with deflections (30). TSD has shown good repeatability of deflection regardless of the driver (31). No correlations were observed between the maximum deflection of FWD and IRI and rut (32). An IRI estimation based on acceleration variance from vehicle mounted accelerometers was conducted by Aleadelat, et al. (2018). It was found that less than 12% of the sections showed errors higher than 30 in./mile (33). Based on Chatterjee, IRI depends on the vehicle model, load, speed, and position of the sensor (34). Several studies have been conducted on IRI measurements from accelerated equipment (35–37). Also, high resolution cameras have been used recently for pavement condition assessment (38). Pave3D 8k is a promising technology for automated pavement survey at traffic speed. It is capable of collecting data from roadways and airport pavements at traffic speed using 3D lasers. This equipment can identify pavement cracking, rutting, macro texture, roughness, and friction. Pave3D 8k has been widely used for evaluation of roadway pavements and bridge decks at traffic speed (39–43).

### 1.3.7 Ground Penetration Radar

Lately, GPR has been used to conduct subsurface investigations on deteriorated pavements for preservation and maintenance. Two types of GPR are currently available, namely air-coupled, and ground-coupled GPR. The air-coupled GPR is a noncontact device with an antenna (i.e., they do not touch the surface during surveying). Since air-coupled GPR systems are typically quicker than ground-coupled ones, they are frequently used as a scanning tool to identify areas that require more extensive testing (44). Differently, ground-coupled GPR must stay in contact with the ground. GPR works by launching discrete electromagnetic wave bursts into a pavement and/or surfaces and then observing the reflections. At layer interfaces, where there is a change in dielectric constant in asphalt pavement, GPR signals are reflected. Also, the signal is influenced by the conductivity and dielectric constant of the material (45). Generally, higher frequency antennas provide better resolution, but the available strength and penetration depth are reduced. Higher strength and greater penetration are possible with lower frequency antennas, but the resolution suffers.

The GPR is being used to determine the thicknesses of pavements for PMS at network and project level. Several studies reported good correlation between thicknesses of asphalt determined by GPR and coring (46,47). A new ASTM standard, namely ASTM D-4748 (48), for determining the thickness of existing pavement layers using GPR was released lately (47).

**1.3.8 Random Forest Models**

Artificial Intelligence (AI) and Machine Learning (ML) are technologies that use algorithms to analyze data and handle tasks by simulating the way human beings learn. Breiman (2004) introduced the Random Forest (RF) machine learning algorithm. It is a non-parametric method which employs a decision tree model (49). This approach is based on bootstrap samples and uses a set of trees with a number of input vectors to create a forest in which each tree generates outputs. The ultimate output is calculated as the average of all the results from each formed tree. Data are typically split into two sets: the training set (bagging) and the confirmation or testing set (out of bag). They are effective classifiers and regressors when the appropriate amount of variance is added. Additionally, the framework provides information about the RF predictive power in terms of the potency of the individual predictors and their relationships. The otherwise theoretical values of strength and correlation are made tangible by using out-of-bag estimation (49). This method has been widely used for prediction in any field of work. An RF model was used to predict the location of potential damage in Pavements (50). Also, RF models were used to predict IRI and friction from distress measurements (51,52). Also, RF models were used to detect pavement distresses (53). As per PMS applications, RF models and other ML techniques were used to predict surface condition indices, structural capacity of pavements, surface temperature, IRI, rutting and other distresses (54–58) . Also, RF models were used to predict TSD variables and/or to use these variables as inputs for RF model predictions (59,60). However, these models are sensitivity to outliers and over fitting, and may result in poor prediction compared to least square regressions (49).

## 1.4 OUTLINE OF THE DISSERTATION

The findings of this study are compiled in this dissertation as three journal publications (all under review), from Chapter 2 to Chapter 4. Chapter 1 and Chapter 5 contain the general introduction and conclusions of this study, respectively. Chapter 2 through Chapter 4 contains data from asphalt and composite pavements near the intersection of I-35 and SH-7 in Oklahoma.

Chapter 1 presents the introduction to PMS and the methods that are used to characterize the condition of pavements. Also, this chapter gives a brief background of FWD, TSD, methods to characterize and understand the condition of pavements and a brief introduction of AI-based methods for prediction, namely RF models.

Chapter 2 presents the outcomes of a forensic investigation study that includes destructive and nondestructive testing for characterization of pavement condition. Different types of distresses were observed at the studied sections on I-35 and SH-7. Coring, volumetrics, SCB, TO, TSR, and HWT tests were conducted as part of the destructive methods. Also, FWD, TSD, Pave3D 8k, and GPR tests were conducted as part of the nondestructive methods. Details of these test results are presented in this chapter.

Chapter 3 presents the use of TSD and FWD data to calibrate the current models that are used to predict the structural condition of pavements. Strains at the bottom of the asphalt layer for both pavement types (AC over native subgrade and composite pavements involving AC over concrete and the concrete over native subgrade) were determined using KENLAYER. Model parameters are used to determine effective structural number and tensile strains at the bottom of the asphalt concrete calibrated for both asphalt and composite pavements using the KENLAYER results and the TSD deflections.

Chapter 4 presents the use of the AI-based models to predict FWD parameters from the TSD inputs and basin indices. Temperature correction was addressed and a comparison between the back-calculated elastic moduli's from the TSD and FWD data were made. Finally, RF and common Linear Regression (LR) models were developed to predict the back-calculated elastic moduli of the pavements and maximum FWD deflection.

Chapter 5 presents the overall summary of the findings from this study. Also, a list of recommendations for future work is presented in this chapter.

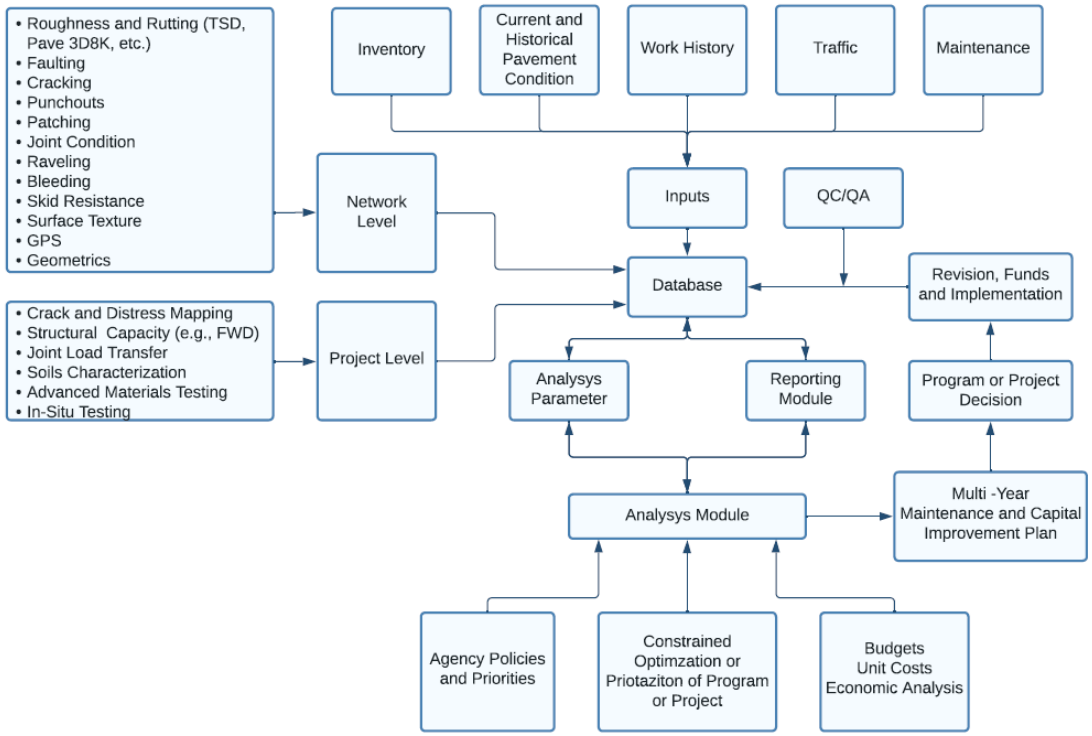


**Figure 1.1 Pavement Management Components**

CHAPTER

# 2

# SUBSURFACE AND FORENSIC INVESTIGATIONS USING TRAFFIC SPEED DEFLECTOMETER (TSD) AND FIELD AND LABORATORY TESTING [1]


## ABSTRACT

Reflection cracking, edge cracking, rut and longitudinal edge depressions are some of the major problems in asphalt pavements near the intersection of Interstate 35 (I-35) and State Highway 7 (SH-7) in Oklahoma. Specifically, reflection cracking and edge cracking were observed on I-35 from Mile Post 45 to Mile Post 59.5, and severe rut and longitudinal joint depressions were observed on SH-7 located approximately 6 miles west of I-35 heading east approximately 5 miles. The purpose of this study was to perform a subsurface investigation using the Traffic Speed Deflectometer(TSD), Ground Penetrating Radar (GPR), Falling Weight Deflectometer (FWD) and/or Fast FWD (FFWD) test, Pave 3D 8k, and laboratory performance tests on asphalt cores, namely Semi-Circular Bend (SCB) test, Texas Overlay (TO) test, Tensile Strength Ratio (TSR) test, Indirect Tensile Asphalt Cracking (IDEAL-CT) test and Hamburg Wheel Tracking (HWT) test. The GPR images exhibited two different types of pavements in the studied section of I-35, namely Jointed Concrete Pavement (JCP) and


[1] This chapter has been submitted to the International Journal of Pavement Research and Technology under the title "Subsurface and Forensic Investigations Using Traffic Speed Deflectometer (TSD) and Field and Laboratory Testing." The current version has been formatted for this dissertation.

Continuously Reinforced Concrete Pavement (CRCP). The JCP section showed severe reflection cracking. Excessive truck loading and changes in pavement section between shoulders and driving lanes are likely causes of edge failures. Overall, good elastic modulus values were observed on I-35 and low modulus values were observed on the eastbound inside lane of SH-7, where major depressions and ruts were observed. The HWT tests showed excessive ruts in the eastbound and westbound lanes of SH-7 indicating potential for rut failure. Significantly high rut and roughness were observed on the eastbound inside lane of SH-7 from TSD measurements. A specialized air-coupled GPR used in this project collected data at highway speed. This can be a useful tool for selective data-driven coring of pavement, which is a destructive process, for project-level evaluations. FFWD or FFWD when used in conjunction with TSD can be a useful tool for validating TSD results and identifying pavement conditions (project level) confidently. Pave 3D 8k and TSD can identify segments with critical rut and roughness.

## 2.1 INTRODUCTION AND METHODOLGY

In recent years, assessment of transportation infrastructure health has been receiving increased attention because of its role in preserving and extending the life of existing infrastructure. Transportation agencies invest billions of dollars each year to construct, assess, preserve, and maintain transportation infrastructure. Roadway pavements are the largest transportation infrastructure nationwide, with a high cost of maintenance and rehabilitation. Currently, 68 percent of roadway pavements in the United States are in poor condition (1). Pavement performance can go down significantly, and the resulting maintenance and rehabilitation cost can increase exponentially with time.

Pavement conditions are typically categorized as functional (level of serviceability) and structural (traffic carrying capacity and withstanding environmental factors throughout its service life). Destructive and non-destructive tests are generally used to determine the overall condition of an existing pavement. Destructive tests including coring, laboratory performance tests (e.g., Hamburg Wheel Tracking (HWT), Semi-Circular Bend (SCB), Indirect Tensile Asphalt Cracking (IDEAL-CT)), and in-situ tests (e.g., Dynamic Cone Penetration (DCP), seismic cone) are used by transportation agencies for project level assessment of pavement conditions. Non-destructive tests including Falling Weight Deflectometer (FWD), Fast Falling Weight Deflectometer (FFWD), Ground Penetration Radar (GPR), Traffic Speed Deflectometer (TSD) and Pave3D 8k are being used for assessment of structural and functional conditions of pavements. All these non-destructive and destructive methods play an important role in conducting forensic investigations of pavements (61). Vehicles equipped with cameras, sensors, and accelerometers, etc.  can capture distresses and geometrics of the various pavement systems (1). Data obtained from these and other tests are used by transportation agencies for Pavement Management Systems (PMS) and to prioritize pavement maintenance, rehabilitation, and reconstruction projects. Some of these measurements are conducted at traffic speed (e.g., TSD, GPR and Pave3D 8k), while traffic control is needed for other measurements (e.g., FWD, FFWD, DCP, seismic cone) (62). Traffic control measures add to cost, time, and safety. As a result, pavement condition assessment using traffic speed data are gaining momentum nationally. To this end, TSD is gaining the attention of state Departments of Transportation (DOTs) nationally, including the Oklahoma Department of Transportation (ODOT). The TSD can assess both structural and functional conditions of pavements without any traffic control. The TSD is an instrumented truck that applies a rear axle load varying from 13 to 28 kips (58 kN to 125 kN). It commonly has seven Doppler laser sensors that are positioned at 8 in. (200 mm), 12 in. (300 mm), 24 in. (600 mm), 36 in. (900 mm), 48 in. (1,500 mm), 60 in. (1,800 mm) and 72 in. (2,100 mm) in front of the loaded axle (i.e., traffic direction) and a single laser located outside the bowl that serves as the reference sensor (15). Although TSD can function at various speeds, it is typically employed at 60 mph (96.5 km/h) with a 1 KHz data collection rate (15). The TSD determines the deflection slope from the vertical pavement deflection velocity and the vehicle horizontal velocity for each location of laser sensor. From these data, a deflection basin is defined and used to represent the profile of the deflected pavement. Pavement deflection is obtained from the deflection slope by integration. As in most field measurements, the TSD data sometimes results in anomalous slope measurements associated with calibration or other measurement issues that might occur at random sensor locations. There are reports that show anomalies in TSD measurements due to the dynamic effect of the TSD load (63). Figure 2.1 show a pictorial view of the aforementioned approach.

The structure of the loading (impact load in FWD and moving half-axle load in TSD) and the measuring sensors are the primary distinctions between the FWD and TSD measurements (geophones for FWD and laser for TSD). Additionally, FWD testing employs multiple drops to verify repeatability, while TSD data are gathered frequently as the instrumented truck travels at traffic speed.

The TSD used in this study can be used for the following pavement applications: (i) identification of pavement changes/anomalies for the network level and the project level evaluation; and (ii) determination of overall pavement structural capacity indicators/indices at the network level (8). TSD has been used previously for forensic investigations, with promising results (64).

Ground penetration radar is a very powerful investigation tool which provides a rapid assessment of pavement subsurface condition. Texas A&M Transportation Institute (TTI) has developed a subsurface data collection and processing system using a 1-GHz air-coupled GPR (Figure 2.2). Subsurface data up to a depth of 24 in. (600 mm) from surface can be collected at highway speed (60-70 mph / 97-113 km/h) using this GPR (65). The GPR has been successfully used to determine the thicknesses of flexible pavement layers, defects in base and asphalt layers, areas of segregation and poor joint density, and delamination in asphalt (66–69).

Pave3D 8k is used as the hardware sensors and software solutions for automated pavement condition survey at 0.02 in. (0.5 mm) resolution. This equipment is capable of collecting pavement surface data to determine crack, rut, macro texture, roughness, and friction. Pave3D 8k has been used widely for evaluations of roads and bridges at traffic speed (43,70–72).

The latest version of the Pave3D 8k vehicle is shown in Figure 2.3, which was used for pavement condition data collection in this study. Pavement surface data are processed using specialized software to determine cracking, transverse rut, and longitudinal roughness. Also, pavement macro-texture can be determined from the Pave3D 8k data in term of Mean Profile Depth (MPD) or Mean Texture Depth (MTD). Moreover, Pave3D 8k data can be used to predict hydroplaning speed and identify grooving and roadway geometric information. The collected profile data from the left and right wheel-paths are analyzed to determine the International Roughness Index (IRI) and rut with an interval of 528 ft (0.1 mile), along the traffic direction.

In this study, pavement distresses were observed in a 14.5 miles section of Interstate 35 (I-35) and a 5 miles section of State Highway 7 (SH-7) in Oklahoma, as shown in Figure 2.4. Raveling, reflection cracking, longitudinal edge cracking and edge failure were observed on the I-35 section beginning at the Carter/Murray County line (Mile Post 45) and extending north to Mile Post 59.5. Figure 2.5 show the longitudinal edge cracking south of Mile Post 52 on I-35 and other distresses observed on the I-35 section.

Longitudinal depressions in the form of ruts near the centerline were observed on the SH-7 section located approximately 6 miles west of I-35 heading east approximately 5 miles in Garvin County (ODOT District 7). Figure 2.6 show a photographic view of the rut on the SH-7 section. Also, it shows a paving fabric layer not stuck down causing shear failure in the upper Hot Mix Asphalt (HMA) layer, which may have caused the surface rut.

The pavement conditions of the SH-7 and I-35 sections were evaluated using TSD’s as part of pooled fund project (Pavement Structural Evaluation with Traffic Speed Deflection Devices, TPF-5(385)). Through measurements of deflections, roughness, texture, rut, and other distresses, TSD can assess both surface and structural conditions of the pavement. The goal of the pooled fund project is to provide the participating agencies guidelines on how to define collection and use of data obtained with TSD for network- and project-level pavement management applications. Figure 2.1 depicts the TSD used in the pooled fund project.

The purpose of the present study was to perform subsurface investigations of the selected pavement sections at SH-7 and I-35 using an air-coupled GPR system to identify the locations of subsurface distresses and to develop data-driven recommendations for maintenance and rehabilitation. The GPR data helped identify the locations where more extensive investigations were needed. Also, in this study, the results from the TSD were compared with the FWD results. The following steps were used in the present study: collection of project information, subsurface investigation using GPR, analysis of GPR data and identification of distressed locations, selective FWD testing, field sampling from distressed locations, laboratory testing and analysis of core samples, and comparison of subsurface investigation results obtained from TSD with those from other field and laboratory data. The following laboratory tests were conducted on the extracted cores: SCB, TO, TSR, IDEAL-CT, HWT, and volumetrics.

## 2.2 RESULTS AND ANALYSIS

Two typical pavement structures were observed on the I-35 section. The section south of Mile Post 52 consisted of 8 to 10 inches of asphalt and 8 inches of Continuous Reinforced Concrete Pavement (CRCP). The section north of Mile Post 52 consisted of 8 to 10 inches of asphalt and 9 inches of plain concrete. The pavement section at SH-7 consisted of 17 to 21 inches of asphalt with fabric at 1.5 inches below the surface.

The collected GPR data were sorted, filtered, and analyzed using the software developed by TTI. The GPR data were used to determine the layer thicknesses, presence of moisture, voids, stripping, and other anomalies in the asphalt pavement which could be responsible for pavement distresses. The output from the GPR was used to identify areas where extraction of cores was needed for further investigation. Figure 2.7 show an example of the GPR analysis for the northbound lane of the I-35 section. Based on the GPR data, the end of the CRCP and the beginning of the Jointed Concrete Pavement (JCP) section occurred at Mile Post 51.5. The GPR data did not detect the presence of CRCP steel; instead, they detected reflection cracking. The main distresses observed south of Mile Post 51.5 (CRCP) were longitudinal edge cracking and edge failure. Also, some surface raveling and edge failure were observed. North of Mile Post 51.5 (JCP), the main distresses were reflection cracking and longitudinal edge cracking. The longitudinal edge failure was likely caused by the joint between the shoulder and the lane inside the stripe paint. The pavement section at the lane consists of 6 inches of HMA over CRCP, whereas the shoulder section consisted of 6 inches of HMA over sand asphalt. Because of this configuration truck loads were generally applied right on the joint, causing higher deflections and failures. Figure 2.8 show the structural differences between the driving lane and the shoulder section and the associated FWD deflections.

Figure 2.9 show a photographic view of the GPR data collection activity on the eastbound lane of the SH-7 section. As noted above, major rut, cracking and longitudinal joint cracking were observed in this section. An increase in moisture over the joint was observed; infiltration of water through the longitudinal joint was the likely cause of increased moisture (73). Presence of relatively high moisture content in the subgrade could be an indication of premature stripping (74). Based on the GPR data, twenty-six (26) locations were identified for coring. Out of twenty-six (26) locations, only sixteen (16) asphalt cores were extracted for laboratory testing. Eleven (11) of these cores were extracted from the I-35 section and the remaining five (5) cores were extracted from the SH-7 section. FWD equipment with seven geophone sensors (W1 to W7) was used in this study. Also, the TSD data were analyzed and matched with the locations of the FWD testing so that the deflection values from both test methods can be compared. Table 2.1 describes the locations of the cores.

### 2.2.1 Back-calculation of Elastic Modulus

The MODULUS 7.0 program was used to analyze the FWD data and calculate the normalized (with respect to 9-kip load) maximum deflection for sensors W1 and W7 as well as elastic moduli of different pavement layers. Figure 2.10 and Figure 2.11 show the elastic modulus values for the HMA and subgrade layers for the I-35 and SH-7 sections, respectively. A mean and a standard deviation of 919.7 and 346.4 ksi. were observed for the surface layer, respectively. The corresponding values for the subgrade were 44.6 and 23.7 ksi. for the eastbound lane of the SH-7 section. For the westbound section, a mean and a standard deviation of 866.6 and 277.7 ksi. were observed for the surface layer, respectively. The corresponding values for the subgrade layer were 42.7 and 13.8 ksi. The elastic moduli for cores 17, 22-23 and 24-25 were found as 510, 636 and 1,052 ksi., respectively. The corresponding mean and standard deviation values were 1,262.2 and 536 ksi., respectively, for the surface layer, and 66.3 and 35.7 ksi., respectively, for the subgrade for the northbound lane of the I-35 section.

Comparatively, for the southbound lane, the corresponding mean and standard deviation values were 1,332.2 and 383.2 ksi., respectively, for the surface layer, and 65 and 35.3 ksi., respectively, for the subgrade. The elastic modulus values for cores 2-3-4, 5-6-7, 12-3, and 14-15 were 918, 596, 1,674, 810 and 1,461 ksi., respectively.

### 2.2.2 Destructive Testing

As noted previously, SCB, IDEAL-CT, TSR, HWT, TO tests were conducted and volumetric properties were determined for the extracted cores to identify potential reasons for the observed distresses. Semi-circular Bend tests were used to determine their fatigue resistance. The Illinois Flexibility Index Test (I-FIT) was conducted in accordance with the AASHTO TP124 test method (75) .  This test was conducted by applying a monotonic load at 50 mm/min until failure. The I-FIT values obtained from these tests are presented in Figure 2.12 . The FI values were found to be very low for samples 2A, 3A and 3B (below 1), and relatively low for sample 2B (below 2.5) compared to the acceptable limit (greater than 8).

Two HWT tests were conducted on samples from the top lifts of the extracted asphalt cores from the SH-7 section following OHD L-55 test method (76).The test results were used to determine their susceptibility to rut and potential for moisture-induced damage. The HWT tests were conducted at 50°C with a wheel pass frequency of 52 passes/minute. The tests were terminated after reaching either a maximum rut depth of 0.8 in (20-mm) or 20,000-wheel passes, whichever reached first. Figure 2.13 presents the HWT test results for cores C22/C23 and C24/C25. From Figure 2.13, asphalt cores C22 and C23 performed well relative to rut and no stripping inflection point was observed. Comparatively, asphalt cores C24 and C25 did not pass the minimum requirement for rut (<0.5 in (12.5) mm for 20,000 passes). Also, stripping inflection point g was observed for these cores. Delamination in core C24 (next to the longitudinal joint) was observed prior to testing. None of the other tested cores showed delamination in the top lift. Bonding between layers plays an important role on the pavement performance (77). Delamination leads to weaking and eventual destruction of such bond.

Texas overlay tests were conducted on samples obtained from the top and bottom sections of cores C5 and C6 on I-35 following the Tex-248-F method (78). Very poor crack resistance was observed for the top specimens collected from 0 to 1.5 inches below the top and bottom specimens prepared from the bottom 1.5 to 3 inches. Figure 2.14 depicts the tested samples; a very dry mix condition was observed. Generally, a mixture with over 300 cycles is considered a good mix (79). From Figure 2.14, the fatigue resistance was found to be very low (less than 8 cycles before the sample broke or failed).

Moisture-induced damage tests were conducted on five (5) cores extracted from the I-35 section. Three (3) of these cores were used as the control subset and the other two (2) cores were used as the conditioned subset. The TSR test was conducted in accordance with AASHTO T-283 method (80). Table 2.2 presents the results obtained for each subset. A low TSR value was observed (0.57). Also, low indirect tensile strengths (below 64 psi.) were observed in all subsets. Cracked or broken aggregates were observed in all subsets and high moisture damage was observed in the preconditioned subset. IDEAL-CT tests were conducted on four (4) cores extracted from the I-35 section. Two (2) of these cores were used as the control subset and other two (2) cores were used as the conditioned subset (the same cores used for the TSR test). The IDEAL CT tests were conducted in accordance with the NCHRP 20-30/IDEAL 195 test method (81). IDEAL-CT indices below 80 (8 to 66) were observed, indicating poor resistance to fatigue. Low indices were observed for all samples. Comparatively, higher IDEAL-CT indices were observed for the pre-condition samples. The IDEAL-CT index for core 4 could not be measured. Table 2.2 show the IDEAL-CT results, and Figure 2.15 show the load vs displacement curves obtained for the tested samples.

### 2.2.3 Non-destructive Testing

Deflection, roughness, and rut depths obtained from the TSD data were compared for both wheels for each bound of the SH-7 and I-35 sections. As noted earlier, TSD can measure these parameters for both wheels. Figure 2.16 show the rut results for both wheels for the eastbound and westbound lanes of the SH-7 section, respectively. As observed during the field visit and from the GPR results, the left wheel path showed significantly higher rut than the right wheel path for both bounds. Significant depressions were observed next to the longitudinal joint.  Rut values of 0.62 and 0.37 in. were observed for the left wheel path and the right wheel path, respectively, for the eastbound lane of SH-7. Asphalt cores 22 and 23 were extracted from these locations. For the westbound lane, the corresponding rut values were found as 0.34 and 0.15 in., respectively, for the left and the right wheel paths from where cores 22 and 23 were extracted. A 0.24 and 0.17 in. rut for left and right wheel, respectively, were observed on the location where C17 is located.  A significantly lower rut was observed at core locations for the west lane compared to the east lane. Figure 2.17 and Figure 2.18 show the results for rut on both wheels for I-35 northbound and southbound, respectively. Slightly higher rut depths were observed for the left wheel in both bounds. Rut depths below 0.2 in. were observed at core locations in both bounds.

Roughness was also measured for both wheels in both segments and bounds. Figure 2.19 show the results for SH-7. Generally, IRI’s below 170 are considered fair, and below 95 are considered good (82). High IRI’s were observed in the left wheel path for the eastbound lane of the SH-7 section compared to the right wheel path. Major depressions were observed in the eastbound at the time of the field survey. Also, the high peaks on IRI result coincide with the high rut peaks shown in previous graphs. Low IRI's (below 90) were observed on core located at the westbound lane of SH-7. For the eastbound lane, a significant difference was observed. The corresponding IRI values were 361 and 69 for the left and right wheel paths, respectively.

Figure 2.20 and Figure 2.21 show the roughness results obtained from the TSD data for the I-35 section. No significant differences were observed for the left and right wheel paths for both bounds. There are some IRI peaks that match the rut peaks observed in the previous figures. However, an acceptable IRI trend (below 175) was observed in the cores extracted from the I-35 section. Table 2.3 describes the mean, standard deviation, minimum and maximum values of deflection, rut and roughness for all sections and segments. Slightly higher ruts, deflections and roughness were observed for the eastbound lane of SH-7 compared to the westbound lane. No significant differences were observed for the I-35 section for both bounds and pavement types (i.e., before and after the intersection with SH-7). Nevertheless, a higher mean deflection was observed for both bounds of the I-35 section, located north of the intersection with SH-7.

Deflections from the TSD testing were compared with the deflections from the FWD testing for both I-35 and SH-7 sections. Figure 2.22 and Figure 2.23 show the comparison between deflections under the center of the load for TSD ($D_0$) and FWD (W1). Correlation values of 0.34, 0.55, 0.47 and 0.26 were observed between the TSD and FWD deflections for the SH-7 eastbound lane, SH-7 westbound lane, I-35 northbound lane, and I-35 southbound lane, respectively. In pursuing these comparisons, it was evident that deflection values were not recorded by TSD at several points. As such, the deflection values obtained from the FWD data could not be compared with the TSD data at these points. Consequently, some gaps in between points are observed in Figure 2.23. Figure 2.24 show the relationships between $W_1$ and $D_0$ for the combined data; the corresponding correlation of and coefficient of determination ($R^2$) were found to be 0.45 and 0.21 were, respectively.

As mentioned above, TSD is capable of measuring roughness and rut as well. Figure 2.25, Figure 2.26, Figure 2.27, Figure 2.28, Figure 2.29, and Figure 2.30 show the comparison for roughness (IRI) and rut at both wheels between TSD and Pave 3D 8k on I-35 and SH-7. Figure 2.31 show the correlation between the TSD and Pave3D 8k measurements of IRI and rut. A higher correlation was observed for IRI compared to rut. A better correlation was observed for IRI values at the left wheel path. As noted, before, roughnesses below 90 in/mile and 170 in/mile are considered good and acceptable, respectively. Both TSD and Pave 3D 8k were capable of detecting good (<90) IRI values with Pave 3D 8k showing higher IRI values (more than 90). For acceptable IRI (<170), TSD shows higher roughness for composite pavements (I-35). For ruts, deformations below 0.5 inches are considered acceptable. TSD showed slightly higher sensitivity to detect ruts higher than 0.5 inch.

## 2.3 CONCLUSSION AND RECOMMENDATIONS

Field (GPR, FWD and TSD) and laboratory tests (SCB, IDEAL-CT, TSR, HWTD, TOT) were performed on selected pavement section on I-35 and SH-7 in Oklahoma to identify the causes of observed reflection cracking, edge cracking, rut and longitudinal edge depressions. The specific findings of this study are listed below:

- The GPR images showed two different types of pavements in the studied section of I-35. It was observed that the pavement structure north of Mile Post 51.5 consisted of Jointed Concrete Pavement (JCP) while the section south of Mile Post 51.5 consisted of Continuously Reinforced Concrete Pavement (CRCP). The JCP section showed severe reflective cracking. The main distresses observed on the CRCP section were longitudinal edge cracking and edge failure. The presence of joints between the shoulder and driving lane inside the stripe paint was a likely cause of the longitudinal edge failure.
- Significant rut, cracking and longitudinal joint cracking were observed on the eastbound lane of SH-7. The GPR images and extracted asphalt cores revealed a very thick layer of HMA in this section. A loose or delaminated fabric layer not attached to the pavement below might have been responsible for causing shear failure and rut in the HMA layer. The GPR data exhibited an increase in moisture over the joint indicating infiltration of water through the longitudinal joint crack. The inside lanes of SH-7 were found to be in fairly good condition.

- The elastic modulus (E) values of the surface and subgrade layers of the I-35 and SH-7 sections were determined using the FWD test data. Overall, good modulus (E) values were observed for the I-35 section and low modulus values were observed for the eastbound inside lane of the SH-7 section, where major depressions and ruts were observed.
- Laboratory performance tests, namely I-FIT (SCB), IDEAL-CT, TO and TSR tests, were conducted on the extracted cores from the I-35 section. The Flexibility Index (FI) from I-FIT test and CT Index from the IDEAL-CT test did not meet the minimum passing criteria for fatigue cracking. Also, very low cycles to failure were observed from the OT test. The results indicated the presence of a very dry mix on the I-35 section that is prone to additional fatigue cracking without appropriate rehabilitation measures.
- The HWT tests were conducted on cores extracted from the eastbound and westbound lanes of the SH-7 section. The results of the HWT tests indicated potential for rut failure of the SH-7 section, without appropriate maintenance and/or rehabilitation measures. The Core 24, which was severely delaminated and located next to the longitudinal joint, was severely damaged during the HWT test. Also, the TSD data exhibited higher rut and roughness for the eastbound lane of the SH-7 section.
- The FWD and TSD deflection data under the center of the loads exhibited a correlation of 0.45. The overall $R^2$ between the FWD and TSD deflection values for both sections were found to be 0.21. A stronger correlation was observed for the westbound lane of the SH-7 section.

- Specialized GPR used in this project, in collaboration with TTI/TAMU, collected data at highway speed. This can be a useful tool for selective data-driven coring of pavement, which is a destructive process.
- FWD or FFWD when used in conjunction with TSD can be a useful tool for validating TSD results and identifying pavement conditions (project level application) confidently. Also, using pavement layer thicknesses from the GPR data at highway speed enhances the utility of TSD data for network-level application.
- Better correlations were observed between the TSD and Pave 3D 8k data. Both tools were able to identify good and acceptable roughness and rut thresholds.

**Table 2.1 Location of Extracted Cores**

| Cores I-35 | Direction | Core Notes |
|---|---|---|
| 2 | NB | Mid lane |
| 3 | NB | 2' S. of core 2 |
| 4 | NB | Over shoulder, delamination and stripping |
| 5 | NB | Mid lane, thick tack and fabric |
| 6 | NB | 2' S. of core 2, fabric |
| 7 | NB | Mid. Shoulder, Delamination |
| 8 | NB | 1' left of shoulder line, thick tack |
| 12 | NB | Mid. Lane over crack, filled crack, thick tack and delamination |
| 13 | NB | 2' right of shoulder line, crack, delamination, stripping |
| 14 | SB | Right wheel path |
| 15 | SB | Shoulder line, delamination, stripping and fully cracked bottom layer |
| **Cores SH-7** | **Direction** | **Core Notes** |
| 17 | WB | Right Wheel thru crack, fabric |
| 22 | EB | Right wheel, fabric, delamination, stripping |
| 23 | EB | Left wheel near center line in rutted area, delamination, stripping, cracked |
| 24 | WB | Left wheel over crack, fabric, delamination |
| 25 | WB | Right wheel |

**Table 2.2 Moisture-Induced Damage and IDEAL-CT Results**

| Specimen Number | 4 | 8 | 14 | 7 | 15 |
|---|---|---|---|---|---|
| Control or Pre-condition | C | C | C | P | P |
| Load, lbf | 1,150 | 1,334 | 1,414 | 955 | 627 |
| IDEAL-CT Index (min. 80) | NA | 8 | 9 | 14 | 66 |
| Indirect Tensile Strength, psi | 55 | 59 | 64 | 41 | 27 |
| Average Control and Pre-Con, psi | 59 | | | 34 | |
| Tensile Strength Ratio (min 0.8/0.75 design/field) | 0.57 | | | | |

**Table 2.3 Deflection, Rut, and Roughness Results Summary**

| Segment | Measure | Mean | Standard Deviation | Maximum | Minimum |
|---|---|---|---|---|---|
| SH-7 Eastbound | $D_0$ (mils) | 3.47 | 1.30 | 9.20 | 0.00 |
| | Rut (in) | 0.26 | 0.08 | 0.49 | 0.05 |
| | IRI (in/mi) | 69.48 | 34.56 | 278.00 | 22.00 |
| SH-7 Westbound | $D_0$ (mils) | 3.26 | 1.61 | 10.60 | 0.00 |
| | Rut (in) | 0.21 | 0.07 | 0.48 | 0.06 |
| | IRI (in/mi) | 56.00 | 28.65 | 291.00 | 20.00 |
| I-35 (north of SH-7) Northbound | $D_0$ (mils) | 0.91 | 1.46 | 9.00 | 0.00 |
| | Rut (in) | 0.13 | 0.06 | 0.43 | 0.03 |
| | IRI (in/mi) | 63.88 | 47.33 | 527.00 | 21.00 |
| I-35 (north of SH-7) Southbound | $D_0$ (mils) | 1.17 | 1.48 | 11.20 | 0.00 |
| | Rut (in) | 0.10 | 0.05 | 0.36 | 0.04 |
| | IRI (in/mi) | 59.48 | 41.44 | 359.00 | 20.00 |
| I-35 (south of SH-7) Northbound | $D_0$ (mils) | 0.41 | 1.16 | 12.20 | 0.00 |
| | Rut (in) | 0.14 | 0.06 | 0.45 | 0.03 |
| | IRI (in/mi) | 70.67 | 39.48 | 465.00 | 30.00 |
| I-35 (south of SH-7) Southbound | $D_0$ (mils) | 0.51 | 1.43 | 19.60 | 0.00 |
| | Rut (in) | 0.08 | 0.04 | 0.49 | 0.03 |
| | IRI (in/mi) | 52.95 | 51.23 | 526.00 | 22.00 |

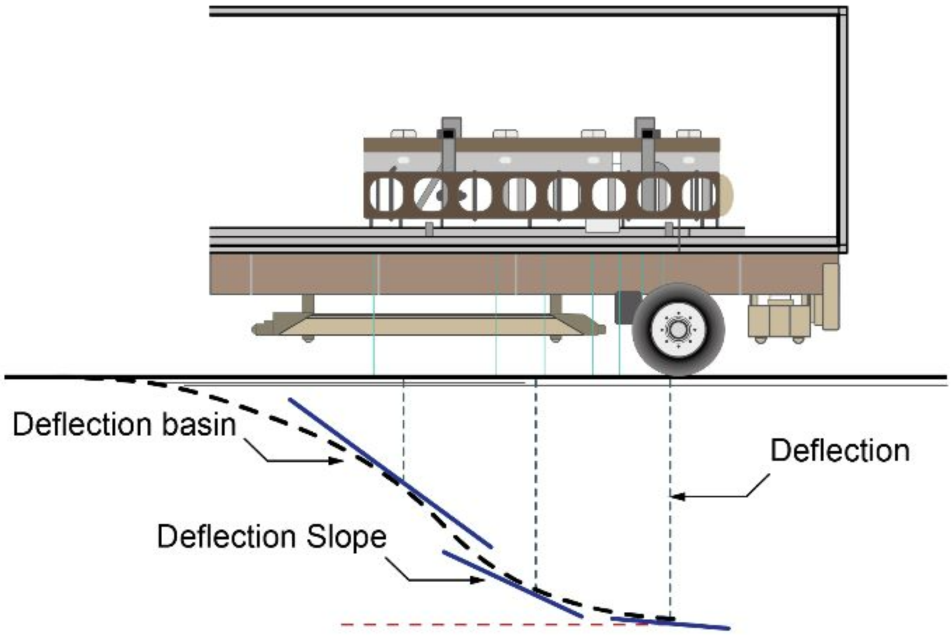


**Figure 2.1 Traffic Speed Deflectometer Deflection Slope (15)**

**Figure 2.2 Ground Penetrating Radar Developed by TTI**

**Figure 2.3 Pave3D 8k Vehicle Developed by OSU (83)**

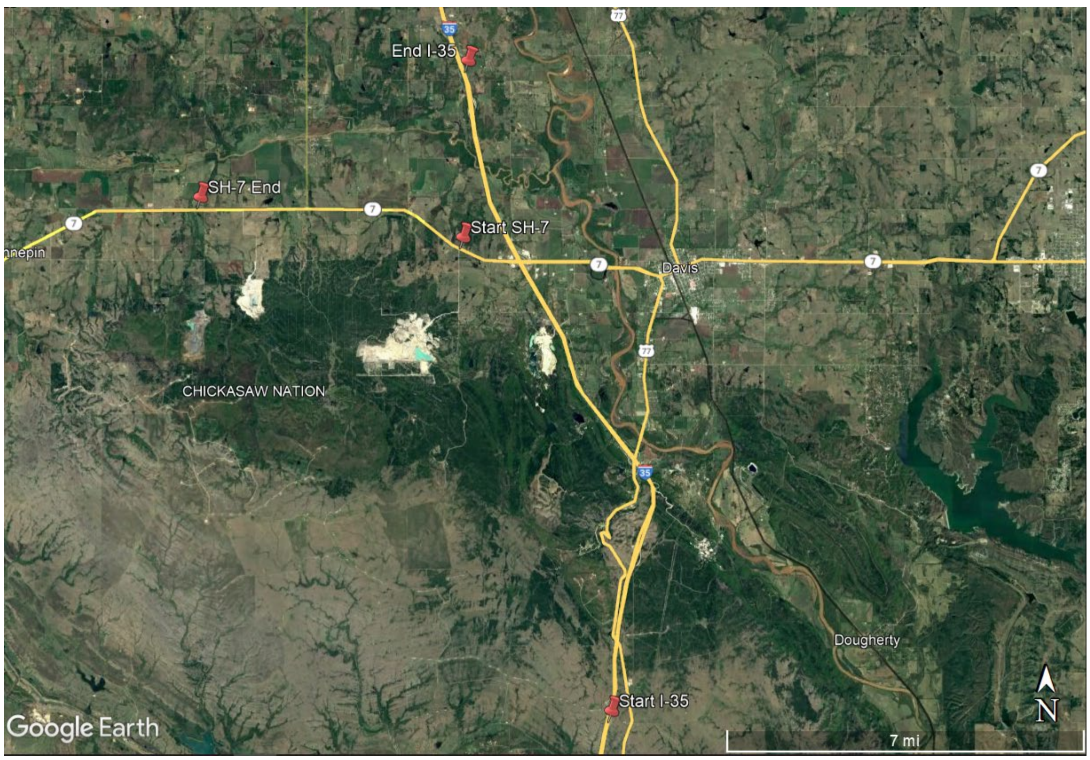


**Figure 2.4 Google Satellite Image of the Test Section**

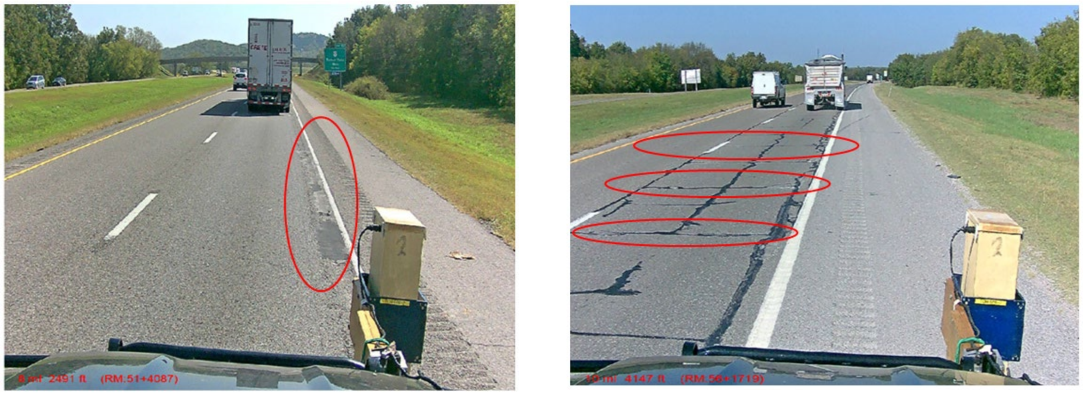

(a) (b)

**Figure 2.5 Distresses Observed on I-35 (a) Edge Longitudinal Cracking, and (b) Reflective Cracking**

(a) (b)

**Figure 2.6 Distresses Observed on SH-7 (a) Rut, and (b) Paving Fabric Delamination**


Figure 2.7 GPR Analysis on I-35 Northbound Mile 51.5


Figure 2.8 Lane and Shoulder Pavement Section on I-35 NB Mile Post 51.5

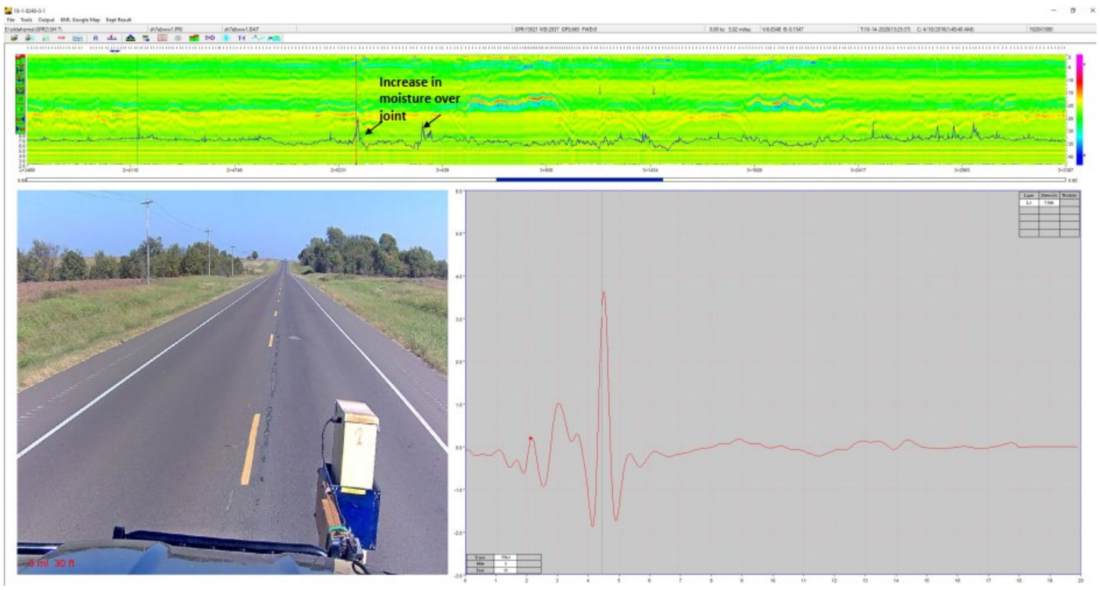


**Figure 2.9 Typical GPR Results for the Eastbound Lane of the SH-7 Section**

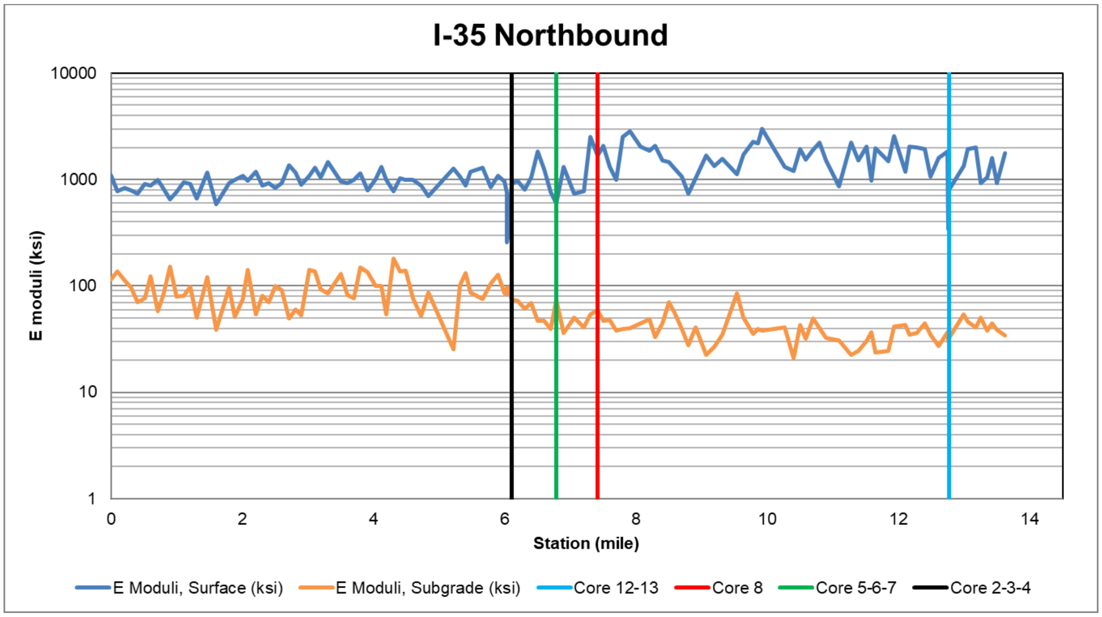


(a)

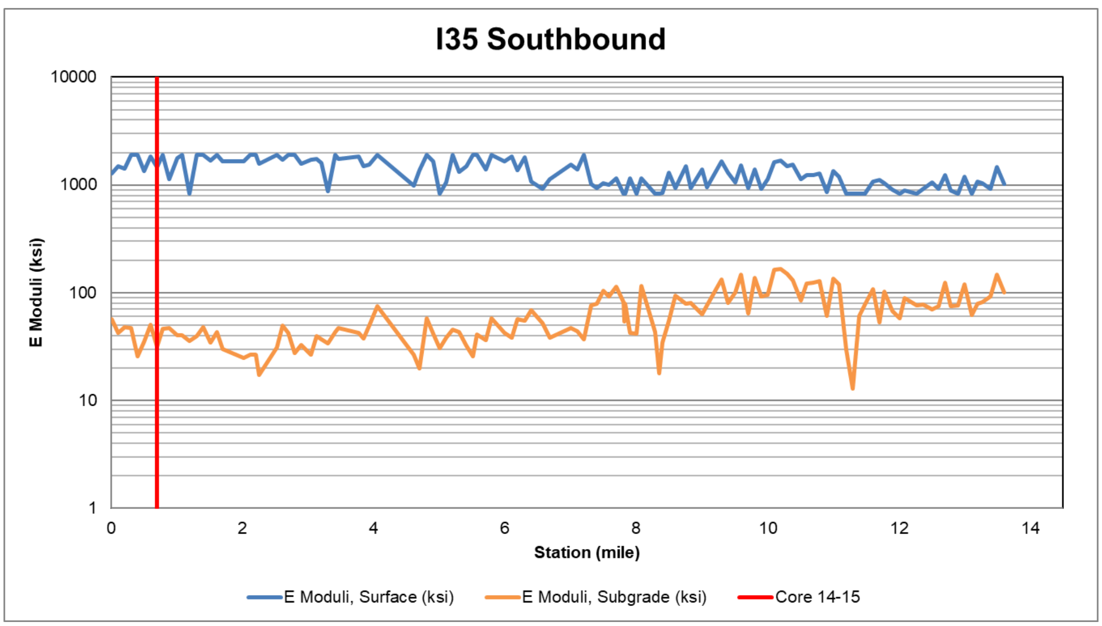


(b)

**Figure 2.10 Elastic Moduli Results for I-35 (a) Northbound (b) Southbound**

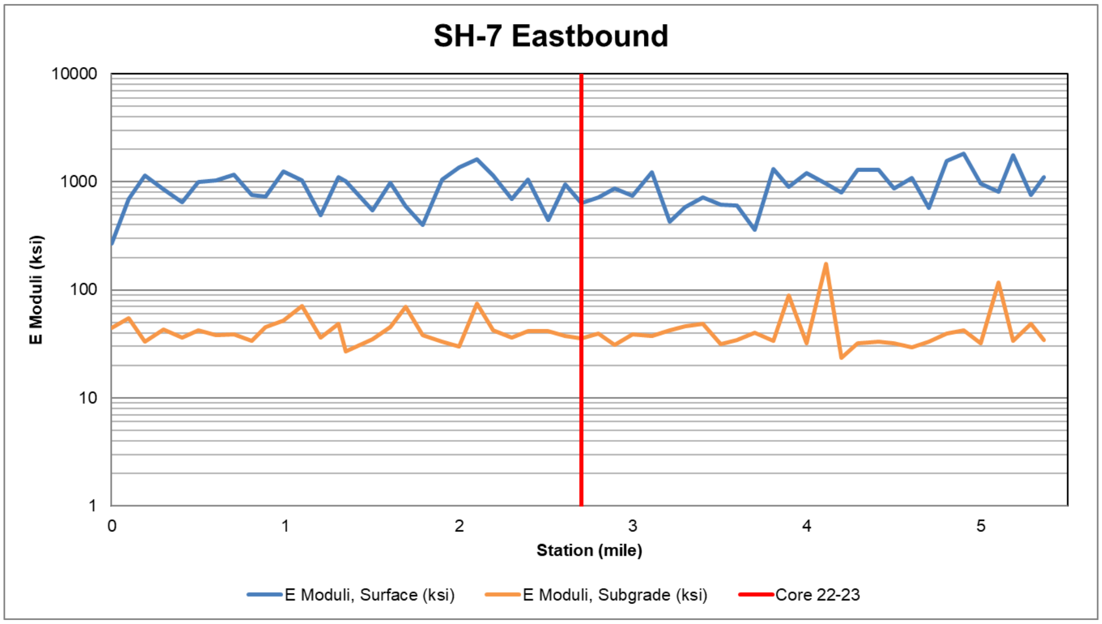


(a)

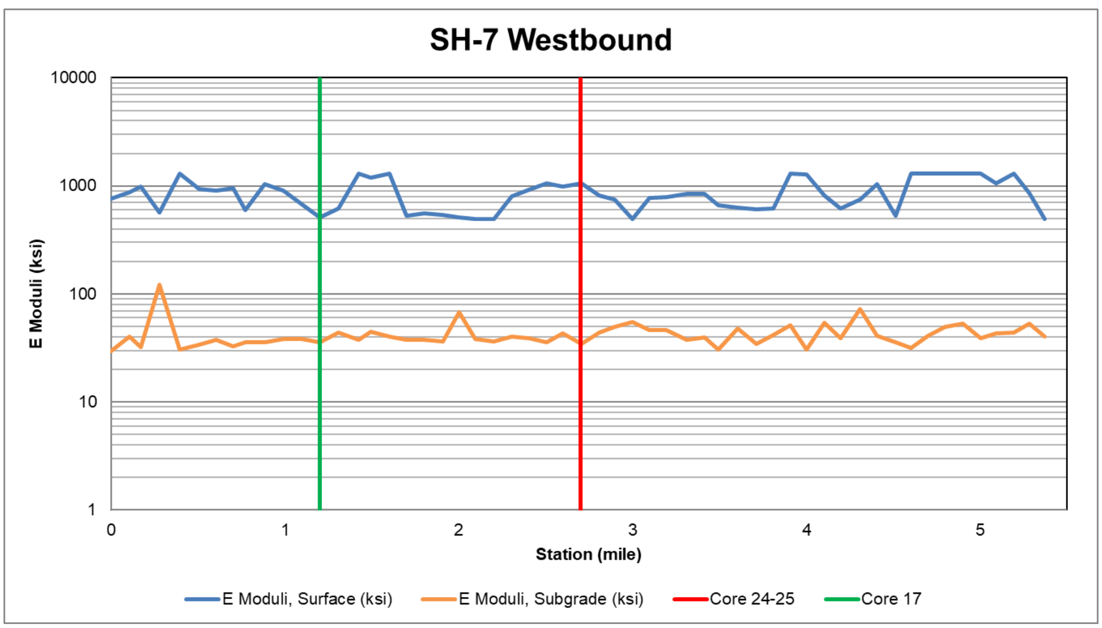


(b)

**Figure 2.11 Elastic Moduli Results for SH-7 (a) Eastbound (b) Westbound**

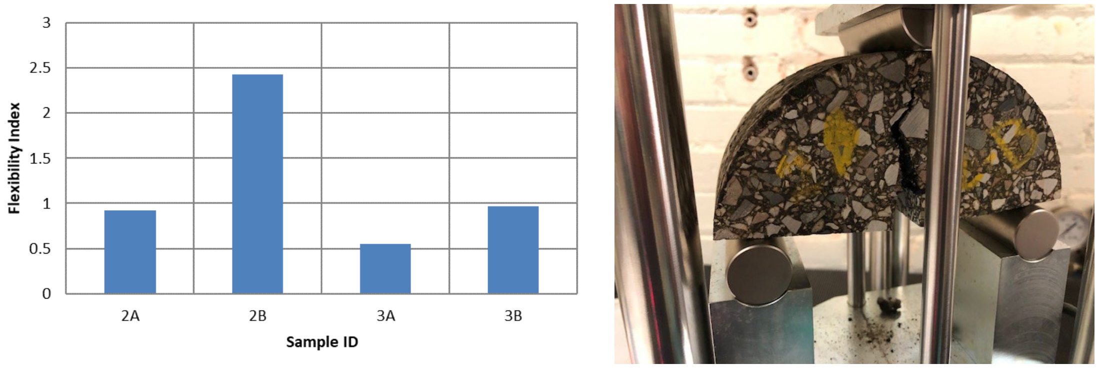


**Figure 2.12 IFIT Results of Asphalt Core Samples**

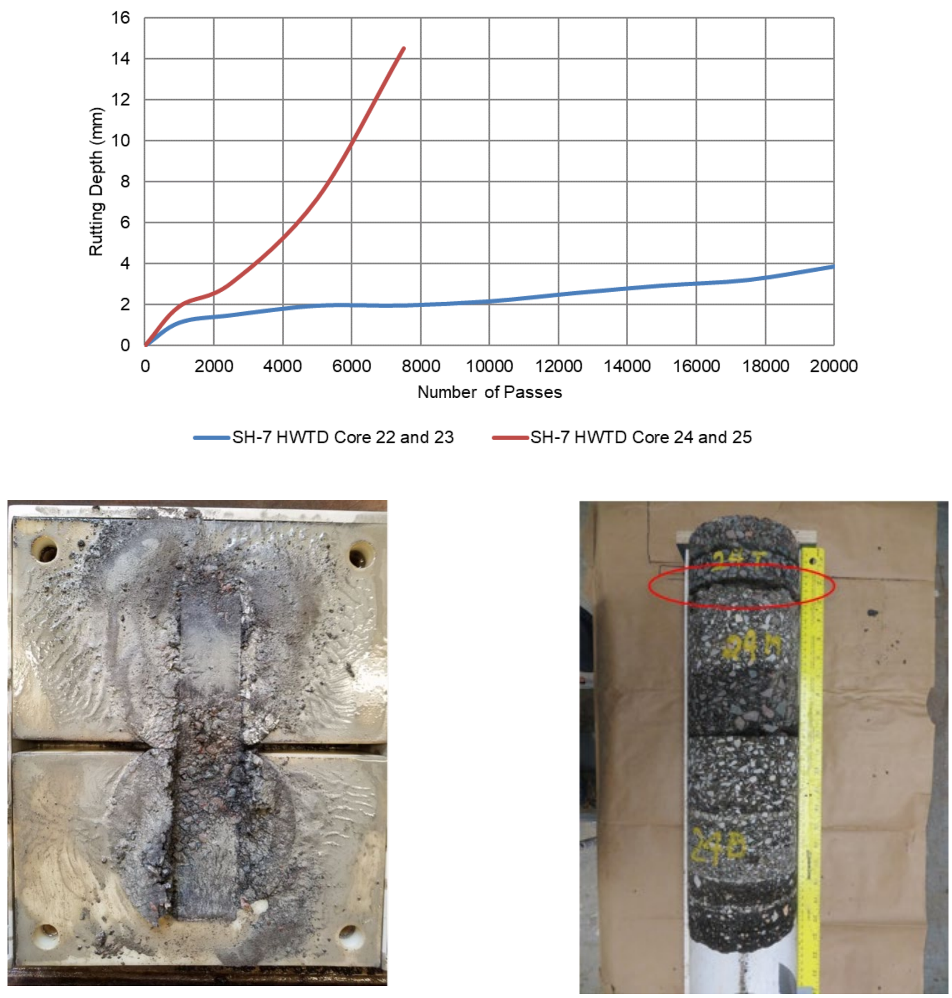


**Figure 2.13 HWT Results**

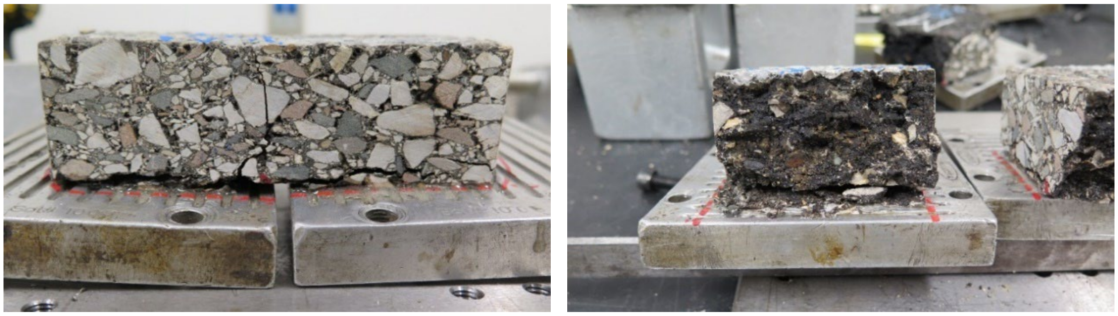

**Figure 2.14 Texas Overlay Test Samples**

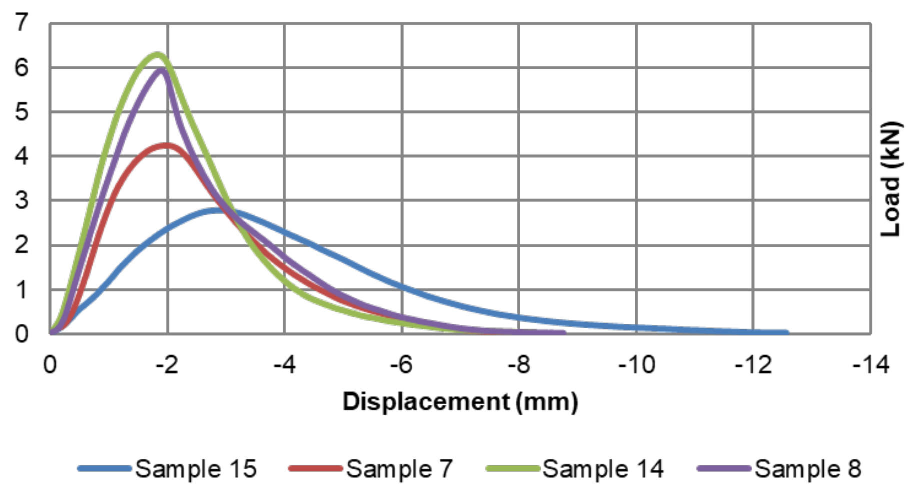


**Figure 2.15 Load vs Displacement, IDEAL-CT Results**

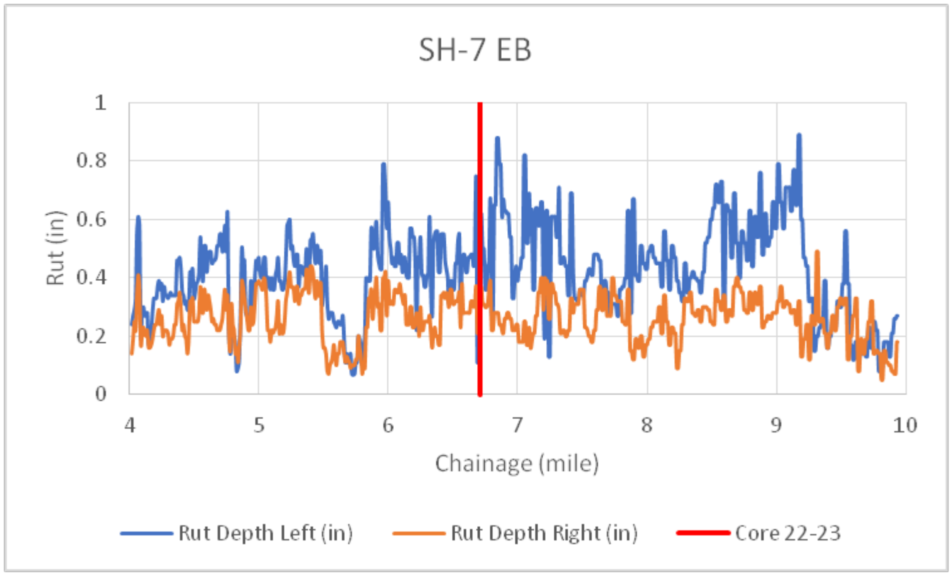


(a)

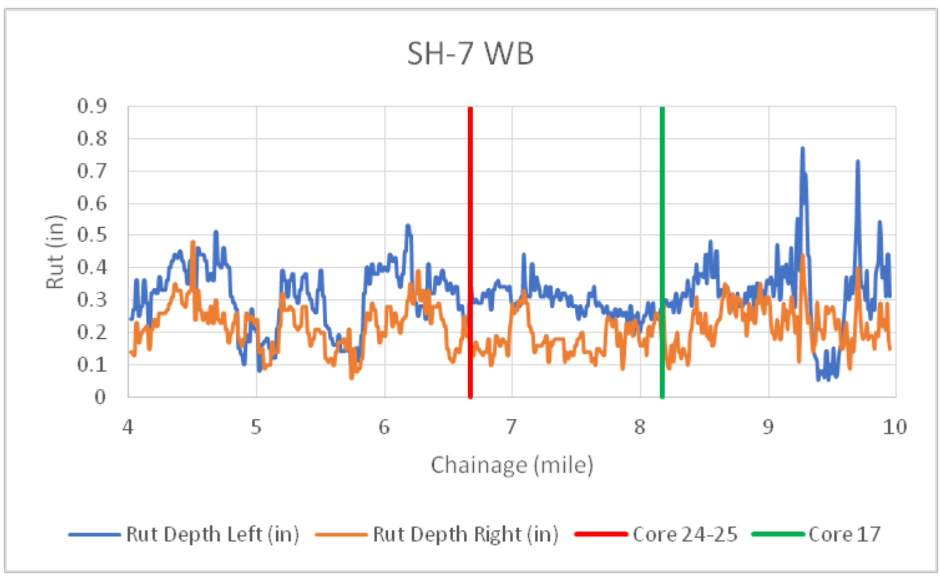


(b)

**Figure 2.16 TSD Wheel Rut SH-7 (a) Eastbound, and (b) Westbound**

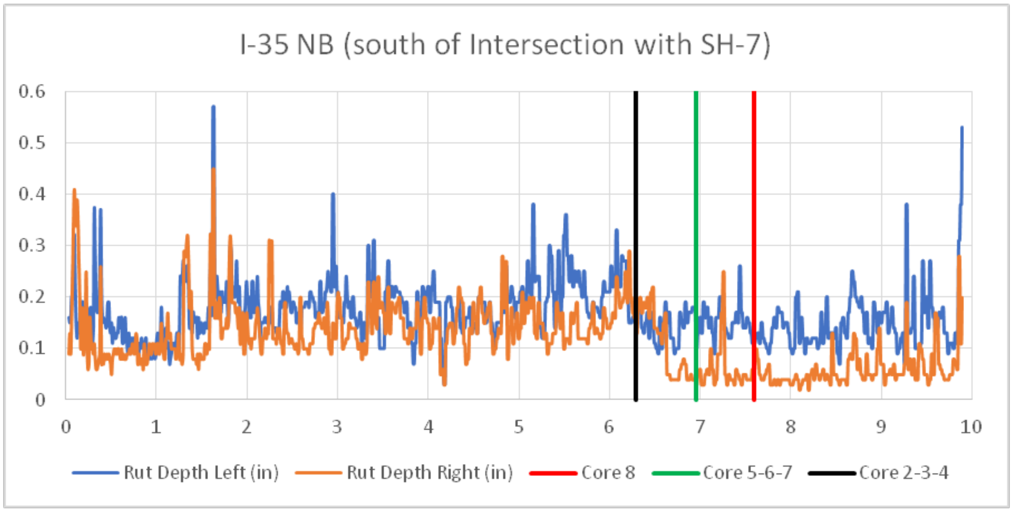


(a)

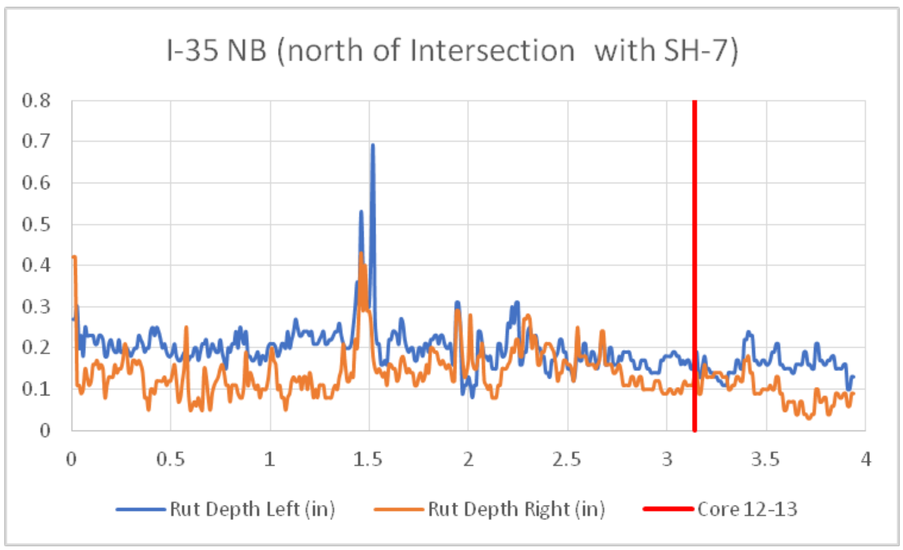


(b)

**Figure 2.17 TSD Wheel Rut I-35 Northbound (a) South of Intersection with SH-7, and (b) North of the Intersection with SH-7**

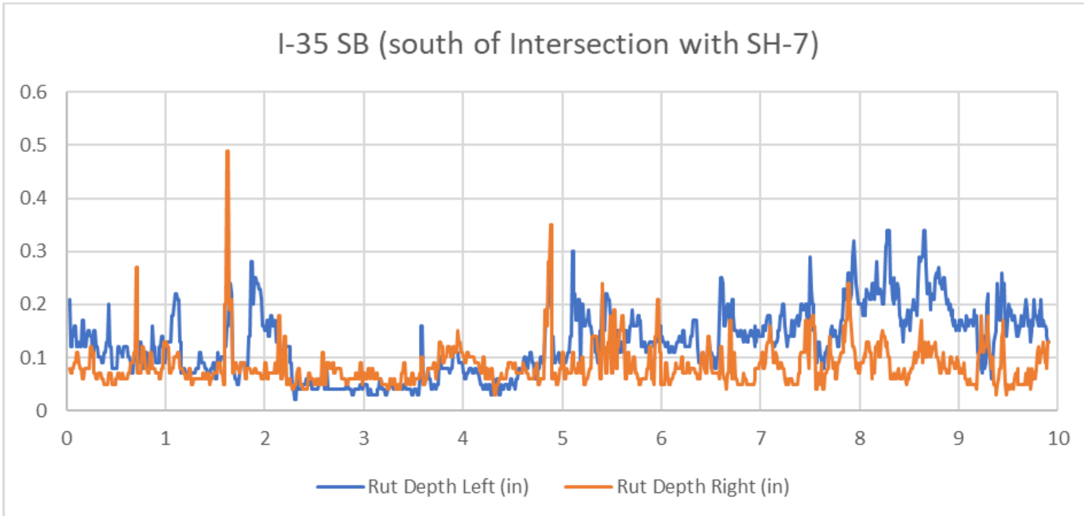


(a)

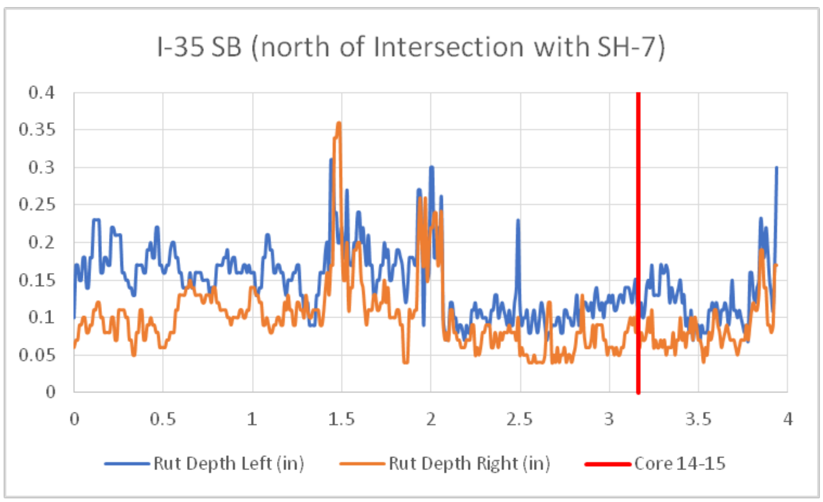


(b)

**Figure 2.18 TSD Wheel Rut I-35 Southbound (a) South of Intersection with SH-7, and (b) North of the Intersection with SH-7**

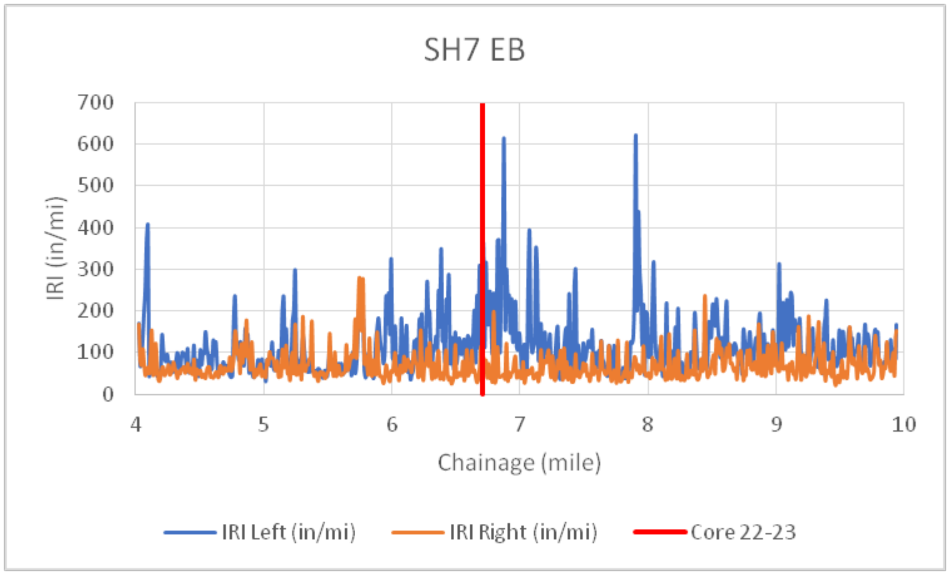


(a)

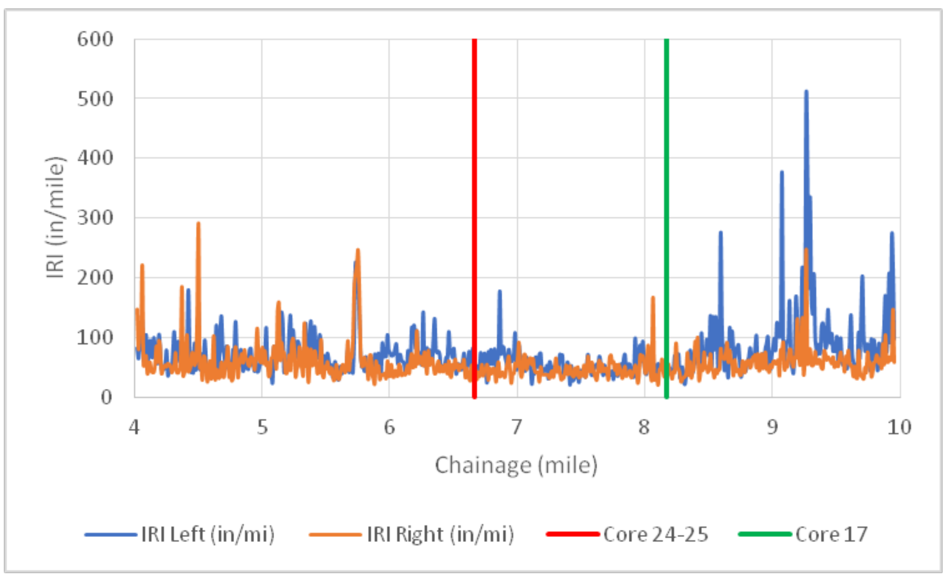


(b)

**Figure 2.19 TSD IRI Roughness SH-7 (a) Eastbound, and (b) Westbound**

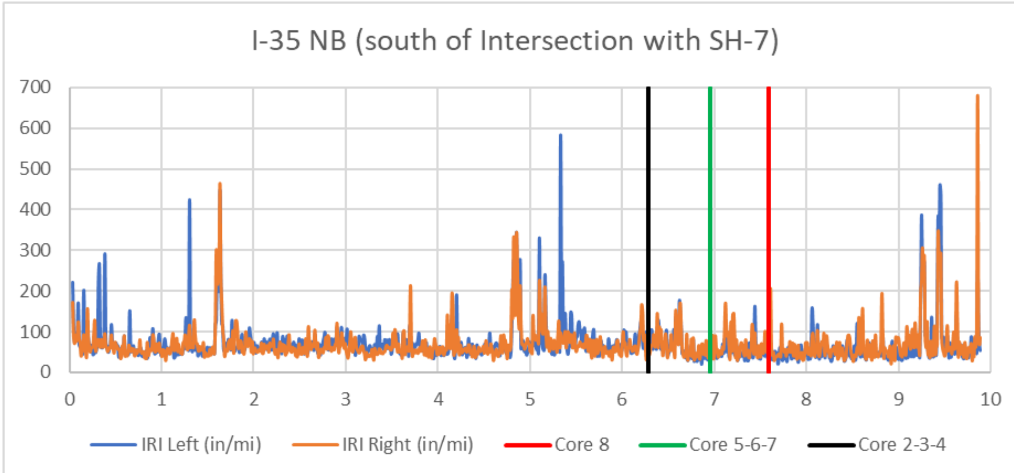


(a)

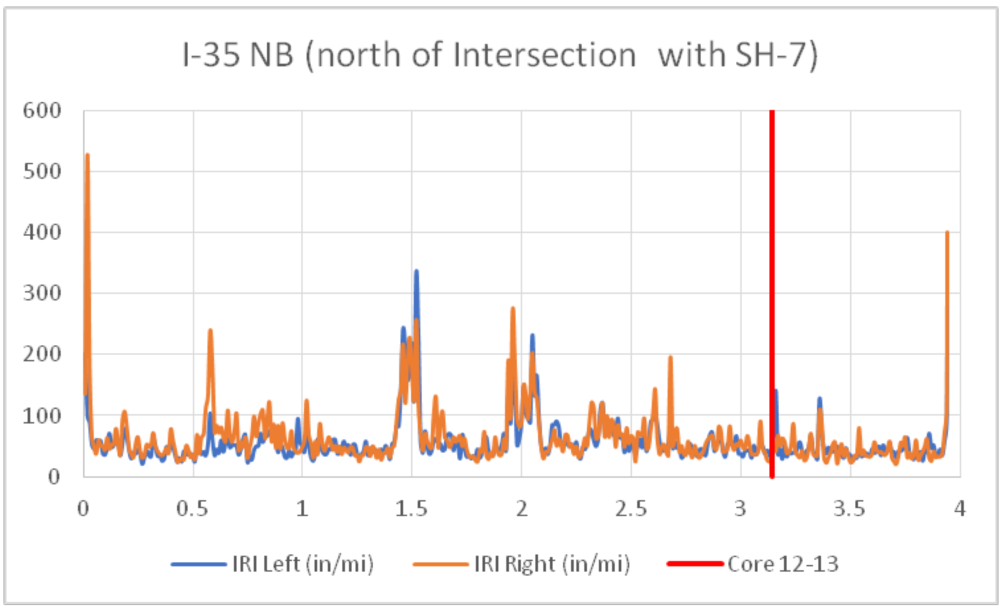


(b)

**Figure 2.20 TSD IRI Roughness I-35 Northbound (a) South of Intersection with SH-7, and (b) North of the Intersection with SH-7**

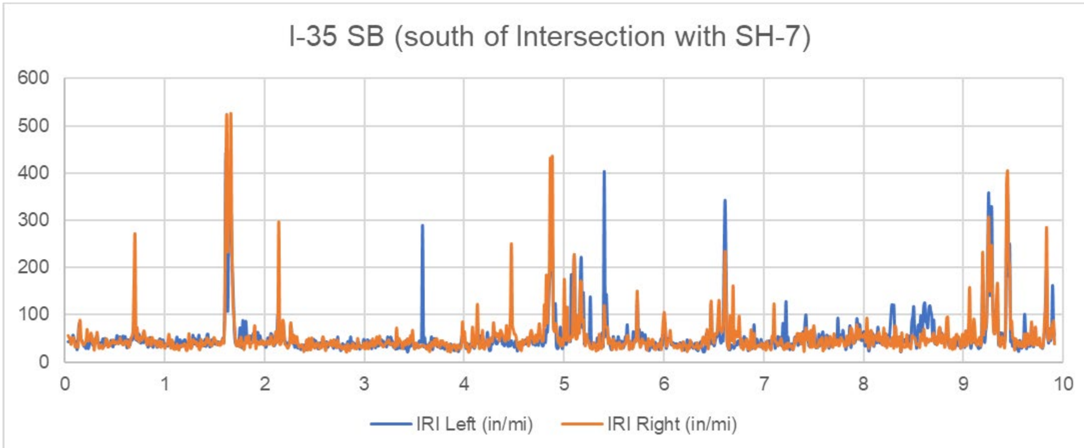


(a)

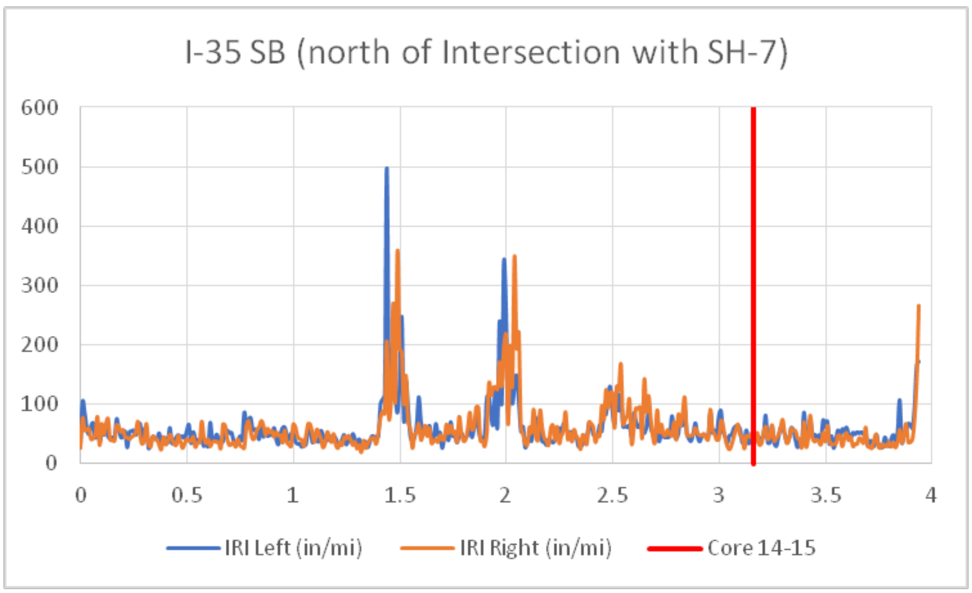


(b)

**Figure 2.21 TSD IRI Roughness I-35 Southbound (a) South of Intersection with SH-7, and (b) North of the Intersection with SH-7**

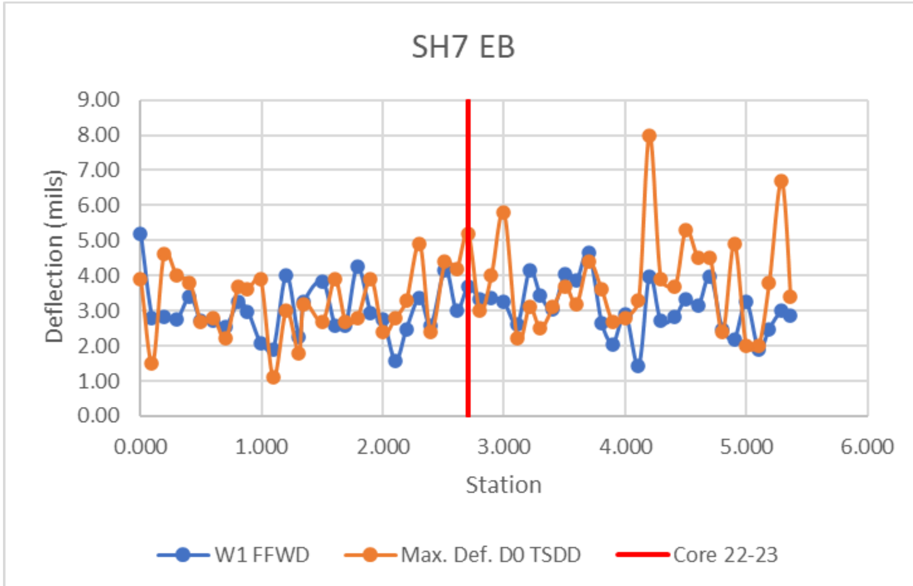


(a)

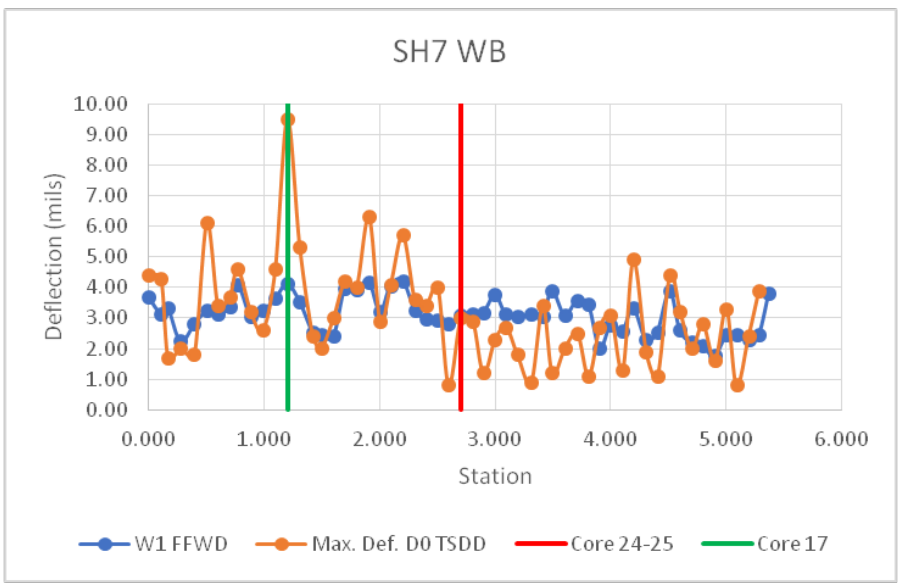


(b)

**Figure 2.22 TSD and FWD Deflections SH-7 (a) Eastbound, and (b) Westbound**

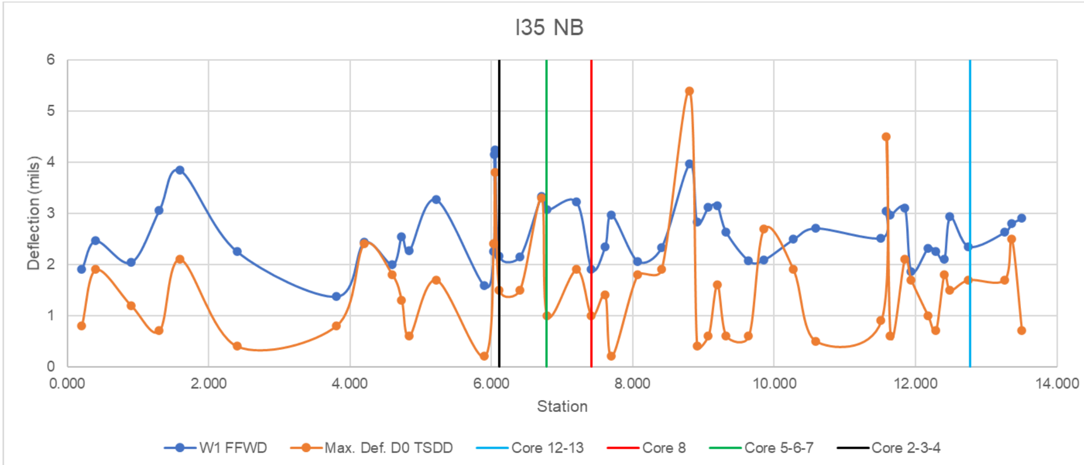


**(a)**


**(b)**

**Figure 2.23 TSD and FWD Deflections I-35 (a) Northbound, and (b) Southbound**

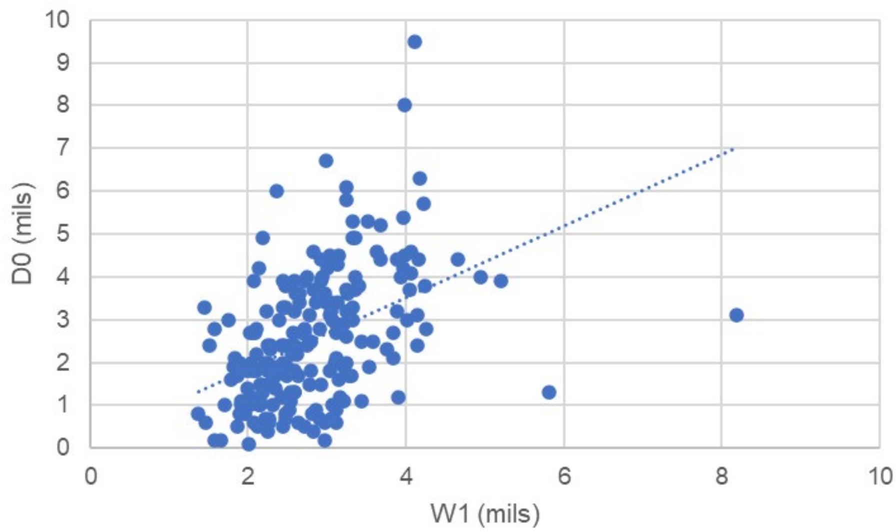


**Figure 2.24 TSD and FWD Deflections Relationship**

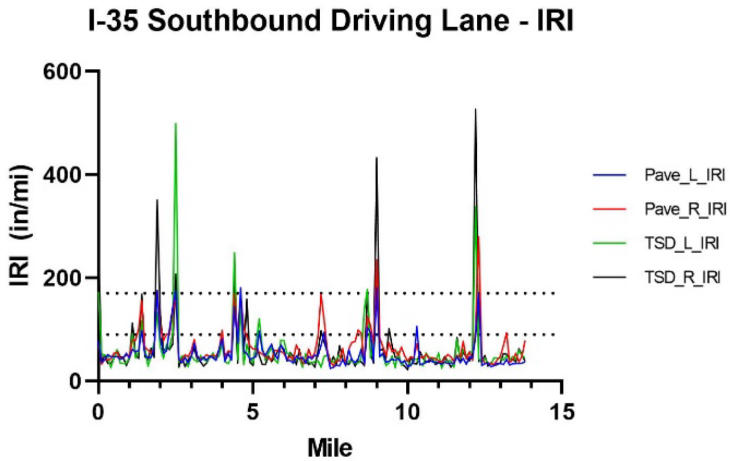


(a)

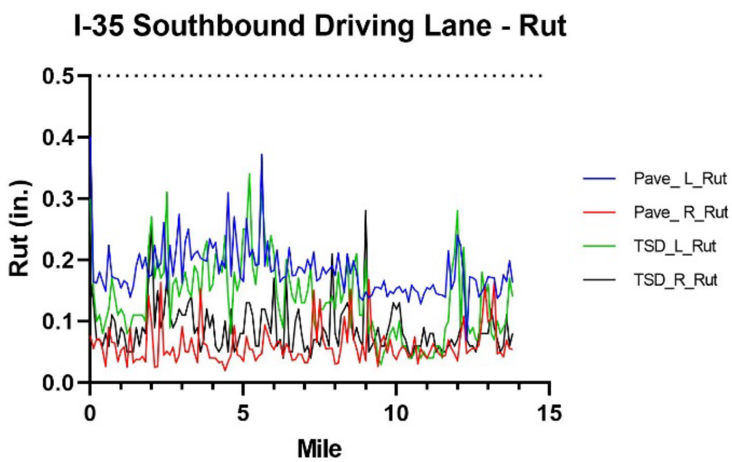


(b)

**Figure 2.25 Roughness (a) and Rut (b) Comparison for TSD and Pave 3D 8k on I-35 Southbound Driving Lane**

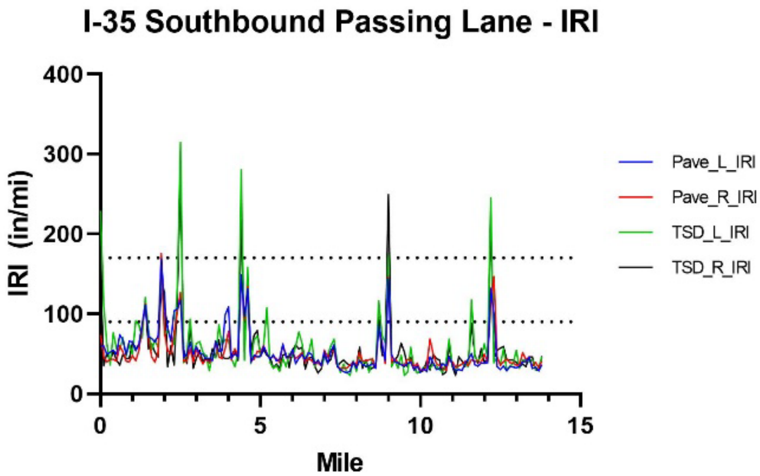


(a)

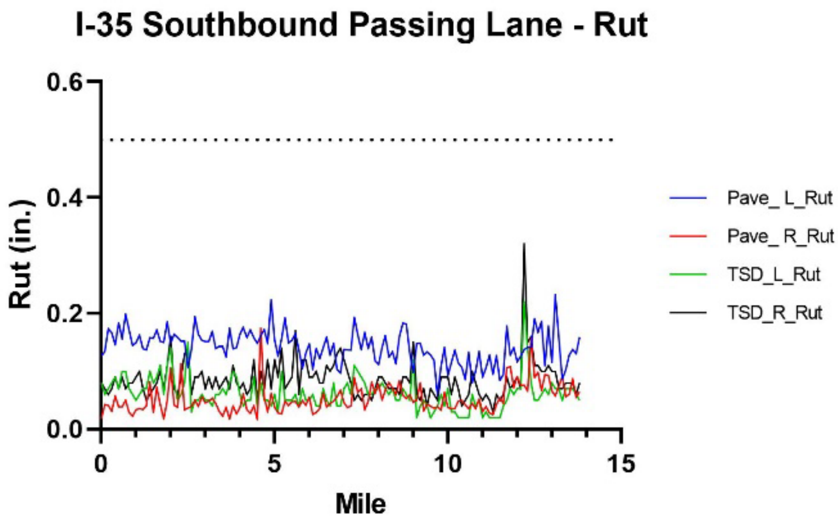


**Figure 2.26 Roughness (a) and Rut (b) Comparison for TSD and Pave 3D 8k on I-35 Southbound Passing Lane**

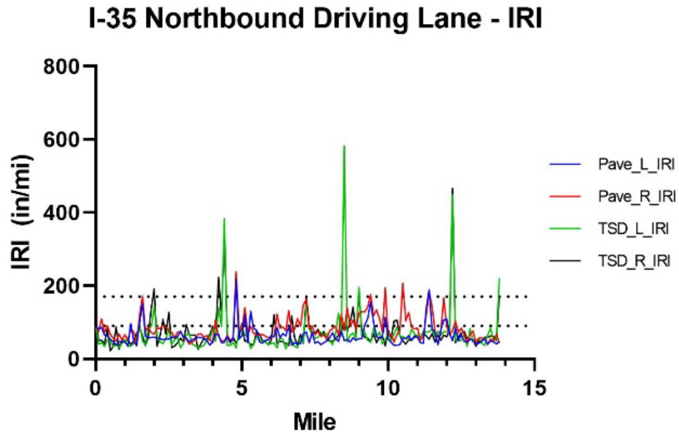


(a)

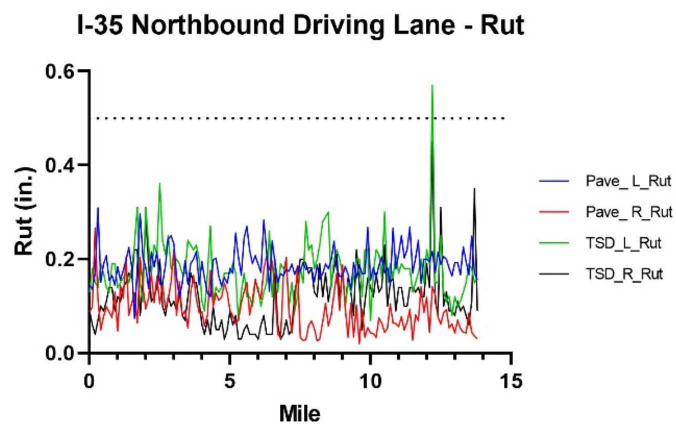


(b)

**Figure 2.27 Roughness (a) and Rut (b) Comparison for TSD and Pave 3D 8k on I-35 Northbound Driving Lane**

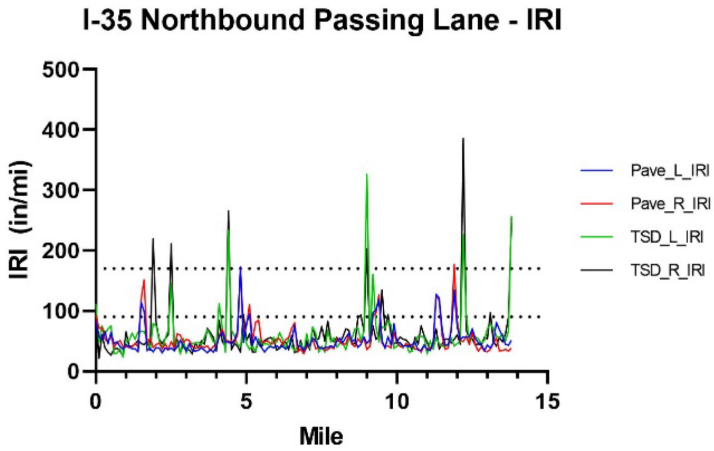


**(a)**

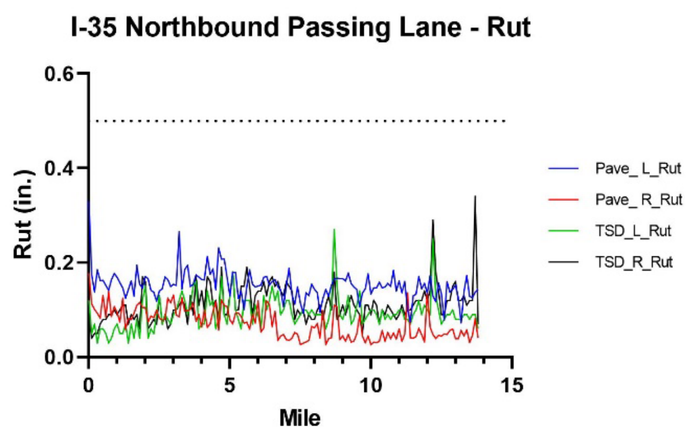


**(b)**

**Figure 2.28 Roughness (a) and Rut (b) Comparison for TSD and Pave 3D 8k on I-35 Northbound Passing Lane**

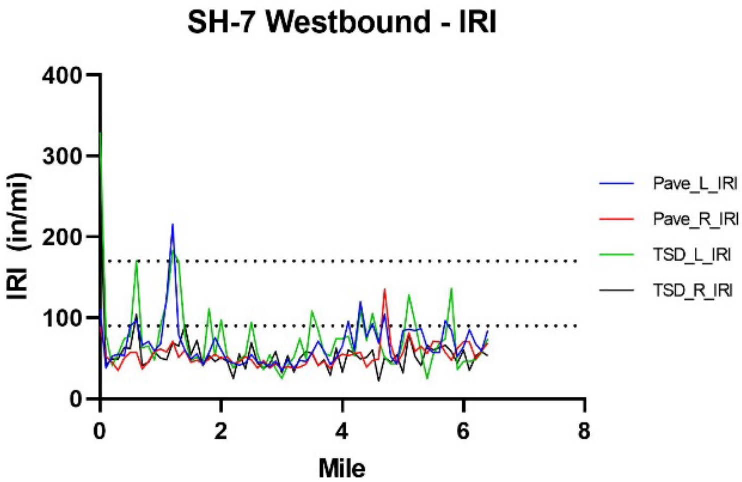


**(a)**

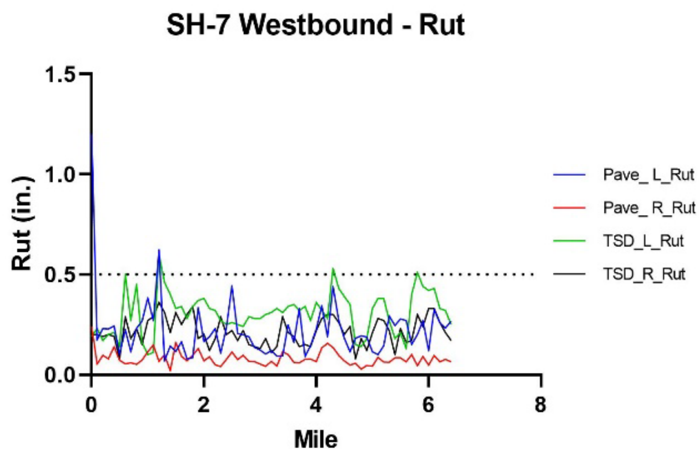


**(b)**

**Figure 2.29 Roughness (a) and Rut (b) Comparison for TSD and Pave 3D 8k on SH-7 Westbound**

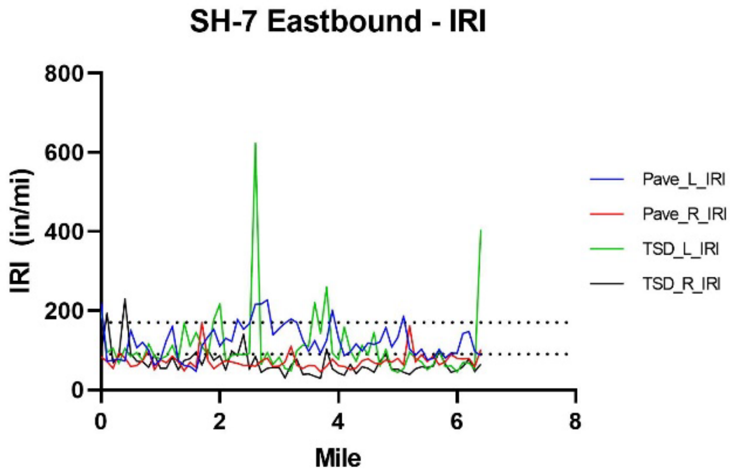


**(a)**

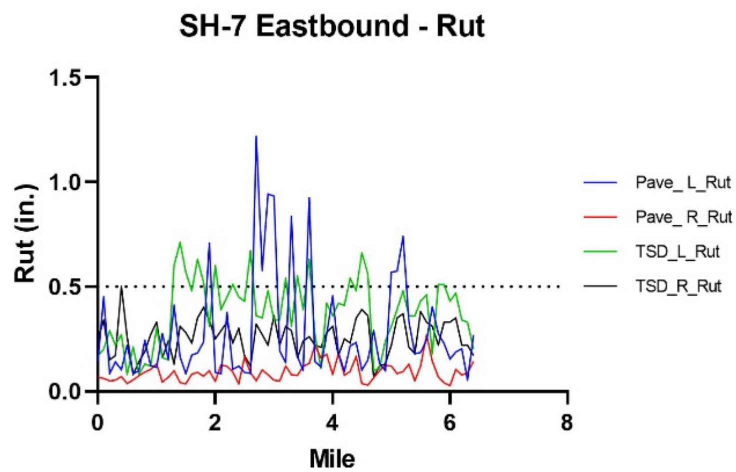


**(b)**

**Figure 2.30 Roughness and Rut Comparison for TSD and Pave 3D 8k on SH-7 Eastbound**

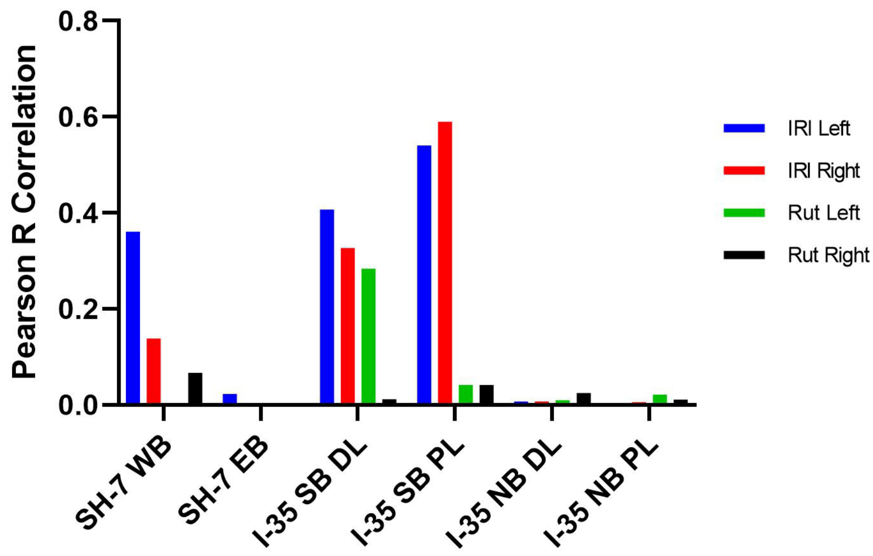


**Figure 2.31 Correlation Between TSD and Pave 3D 8k**

CHAPTER

# 3

# CALIBRATION OF EFFECTIVE STRUCTURAL NUMBER AND TENSILE STRAINS MODELS USING TRAFFIC SPEED DEFLECTOMETER (TSD) DATA FOR ENHANCED PROJECT-LEVEL ASSESSMENT [2]


## ABSTRACT

Pavement deterioration models provide the basis for predicting future changes in network conditions, estimating future funding needs, and determining the effectiveness and timing of maintenance and rehabilitation activities. Determining the accurate structural condition of pavements helps identify effective maintenance strategies which enhance the sustainability and service life of pavements. This study aims to use Traffic Speed Deflectometer (TSD) and Fast Falling Weight Deflectometer (FFWD) for project-level evaluation of pavements and use pavement properties to calibrate current models that help to predict the structural condition of pavements. Model parameters were calibrated to determine effective structural number and tensile strains at bottom of asphalt concrete for asphalt and composite pavements from TSD deflections. A significant improvement in the calibration was observed for asphalt concrete pavements.


[2] This chapter has been submitted to the Sustainability (2023) Special Issue “Advances in Sustainable Asphalt Materials and Pavements.” under the title “Calibration of Effective Structural Number and Tensile Strains Models Using Traffic Speed Deflectometer (TSD) Data for Enhanced Project-Level Assessment.” The current version has been formatted for this dissertation.

## 3.1 INTRODUCTION

Transportation, specifically highway infrastructure, plays a crucial role in the socioeconomic development of a country. Over the last few decades, the United States (U.S.) has invested heavily to develop its highway infrastructure network. As the infrastructure systems are reaching a mature state, the state transportation agencies are changing their focus from constructing new highways to maintaining the existing ones to meet minimum performance requirements required by the Federal Highway Administration (FHWA) for federal funding. In 2017, over $80 billion was spent only to operate, maintain, and rehabilitate the U.S. highway infrastructure (84). However, rapid deterioration of the highway infrastructure and limited resources at transportation agencies have necessitated the need for incorporating technically appropriate maintenance solutions that are economically viable and environmentally sustainable. Therefore, there is a need for a well-equipped Pavement Management System (PMS) to provide decision-makers with the required information to ensure efficient and sustainable management of highways.

Transportation agencies collect pavement health or condition data and populate the PMS to optimize agency resources for pavement maintenance and rehabilitation needs. Generally, PMS uses condition indices or scores of roadway pavements at different levels. The American Association of State Highway and Transportation Officials (AASHTO) defines PMS as “a set of tools or methods that assist decision-makers in finding optimum strategies for providing, evaluating, and maintaining pavements in a serviceable condition over a period of time” (2). The PMS helps with the decision-making for long-term "needs-based" budgeting at the network level to handle the overall state of the network. At project level, PMS covers the most economical methods of maintenance and rehabilitation for each road segment. Several Maintenance, Rehabilitation, and Reconstruction (MRR) strategies have been proposed in different studies for project-level assessment (85–88). Allocating limited resources in the most effective way possible to maximize benefits during the asset life cycle is a crucial component of asset management.

Roadway pavement condition data involves structural condition (e.g., structural number, layer modulus, drainage) as well as surface condition (e.g., roughness, rut, crack, patch) and other factors (e.g., safety, traffic, accidents) to determine the condition or rating of the pavement. The structural condition of pavements plays an important role in the project-level PMS. The structural capacity is an indicator of the remaining service life and the condition of the pavements. Pavement performance can go down significantly, and the resulting maintenance and rehabilitation cost can increase exponentially with time, as shown in Figure 3.1.

Destructive and non-destructive methods are used to assess the condition of pavements at project level. Falling Weight Deflectometer (FWD) or Fast Falling Weight Deflectometer (FFWD) are tools that are commonly used in PMS at project-level. Since the 1980's, FWD has been one of the most widely used devices for pavement condition assessment in the U.S. In this test, deflection basin is measured under an impact load using geophones or force-balance seismometers (89). The size of the plate and impact load depend on the material being tested (asphalt, stabilized subgrade, compacted subgrade, etc.). Generally, an impact load is applied on a circular plate 12 in. (300 mm) in diameter and placed on the surface of the pavement. Deflections at the center of the load as well as 12 in. (300 mm), 24 in. (600 mm), 36 in. (900 mm), 48 in. (1,200 mm), 60 in. (1,500 mm), and 72 in. (1,800 mm) from the center of the plate are collected with a FWD.

Recently, Traffic Speed Deflectometer (TSD) has emerged as a useful tool for measuring surface deflections of pavements at close intervals as well as roughness, texture, and rut at traffic speed. The TSD is an instrumented truck that applies a rear axle load varying from 13 to 28 kips (57 kN to 125 kN) on the pavement and measures deflections. It commonly has seven Doppler laser sensors that are positioned at 0, 8 in. (200 mm), 12 in. (300 mm), 24 in. (600 mm), 36 in. (900 mm), 48 in. (1,500 mm), 60 in. (1,800 mm) and 72 in. (2,100 mm) in front of the loaded axle (i.e., traffic direction) and a single laser located outside the bowl that serves as the reference sensor (15). TSD can operate at different speeds, although 60 mph (96.5 km/h) with a data collection rate of 1 KHz is commonly used (15). The TSD determines the deflection slope from the vertical pavement deflection velocity and the vehicle horizontal velocity for each location of laser sensor. From these data, a deflection basin is defined and used to represent the profile of the deflected pavement. Pavement deflection is obtained from the deflection slope by integration. Figure 3.2 show a pictorial view of the TSD data collection approach. Additional details on TSD can be found elsewhere (5), (90), (91), (15), (92), and (8). As data are collected at traffic speed, no traffic control is needed. TSD is gaining popularity within transportation agencies for pavement condition assessment and management at network level.

The main differences between the FWD and TSD measurements are the nature of loading (impact load in FWD and moving half-axle load in TSD) and measuring sensors (geophones in FWD and Doppler laser in TSD). In addition, multiple drops are used in FWD testing that allows verification of the repeatability, while TSD data are collected at close intervals as the instrumented truck moves at traffic speed. One can argue that some accuracy is lost in TSD due to the averaging process and the approach used in defining pavement deflection basin. No such issues exist with FWD testing. In addition, the tensors for stress and strain rotate during data collection in TSD and it remains constant for FWD. Also, other factors, namely damping, tire pressure, and truck dynamics can influence TSD data (16).

Despite the advantages of using TSD in quantifying both surface and structural conditions of roadway pavements, there are issues pertaining to using deflection data in determining tensile strain at the bottom of Asphalt Concrete (AC) layer and assessing structural capacity or remaining service life of the pavement. The Effective Structural Number ($SN_{eff}$) and the tensile strain at the bottom of the AC are indicators of the remaining service life of the pavement, and the damage induced in the pavement by traffic loading. An accurate estimation of the $SN_{eff}$ and tensile strain at the bottom of the AC can help to characterize the condition of pavements with more certainty and potentially detect deficiencies that can lead to a faster deterioration of the pavement and a higher maintenance cost in future.

To this point, there are several approaches to determine the $SN_{eff}$ and tensile strains at the bottom of the AC from FWD, modeling or other non-destructive methods (6,7,93–96). For example, Rhode proposed a model and estimated necessary values for coefficients to calculate $SN_{eff}$ from FWD deflections and thicknesses of AC (7). Based on Rhode's work, Nasimifar proposed new coefficients to estimate $SN_{eff}$ from TSD deflections (26). Also, AASHTO proposed a method to calculate $SN_{eff}$ from given layer coefficients that are related to the elastic moduli and thicknesses of the pavement layers (2). Rada et al. proposed a model to estimate tensile strains at the bottom of AC for different layer thicknesses from basin indices that can be calculated from TSD deflections (8).

The main objective of this study was to review, compare, analyze, and model the TSD data from Interstate 35 (I-35) and State Highway 7 (SH-7) pavement sections that were collected as a part of a pooled fund study (TPF-5 (385), Pavement Structural Evaluation with Traffic Speed Deflection Devices), conducted by Virginia Tech Transportation Institute (VTTI). TSD data were collected from several miles of pavement on I-35 and SH-7 in Oklahoma. Specifically, a 14.5-mile segment of I-35 pavement that began at the Carter/Murray County line Mile Post 45 (34.376384, -97.144182) and extended north to Mile Post 59.5 (34.559871, -97.193138) was studied. The SH-7 pavement section started 1-mile west of the intersection with I-35 (34.510042, -97.194876) and extended 5 miles west (34.521343, -97.284874) in Garvin County. Also, FWD data were collected on the same sections of I-35 and SH-7.

In this study, TSD and FWD data were analyzed and compared using statistical and traditional regression methods. The KENLAYER software (6) was used to calculate the deflections, strains, and stresses for the asphalt concrete pavements of SH-7 and composite pavements of I-35. The parameters or coefficients of models proposed by Rada et al. (8), AASHTO (2), and Rhode (7) were calibrated by comparing the TSD and FWD data with KENLAYER outputs. As noted above, a sustainable pavement management plan can only be realized from the true understanding of the conditions of the pavements. An understanding of $SN_{eff}$ and tensile strains at the bottom of AC can lead to a better estimation of the remaining service life of the pavements and improved maintenance, repair and rehabilitations decisions.

### 3.2 METHODOLOGIES

In this study, the pavement conditions of a 14.5-mile section of I-35 and a 5-mile section of SH-7 were studied. Figure 3.3 show the satellite view of the studied I-35 and SH-7 sections. Based on previous plans, the I-35 section had several modifications over the years. Two different pavement types were observed in the I-35 sections. The section south of Mile Post 52 consisted of an 8- to 10-inch-thick asphalt layer supported by an 8-inch thick Continuously Reinforced Concrete Pavement (CRCP). The section north of Mile Post 52 had an 8- to 10-inch-thick asphalt layer over a 9-inch-thick Jointed Concrete Pavement (JCP). The SH-7 section consisted of 17 to 21 inches of asphalt with fabric at 1.5 inches below the surface. Layer thicknesses were determined using a Ground Penetration Radar (GPR) and coring.

A TSD with nine Doppler laser sensors was used for collecting pavement condition data with the help of Australian Road Research Board (ARRB) Systems. The vertical pavement deflection velocities and the vehicle horizontal velocities were recorded at 0 in., 8 in. (200 mm), 12 in. (300 mm), 18 in. (450 mm), 24 in. (600 mm), 36 in. (900 mm), 48 in. (1,200 mm), 60 in. (1,500 mm), and 72 in. (1,800 mm) from the center of the wheel load. Deflections were calculated using the Area Under the Curve (AUTC) model by numerically integrating the deflection bowl. It was observed that the deflection readings of several stations on I-35 section were not recorded by TSD.

Minimal deflection reading, laser reading error, and/or high speed of TSD may have been responsible for this issue (90,97).

### 3.2.1 KENLAYER Analysis

A Dynatest FFWD with seven geophone sensors (W1 to W7) was used for the FWD or FFWD test. The FWD tests were conducted at 359 locations or stations on the I-35 and SH-7 pavement sections. Modulus 7.0 (98) software was used to back calculate elastic moduli for pavement layers and subgrade. For the purpose of this study, the strains at the bottom of the asphalt layer were determined using the KENLAYER software (6). The KENLAYER analyzes pavement using an elastic multi-layer system under a circular load applied on the pavement surface. During this analysis, load can be applied to layer systems using single, double, double tandem or double tridem wheels. In this study, two typical sections were adopted, one for I-35 that has 10 inches of asphalt concrete over 10 inches of Portland cement concrete and native subgrade, and the other being the pavement at the SH-7 section with 20 inches of asphalt concrete over native subgrade. The back-calculated elastic moduli from Modulus 7.0 were used in the KENLAYER analysis for each FWD location that matches with the TSD data. Figure 3.4 and Figure 3.5 show the typical layers for both sections. A contact radius of 3.9 in (99 mm.), contact tire pressure of 116 psi (800 kPa) and a dual spacing of 13.5 in. (342 mm.) were used as the load group. These values are standard for TSD loading. Also, deflection responses beneath the center of the wheel and tensile strain at the bottom of the AC layer were calculated. The following Poisson's ratios were used in the analyzes by the KENLAYER software: 0.35 for AC, 0.15 for PCC and 0.45 for native subgrade. A total of 147 analyzes for I-35 and 110 analyzes for SH-7 were conducted using the KENLAYER software. Parameters such as wheel contact radius and pressure, wheel spacing, asphalt elastic moduli for asphalt, concrete and subgrade, and Poisson's ratios were used as input parameters for each specific analysis.

### 3.2.2 Approach of Strains and Effective Structural Number Calibration

In this study, deflection basin-related indices or deflection bowl parameters were used to analyze deflection data from FWD and TSD and calibrate the model parameters. The deflection bowl parameters tend to focus mainly on the deflection under the center of the load (maximum deflection) and differences in deflection among the sensors as an indicator of stiffness of different layers within the pavement structure, including the stiffness of the subgrade, and the remaining life. The most common basin indices are Surface Curvature Index (SCI) (Equation (3.1)) and Deflection Slope Index (DSI) (Equation (3.2)). These indices are closely related to the condition of the upper layers of pavements. The SCI with r = 12 in. (300 mm.) is commonly used for deflection bowl analysis. Typically, s = 4 in. (100 mm.) and r = 12in. (300 mm.) are used to calculate DSI. Several other basin indices have been proposed by several researchers (17). Their applications differ based on the layer that is intended to be analyzed. The Area under the pavement (AUPP) is a deflection basin parameter that has been utilized successfully to link to horizontal strain at the base of the AC layer as well as to assess pavement stiffness (lower AUPP equates to higher stiffness and vice versa)(99).

Surface Curvature Index ($SCI_r$) = $D_0 - D_r$ Equation 3.1

Deflection Slope Index ($DSI_{s\text{-}r}$) = $D_s - D_r$ Equation 3.2

Area Under Pavement Profile (AUPP) = $\frac{(5D_0 - 2D_{12} - 2D_{24} - D_{36})}{2}$ Equation 3.3

where,

$D_s$ and $D_r$ represent deflections ‘’s’’; and

‘’r’’ inches away from the center of the load.

Rada et al. (8) proposed several TSD basin indices and models to calculate tensile strains at the bottom of the AC layer. The most prominent basin index was $DSI_{4-12}$. Equation (3.4) describes the maximum fatigue strain as a function of $DSI_{4-12}$. Coefficients or parameters “a” and “b” from Equation (3.4) were calibrated by comparing strains from KENLAYER analysis and $DSI_{4-12}$ from TSD deflections. A non-linear regression analysis was used to calibrate model coefficients. Coefficients “a” and “b” were calibrated with a 90% confidence level along with outliers’ detection and removal techniques. Table 3.1 show the most significant models based on AC layer thickness.

Maximum Fatigue Strain (microstrain), $\varepsilon = a * {DSI_{4-12}}^{b}$ Equation 3.4

Design of pavement by the AASHTO method uses a structural indicator of pavements, known as “Structural Number (SN)” (previously called “thickness index”). It is used to determine the structural capacity or traffic load carrying capacity of a given pavement structure. In this method, contributions of all layers within the pavement structure are added to obtain the overall capacity of the pavement (17). The SN determines the total number of ESAL a given pavement can support during its service life. Equation (3.5) describes the SN based on the layer coefficients, drainage coefficients, and layer thicknesses.

Structural Number (SN) = $a_1 D_1 + a_2 D_2 m_2 + a_3 D_3 m_3 + \cdots$ Equation 3.5

where,

$a_i$ = $i^{th}$ layer coefficient;

$D_i$ = $i^{th}$ layer thickness; and

$m_i$ = $i^{th}$ layer drainage coefficient

The coefficients for asphalt concrete layer $a_1$ can be determined by Equation (3.6) and Figure 3.6 as provided in the 1993 AASHTO Guide (2).

Layer Coefficient $a_1 = 0.4 * log\left(\frac{E}{435.1}\right) + 0.44$ Equation 3.6

where,

$a_1$ = $1^{st}$ layer coefficient (AC);

Rhode (7) proposed Equation (3.7) to calculate the $SN_{eff}$ from the FWD measurements. For an asphalt pavement, Rhode's proposed 0.4728, -0.4810, and 0.7581 as $k_1$, $k_2$, and $k_3$, respectively. The $k_1$, $k_2$, and $k_3$ values for determining $SN_{eff}$ with the TSD data were proposed by Nasimifar et al. (26) as 0.4369, -0.4768, and 0.8182, respectively.

Effective Structural Number ($SN_{eff}$) = $k_1 SIP^{k_2} Hp^{k_3}$ Equation 3.7

where,

HP = total thickness (mm); and

SIP = structural index of pavement = $D_0$ - $D_{1.5HP}$ .

In the present study, the model parameters proposed by Rhode (7) were calibrated by comparing the TSD data with KENLAYER outputs. To calibrate Rhode's (7) model parameters, $k_1$, $k_2$, and $k_3$, two approaches were used in this study. The first approach involves using a non-linear regression calibration using FWD $SN_{eff}$ (Rhode method) and measured TSD deflections. The second approach used a non-linear regression calibration based on calculated AASHTO $SN_{eff}$ and measured TSD deflections. In this approach, back-calculated moduli's from FWD were used to determine the asphalt layer coefficients using the AASHTO 1993 design charts. Layer coefficient $a_1$ was calculated for each E modulus obtained from the I-35 and SH-7 sections based on the AASHTO 1993 design chart. A layer coefficient "$a_2$" of 0.5 was assumed for the CRCP and JCP layers present in the I-35 section. Equation (3.5) was used to calculate $SN_{eff}$ with an assumed drainage coefficient of 1 for the CRCP and JCP layers. A non-linear regression analysis was used to calibrate parameters $k_1$, $k_2$, and $k_3$, in Equation (3.7) for composite pavement sections on I-35. Coefficients $k_1$, $k_2$, and $k_3$ were calibrated with a 90% confidence level along with outliers' detection and removal techniques.

Also, an attempt was made to compare the elastic moduli obtained from the FWD and TSD data. Modulus 7.0 was used to back calculate surface and subgrade elastic moduli from the FWD deflections. A similar approach was used to back calculate surface and subgrade elastic moduli from the TSD deflections as well. For this purpose, the TSD data were formatted to Modulus 7.0 standards.

## 3.3 RESULTS AND DISCUSSION

### 3.3.1 Traffic Speed Deflectometer Data

As mentioned above, FWD and TSD deflections, roughness and rut data were collected on I-35 and SH-7 sections. Figure 3.7, Figure 3.8, Figure 3.9, and Figure 3.10 show the deflection readings for the I-35 and SH-7 sections. For northbound I-35, mile 0 represents the starting point (Mile Post 45). For southbound I-35, mile 0 represents the ending point (Mile Post 59.5). For westbound SH-7, mile 0 represents the starting point

(1 mile west of I-35). For eastbound SH-7, mile 0 represents the ending point (6 miles west of I-35). Generally, the passing lane had higher deflections compared to the driving lane of I-35 for both southbound and northbound lanes. For the SH-7 section, higher deflections were observed for both directions close to the starting point (1 mile west of I-35). A total of 535 and 543 points were analyzed for southbound driving lane and passing lane of I-35, with a mean maximum deflection ($D_0$) of 1.9 and 2.2 mils, respectively. A total of 509 and 882 points were analyzed for the northbound driving lane and passing lane of I-35, with a mean maximum deflection ($D_0$) of 1.9 and 2.6 mils, respectively. A total of 641 and 647 points were analyzed for the westbound and eastbound lanes of SH-7, respectively (Figures 8 and 9). The mean maximum deflections ($D_0$) of 3.6 and 3.9 mils were observed for the westbound and eastbound lanes of SH-7, respectively. From Figures 3.7 to 3.9, higher deflections were observed in passing lanes on I-35, where no reflection cracking due to JCP and CRCP pavements was observed.

### 3.3.2 Falling Weight Deflectometer Data

Falling Weight Deflectometer or FFWD data were collected on the I-35 and SH-7 sections. Modulus 7.0 was used to back calculate elastic moduli for pavement layers and subgrade. The deflection and elastic moduli values for the northbound and southbound sections of I-35 are shown in Figure 3.11, while the deflection and elastic moduli values for the eastbound and westbound sections of SH-7 are shown in Figure 3.12. For safety reasons, FWD tests were performed only on the right-most lane (next to shoulder) in each direction (i.e., driving lane). The deflection values at the center of the FWD loading plate correspond to the W1 sensor, which is an indicator of the overall structural condition of the pavement at the time of testing. The W7 sensor, on the other hand, indicates deflection at 60 inches (1500 mm) from the center of the load, which is an indicator of the subgrade strength. The air temperature during testing ranged from 32°F to 51°F (0 to 11 °C), as per temperature data collected from the Mesonet site located at Pauls Valley, Oklahoma. For the northbound lane of I-35, FWD tests were conducted at 124 locations. Comparatively, FWD tests at the southbound lane of I-35 were conducted at 123 locations. For the eastbound and westbound lanes of SH-7, FWD tests were conducted at 56 locations in each direction. These measurements and calculations were used in this study to obtain tensile strains at the bottom of asphalt layer, to compare with TSD data, and to calibrate model parameters.

### 3.3.3 KENLAYER Analysis and Comparison with TSD and FWD Data

A total of 147 analyses for I-35 and 110 analyses for SH-7 were done using the KENLAYER software. Each analysis was conducted using a different set of elastic moduli. Figure 3.13, Figure 3.14, Figure 3.15, and Figure 3.16 show the tensile strains at the bottom of AC layer and the deflections at top of the AC layer from the KENLAYER analyses, along with FWD and TSD maximum deflections ($D_0$) for comparison purposes. It can be observed that the KENLAYER and FWD deflections are similar in all directions for both the I-35 and SH-7 sections. This was expected as the elastic moduli input for KENLAYER analyses was based on the FWD data. Better relations were observed between TSD, FWD and KENLAYER deflections for the SH-7 section compared to the I-35 section. Figure 3.17 and Figure 3.18 show the Pearson (r) correlations between the tensile strain at the bottom of AC and TSD and FWD deflections for I-35 and SH-7 sections, respectively. From Figure 16, tensile strain at the bottom of the AC layer from the KENLAYER analyses was found to exhibit a better correlation with the FWD deflections.

Figure 3.18 exhibited relatively higher correlations between deflections obtained from TSD, KENLAYER and FWD for the SH-7 section. Strong correlations were observed (with a r value >0.53 for the I-35 section and >0.84 for the SH-7 section) between the tensile strains at the bottom of the AC layer obtained from the KENLAYER analyses and FWD deflections. Also, for the SH-7 section, tensile strains at the bottom of the AC layer showed better correlations with TSD compared to that of the I-35 section. For the I-35 section, an overall compressive strain at the bottom of the AC layer was observed (Figure 3.13 and Figure 3.14). This is due to the composite nature of the I-35 section which produced a neutral axis below the asphalt layer and resulted in compressive strain at the bottom of the asphalt layer. Tensile strains were observed at the bottom of the asphalt layer for the SH-7 section due to the direct contact with a softer layer or native subgrade.

Figure 3.19 and Figure 3.20 show the $DSI_{4-12}$ values obtained from the TSD data for the I-35 and SH-7 sections, respectively. The depth of the AC layers were 10 inches for the I-35 section and 20 inches for the SH-7 section. Equation (3.4) describes the maximum fatigue strain as a function of $DSI_{4-12.}$

### 3.3.4 Calibration of Tensile Strains Model Coefficients

As noted earlier, when calculating tensile strains at the bottom of the AC layer by the KENLAYER software, several data points on I-35 showed compressive strain instead of tensile strain. This change in behavior generally occurs when the AC elastic moduli values were below 1,700 ksi, as can be observed in Figure 3.21. This is due to the composite nature of the I-35 section mentioned above. This was not observed for the SH-7 section, where a softer native subgrade (assumed semi-infinite) layer was present underneath the AC layer. Only 42 data points showed tensile strains at the bottom of the AC layer on the I-35 section. These 42 data points were used to fit the non-linear Equation (4) proposed by Rada et al. (8) and to calculate the corresponding parameters "a" and "b" The coefficient "a" ranged from -0.9054 to -0.3310, and the coefficient "b" ranged from -0.06168 to 0.5535 with the best fit values being -0.5645 and 0.2297 for coefficients "a" and "b," respectively. Figure 3.22 show a comparison between strain at the bottom of the AC from KENLAYER and the strains calculated from calibrated Rada et al. (8) model. As mentioned above, for the SH-7 section, strains at the bottom of the AC layer were in tension. The corresponding coefficient "a" ranged from -25.9 to -23.22, and coefficient "b" ranged from 0.1657 to 0.3486 with the best fit values being -0.2457 and 0.2566 for coefficients "a" and "b", respectively. Figure 3.23 show a comparison between the tensile strains and the model calculated strains. An r correlation of 0.5 was observed.

### 3.3.5 Calibration of Effective Structural Number Model Coefficients

In this study, an attempt was made to calibrate the parameters of the Equation (3.7) for accurate determination of $SN_{eff}$ from TSD measurements. As shown in Equation (3.7), the model uses a Structural Index of Pavement (SIP) to calculate the $SN_{eff}$ from the deflection measurements. Figure 3.24 and Figure 3.25 show the correlations between $SN_{eff}$ and SIP based on the FWD and TSD and the Rhode (7) and Nasimifar et al.(26) models for the I-35 and SH-7 sections. A poor correlation ($r<0.1$) was observed for $SN_{eff}$ from FWD and TSD data for I-35 as shown in Figure 3.24.

However, a better correlation was observed for SIP from FWD and TSD. A higher r correlation was observed for SH-7 data for SIP and $SN_{eff}$ from FWD and TSD. The r values of 0.54 and 0.52 were observed for $SN_{eff}$ and SIP between FWD and TSD data sets for SH-7.

As noted earlier, to calibrate $k_1$, $k_2$, and $k_3$ in Equation (3.7) for TSD measurements, two approaches were used in this study. The first approach involves using a non-linear regression calibration from FWD $SN_{eff}$ (Rhode method) and measured TSD deflections. The second approach used a non-linear regression calibration based on calculated AASHTO $SN_{eff}$ and measured TSD deflections. In this approach, back-calculated elastic moduli's from FWD were used to determine the asphalt layer coefficients using the AASHTO 1993 design charts. Figure 3.6 showed the $a_1$ layer coefficient based on the asphalt concrete elastic moduli.

***3.3.5.1 Calibration of Effective Structural Number Model based on Rhode's Method***

A non-linear regression analysis was used to calibrate parameters $k_1$, $k_2$, and $k_3$, in Equation (3.7). For this purpose, target $SN_{eff}$ values were calculated by the Rhode equation using the FWD data. The SIP and layer thicknesses from TSD were used to fit the model and to calculate the parameters. The parameters $k_1$, $k_2$, and $k_3$ were modeled with 90% confidence interval along with outliers' detection and removal. For the I-35 section, the calibrated values for the parameters $k_1$, $k_2$, and $k_3$ were found as 0.2796, -0.01121, and 0.6296, respectively. Figure 3.26 show the $SN_{eff}$ values calculated by the Rhode's equation using the FWD data and the $SN_{eff}$ values from TSD data using the calibrated model parameters for the I-35 sections. The overall correlation was observed to be low. For the SH-7 section, the calibrated values for the parameters $k_1$, $k_2$, and $k_3$

were found as 0.3131, -0.1797 and 0.6639, respectively. Figure 3.27 show a comparison of the $SN_{eff}$ values calculated by the Rhode equation using the FWD data and the predicted $SN_{eff}$ values from TSD data using calibrated model parameters for the SH-7 sections. An improved correlation with an R value of 0.55 was observed for the SH-7 section. As described in previous sections, the application of Rada et al. (8) and Rhode (7) equations may be limited for composite pavements.

#### *3.3.5.2 Calibration of Effective Structural Number Model based on AASHTO Method*

Layer coefficients $a_1$ were calculated for each elastic moduli obtained from the I-35 and SH-7 sections based on the AASHTO 1993 design chart shown in Figure 3.6. A layer coefficient "$a_2$" of 0.5 was assumed for the CRCP and JPCP layer present in the I-35 section. Equation (3.5) was used to calculate $SN_{eff}$ with an assumed drainage coefficient of 1 for the CRCP and JCPC layers. Coefficients $k_1$, $k_2$, and $k_3$ were modeled with a 90% confidence interval along with the outliers' detection and removal techniques. For the I-35 section, the parameters $k_1$, $k_2$ and $k_3$ were found to be 0.3122, 0.00247, and 0.6457, respectively. Figure 3.28 show the $SN_{eff}$ values calculated by the AASHTO method and the predicted $SN_{eff}$ values from TSD data using calibrated model parameters for I-35 sections. An overall low correlation was observed. For the SH-7 section, the corresponding values for parameters $k_1$, $k_2$, and $k_3$ were 0.2747, 0.09122, and 0.6470, respectively. Figure 3.29 show the $SN_{eff}$ values calculated by the AASHTO method and the predicted $SN_{eff}$ values using the model parameters for SH-7. Overall, better results were observed for SH-7, with an r correlation higher than 0.4.

### 3.4 CONCLUSIONS

The main objective of the study was to review, compare, analyze, and model the TSD data from I-35 and SH-7 sections that were collected in the State of Oklahoma. Data from TSD was compared with FWD data. In this study, the KENLAYER software was used to model deflections, strains, and stresses for asphalt concrete pavements for SH-7 section, and composite pavements for the I-35 section. Also, GPR data and coring were further analyzed to determine thicknesses. The models for calculating tensile strain at the bottom of the AC layer and $SN_{eff}$ were calibrated for TSD data. The overall findings of this study are listed below:

- The TSD data for the I-35 sections exhibited some limitations because deflection values were not recorded at several locations. Properties of the pavement sections (composite, stiffer), minimal deflection, speed, and/or laser not recording velocities, among other factors, could have played a role in this regard. As a result, several FWD deflections could not be included in the comparison.
- The elastic modulus values for the surface and subgrade layers of I-35 and SH-7 sections were determined using the FWD test data. Overall, good modulus (E) values were observed for the I-35 section but low modulus values were observed for the eastbound inside lane of the SH-7 section. The TSD Data were organized in the format used by Modulus 7.0 and used to back calculate elastic moduli. Attempts were made to correlate FWD deflections with the TSD deflections. Deflections from TSD testing showed better correlations for the SH-7 section when compared with the FWD and KENLAYER deflections.

- Tensile strains at the bottom of asphalt concrete layer obtained from the KENLAYER exhibited different trends for composite pavements, tension in the bottom of AC in composite pavements were not observed in all the studied sections. A stiffer layer beneath the asphalt concrete resulted in compression instead of tensile strains at the bottom of the asphalt concrete layers in several cases. For the I-35 section, this phenomenon occurred when the elastic moduli of the asphalt layers were below 1,700 ksi. For non-composite pavements, tensile strains were observed at the bottom of asphalt concrete layer for all sections, as expected. Parameters or coefficients used for determining tensile strains from the TSD basin parameters (DSI) were calibrated in this study. Better correlations (between the calibrated coefficients and those used in TSD) were observed for the SH-7 section, in general.
- Parameters or coefficient for effective structural number from TSD data were calibrated using FWD data. The Rhode method correlated better than the AASHTO method. Also, better correlations were observed for the SH-7 section, in general.

TSD is gaining popularity in pavement management at network level. From the results presented in this paper it is evident that its application for project level is promising. The structural capacity of roads can be assessed at a much faster rate and with wider coverage. This can help the decision making of PMS for MRR's applications. Hence, the remaining service life of pavement could be extended. Also, TSD can be used at traffic speeds and with minimal operational requirements and safety procedures.

The application of TSD at network and project level is very promising and can lead to understanding and assessing pavements faster and with less use of resources. The daily cost of operating the TSD is higher than testing with the FWD based on the original expenditure. However, the costs per mile for TSD are significantly lower than those for FWDs, based on the daily productivity of the two devices, the cost per mile is significantly lower for TSD compared to FWD. The fact that the TSD does not give the same quantitative results as the FWD does not mean either device is not accurate.

**Table 3.1 TSD index $DSI_{4\text{-}12}$ and Maximum Fatigue or Tensile Strain (8)**

| AC Layer Thickness (in.) | Maximum Fatigue Strain (microstrain) | $R^2$ |
| --- | --- | --- |
| 3 – 6 (thin AC) | $69.1 * DSI_{4\text{-}12}^{0.9348}$ | 0.88 |
| 6-16 (thick AC) | $76.22 * DSI_{4\text{-}12}^{0.8924}$ | 0.97 |
| Unknown | $76.24 * DSI_{4\text{-}12}^{0.8969}$ | 0.97 |

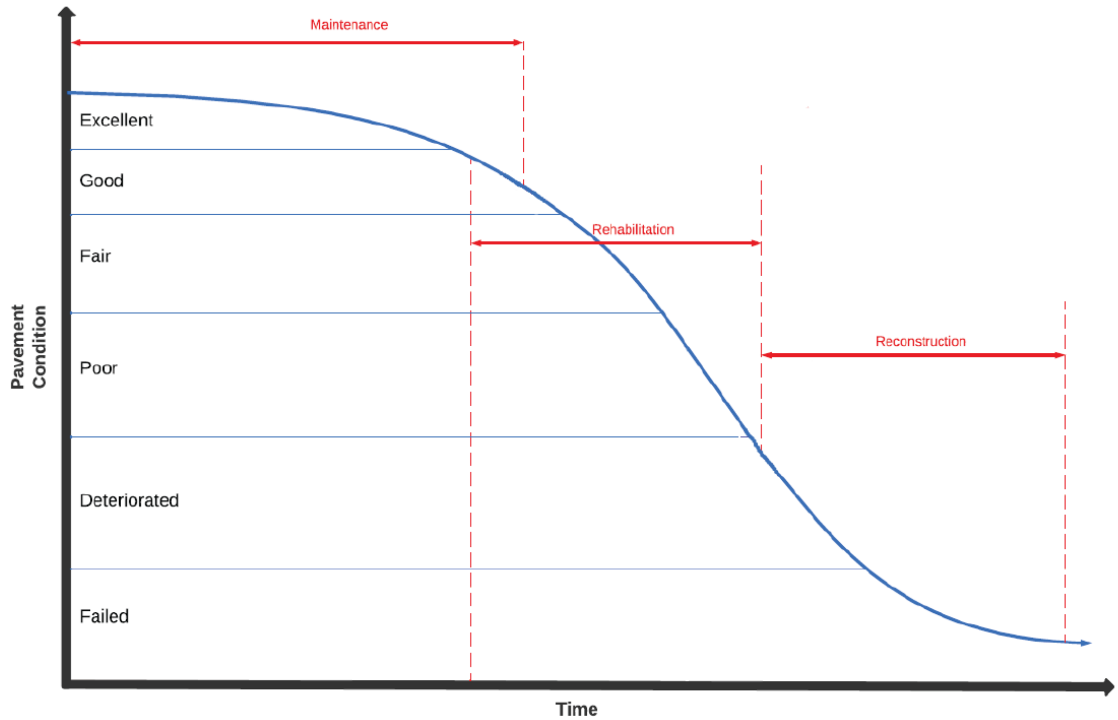


**Figure 3.1 Condition of Pavement Over Time**

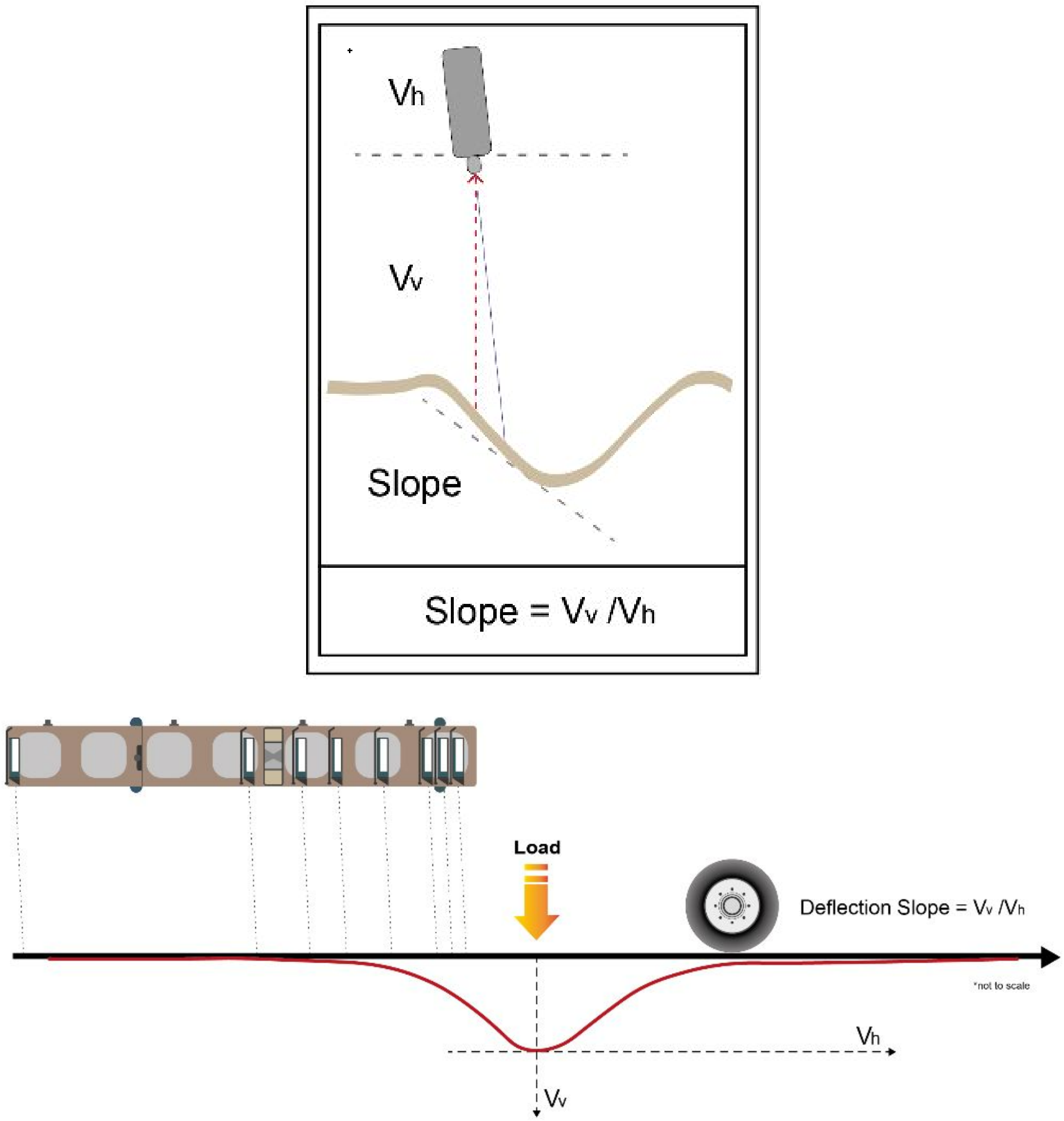


**Figure 3.2 Deflection Slope from Traffic Speed Deflectometer (15)**

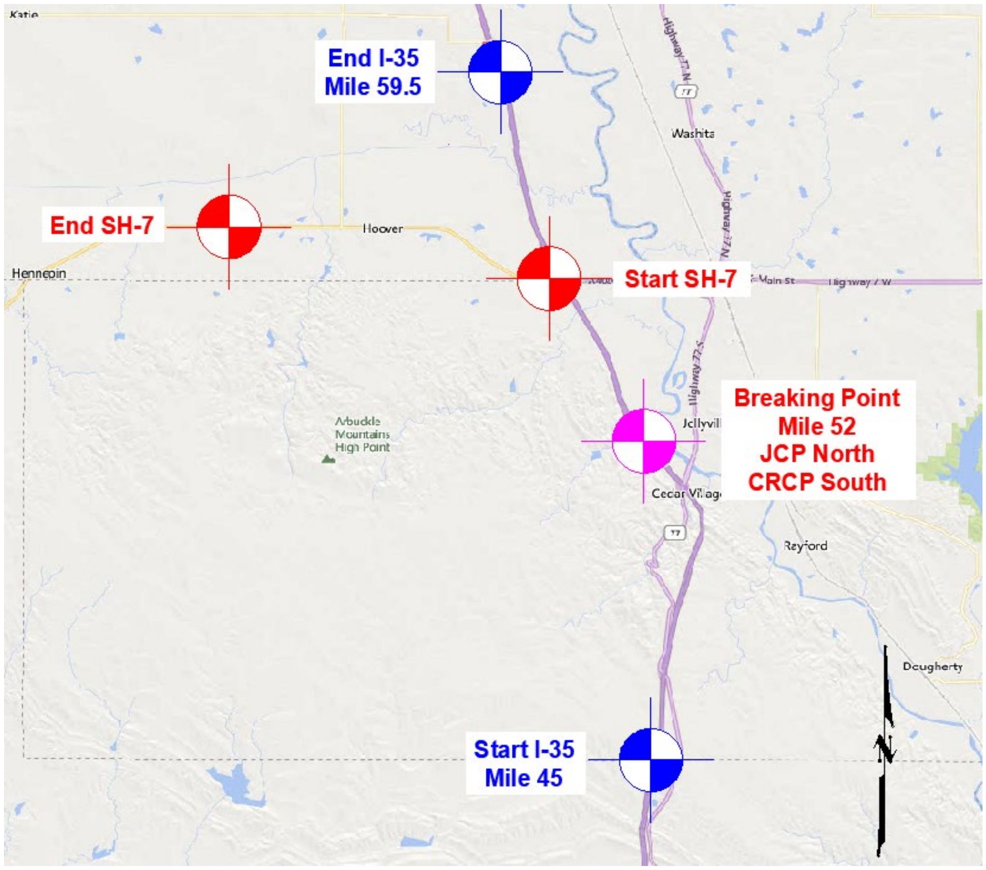


**Figure 3.3 Satellite View of State Highway 7 and Interstate 35 Sections**

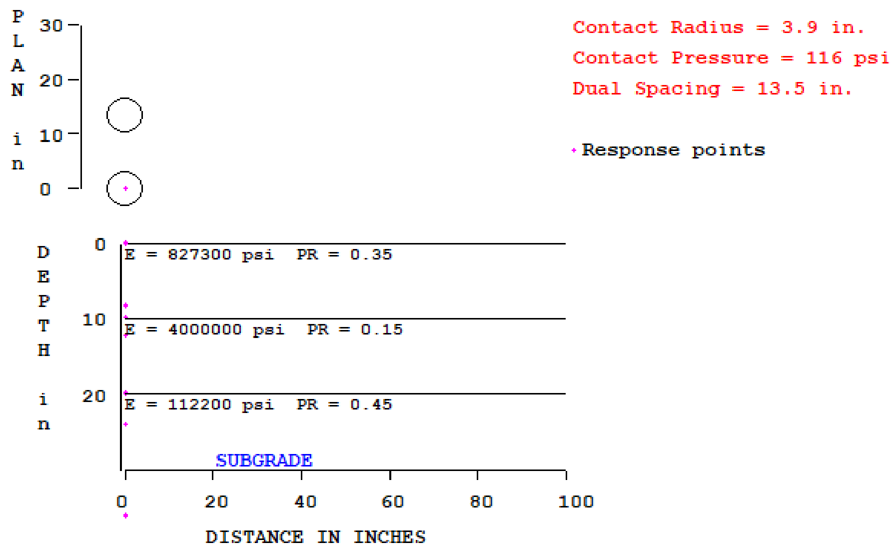


**Figure 3.4 Typical Section of I-35 used in KENLAYER Analysis**

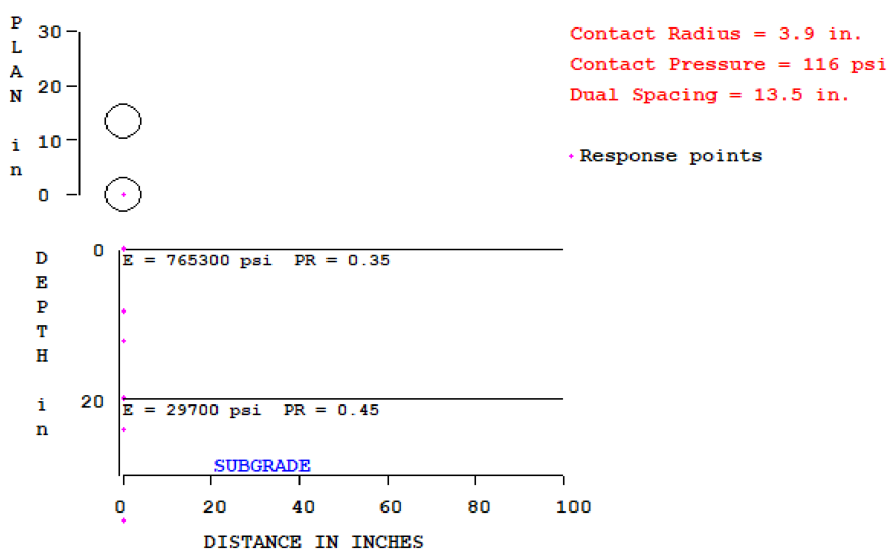


**Figure 3.5 Typical Section of SH-7 used in KENLAYER Analysis**

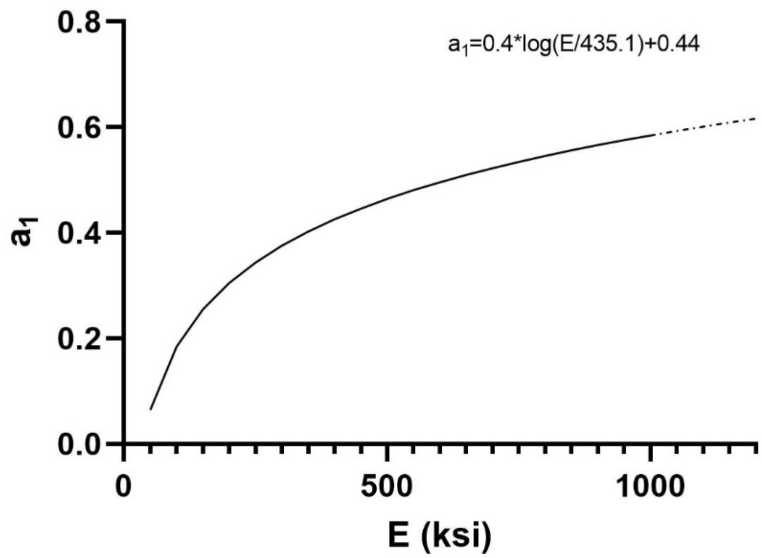


**Figure 3.6 Relationship of Layer Coefficient $a_1$ and Elastic Moduli of AC (2)**

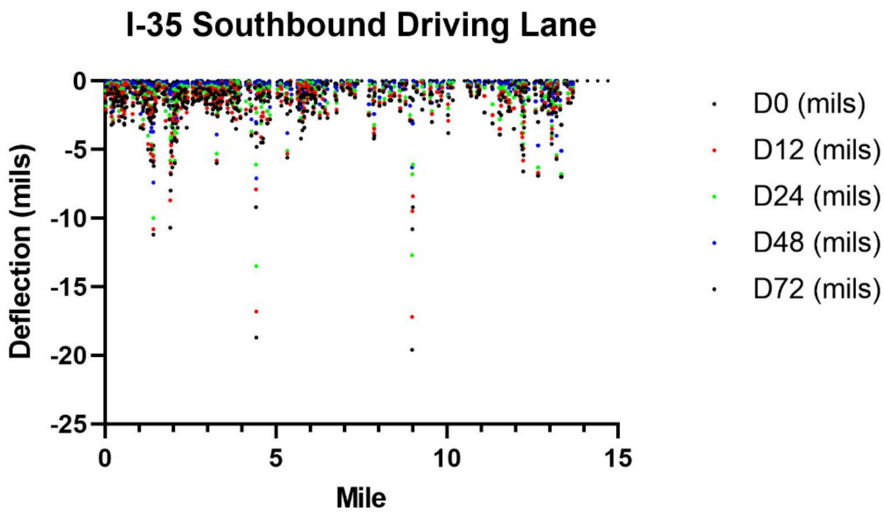


(a)

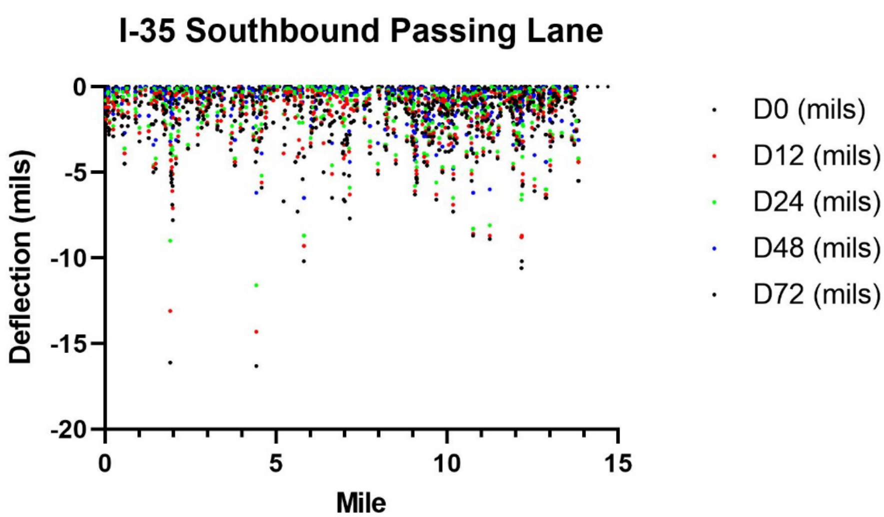


(b)

**Figure 3.7 TSD Deflections on the (a) Driving and (b) Passing Lanes of Southbound I-35**

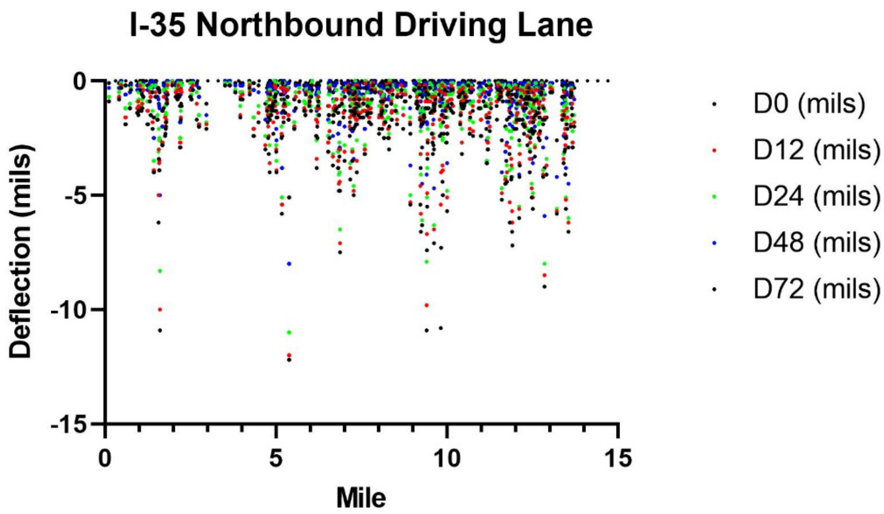


(a)

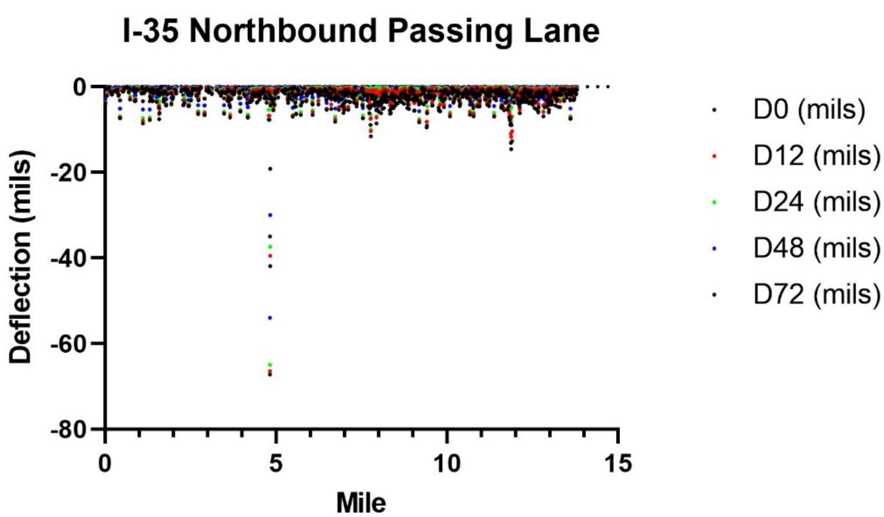


(b)

**Figure 3.8 TSD Deflections on the (a) Driving and (b) Passing Lanes of Northbound I-35**

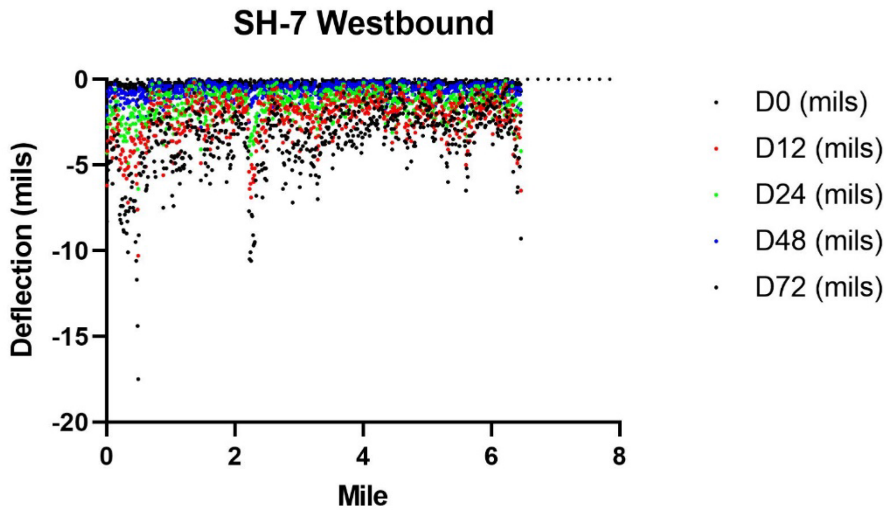


**Figure 3.9 TSD Deflections on Westbound SH-7**

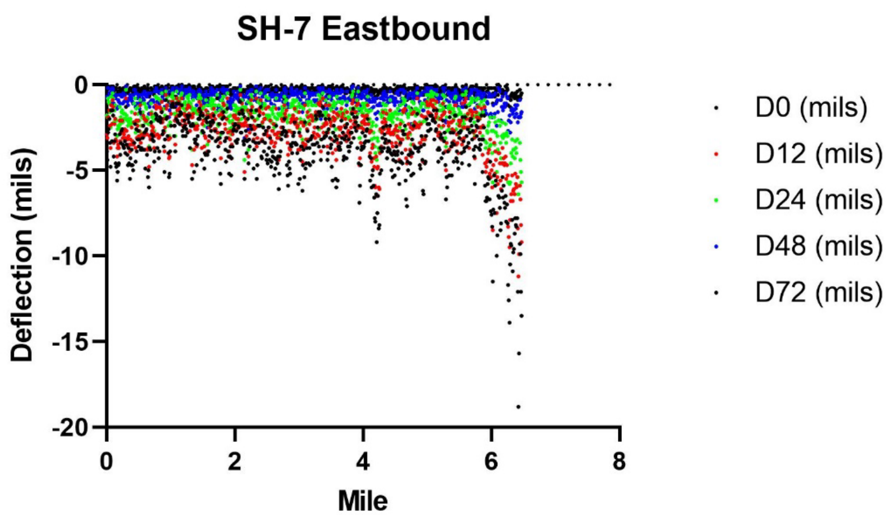


**Figure 3.10 TSD Deflections on Eastbound SH-7**

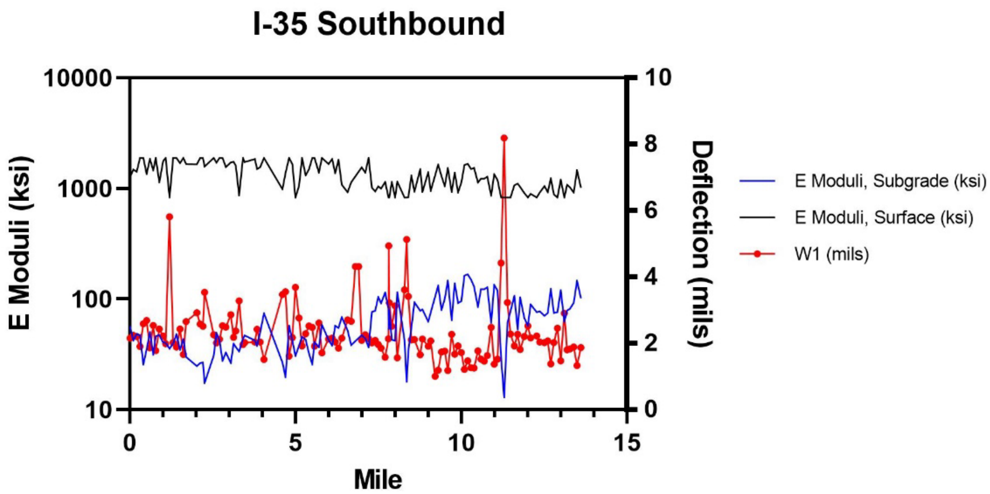


(a)

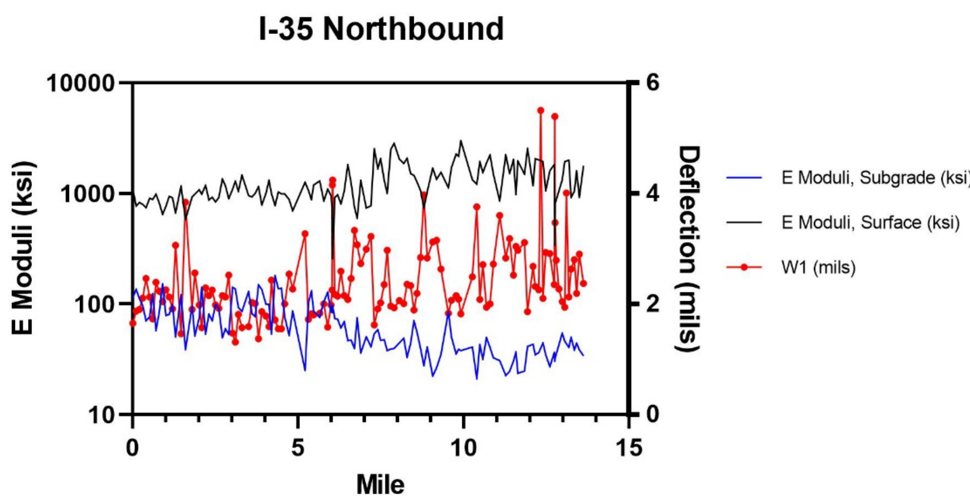


(b)

**Figure 3.11 FWD Elastic Moduli and Deflections for (a) Southbound and (b) Northbound Lanes of I-35**

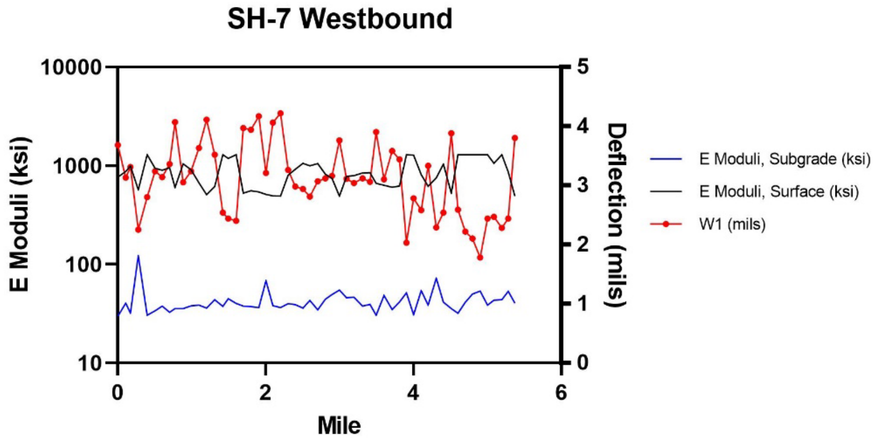


**(a)**

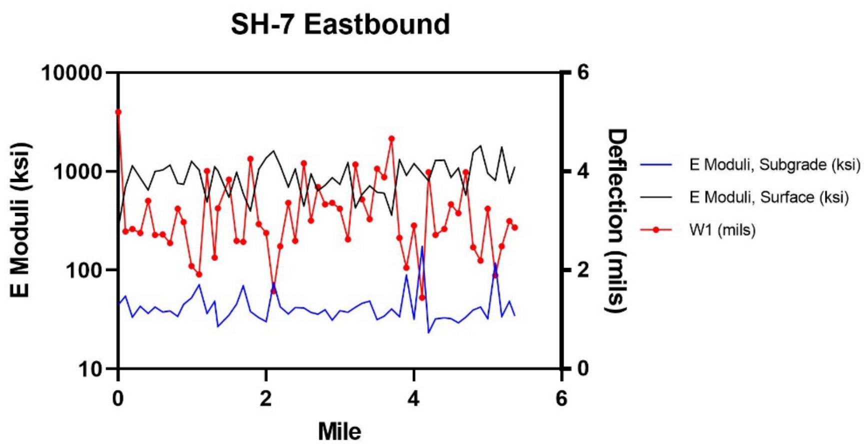


**(b)**

**Figure 3.12 FWD Elastic Moduli and Deflections for (a) Westbound and (b) Eastbound Lanes of SH-7**

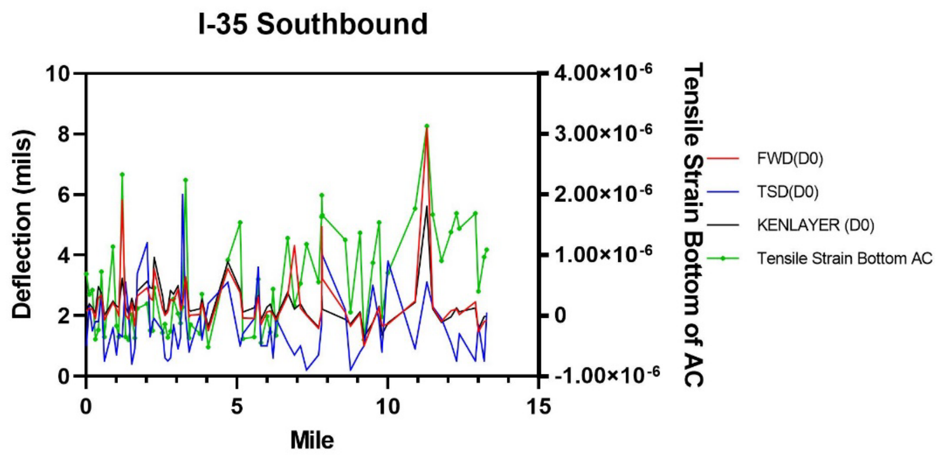


**Figure 3.13 Comparison of deflections and strains obtained from different methods for the southbound lanes of I-35**

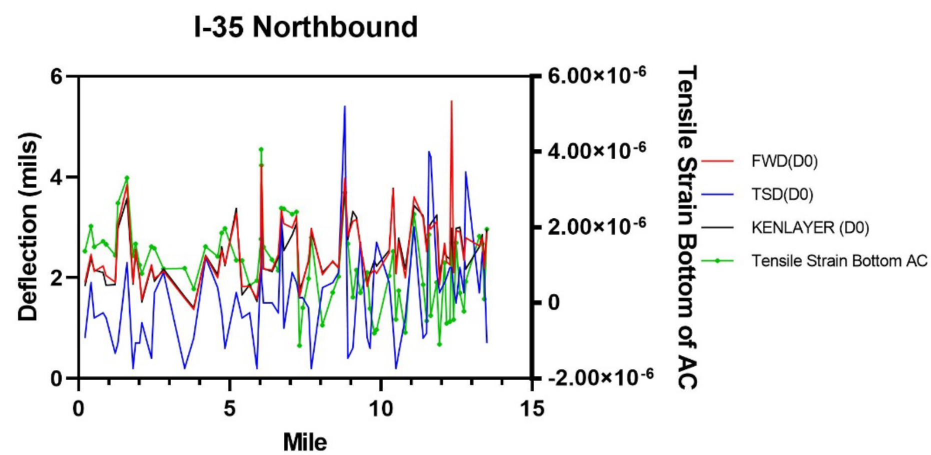


**Figure 3.14 Comparison of Deflections and Strains Obtained from Different Methods for the Northbound Lanes of I-35**

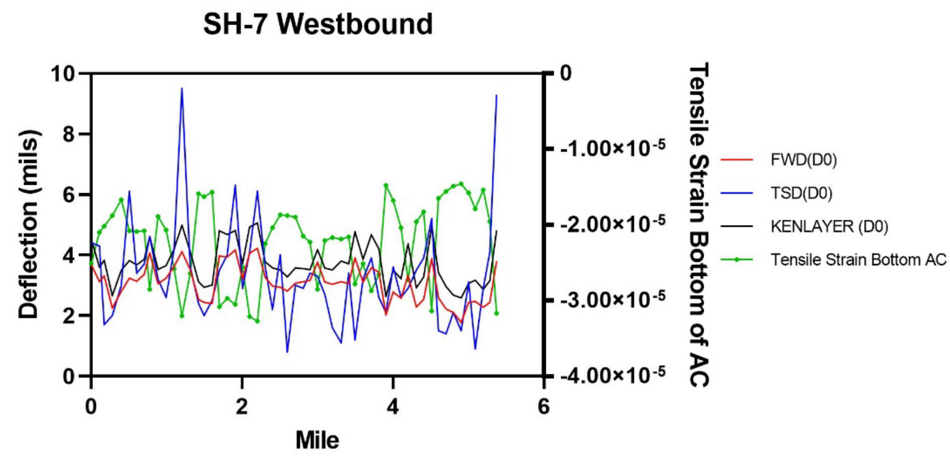


**Figure 3.15 Comparison of Deflections and Strains Obtained from Different Methods for the Westbound Lanes of SH-7**

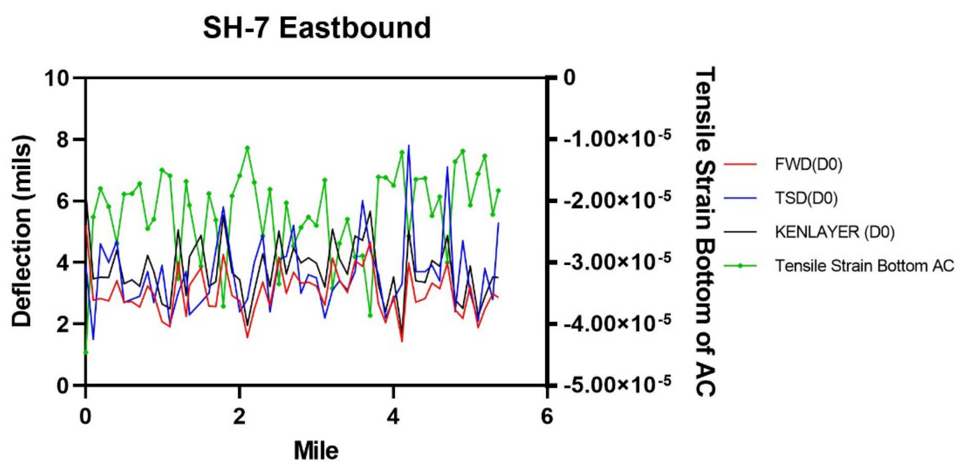


**Figure 3.16 Comparison of Deflections and Strains Obtained from Different Methods for the Eastbound Lanes of SH-7**

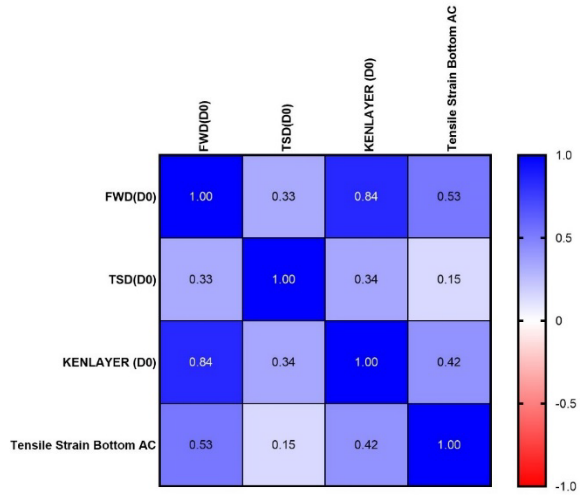


**Figure 3.17 Pearson (r) Correlation Matrix for Deflections and Tensile Strains for the I-35 Section**

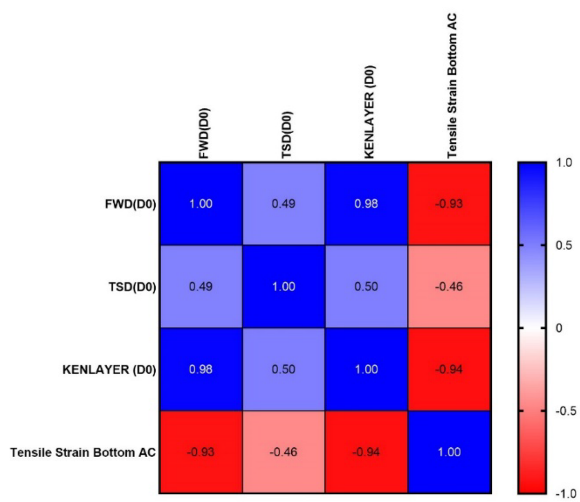


**Figure 3.18 Pearson (r) Correlation Matrix for Deflections and Tensile Strains for the SH-7 Section**

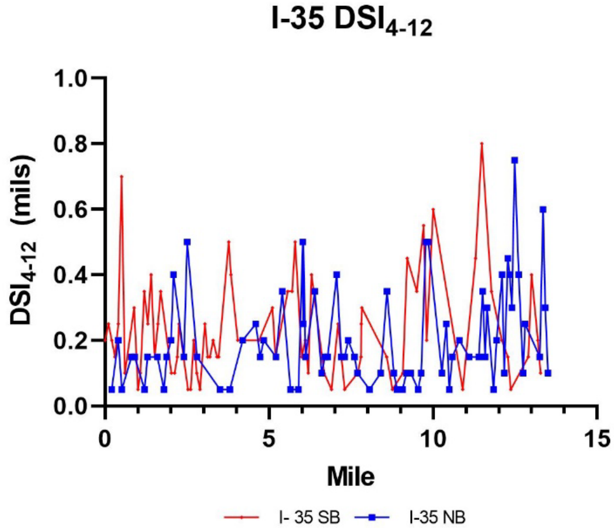


**Figure 3.19 Deflection Slope Index (DSI) Obtained from the TSD Data for the I-35 Section**

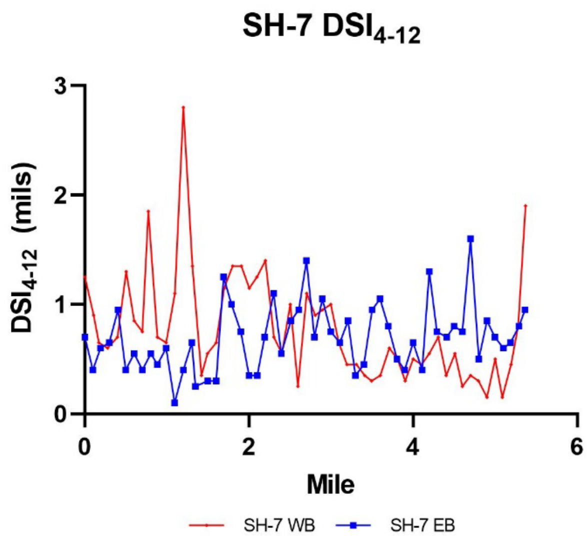


**Figure 3.20 Deflection Slope Index (DSI) Obtained from the TSD data for the SH-7 Section**

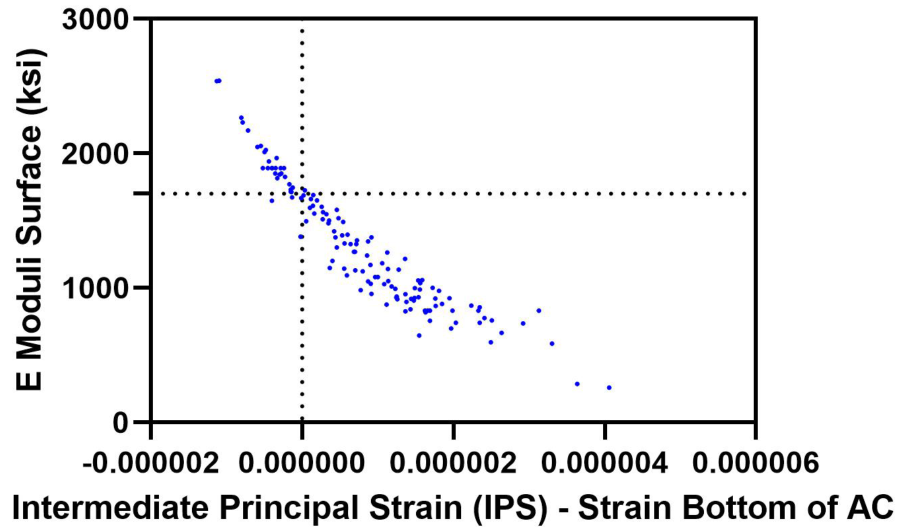


**Figure 3.21 Tensile Strains and Surface E Moduli for the I-35 Section**

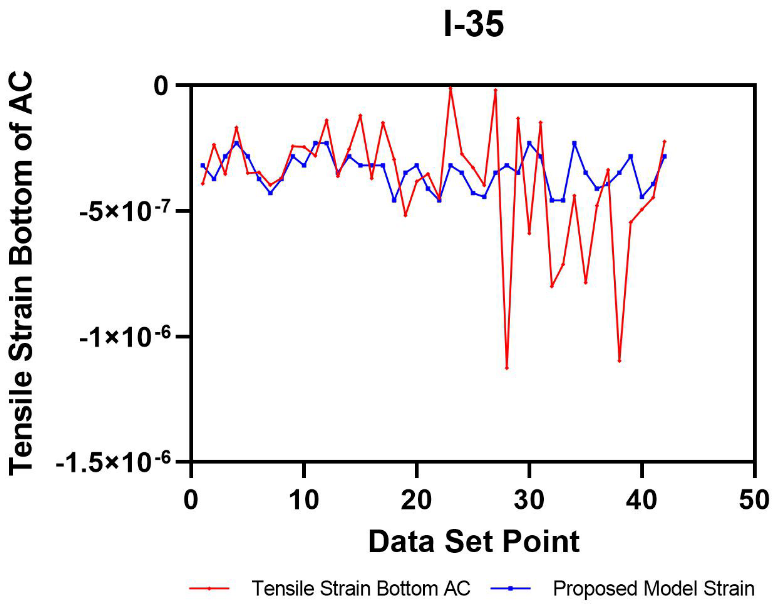


**Figure 3.22 Comparison of Tensile Strains from KENLAYER and Calibrated Rada et al. (8) Model for the I-35 Section**

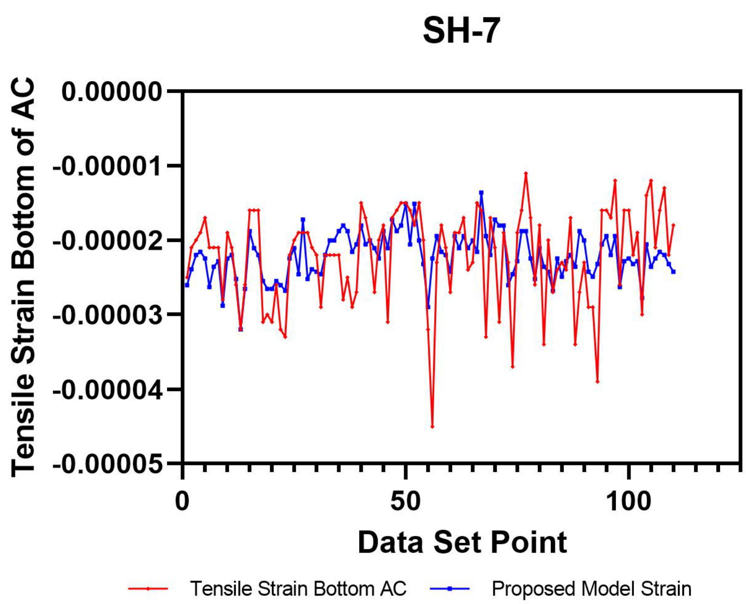


**Figure 3.23 Comparison of Tensile Strains from KENLAYER and Calibrated Rada et al. (8) Model for the SH-7 Section**

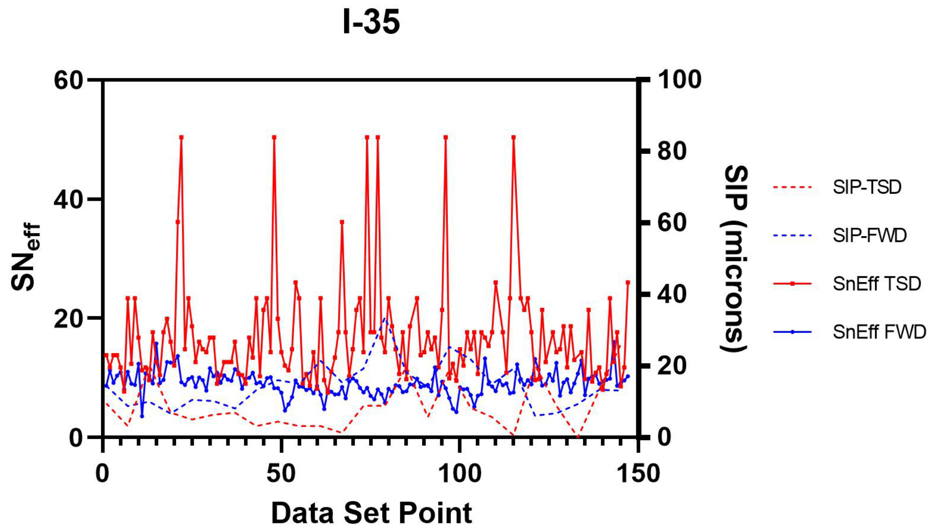


**Figure 3.24 Comparison of $SN_{eff}$ and SIP for the I-35 Section**

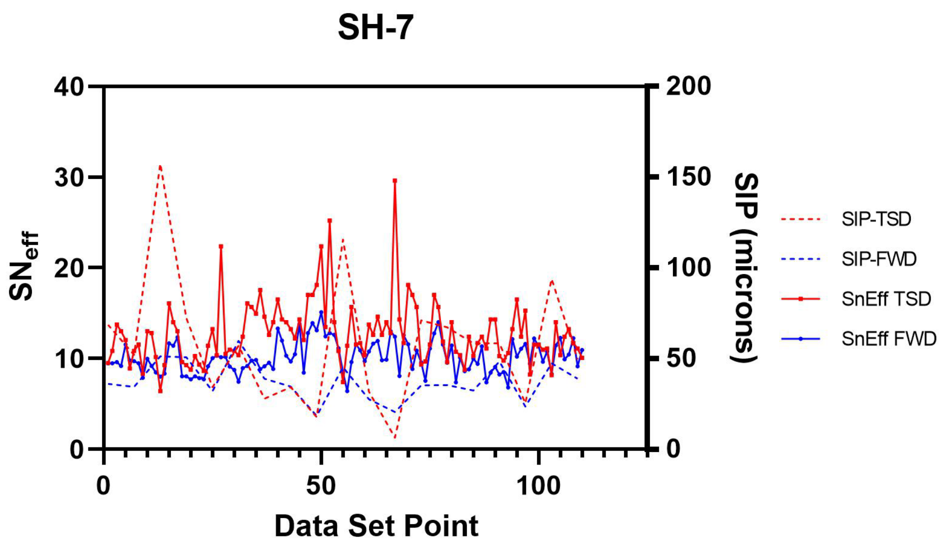


**Figure 3.25 Comparison of $SN_{eff}$ and SIP for the SH-7 Section**

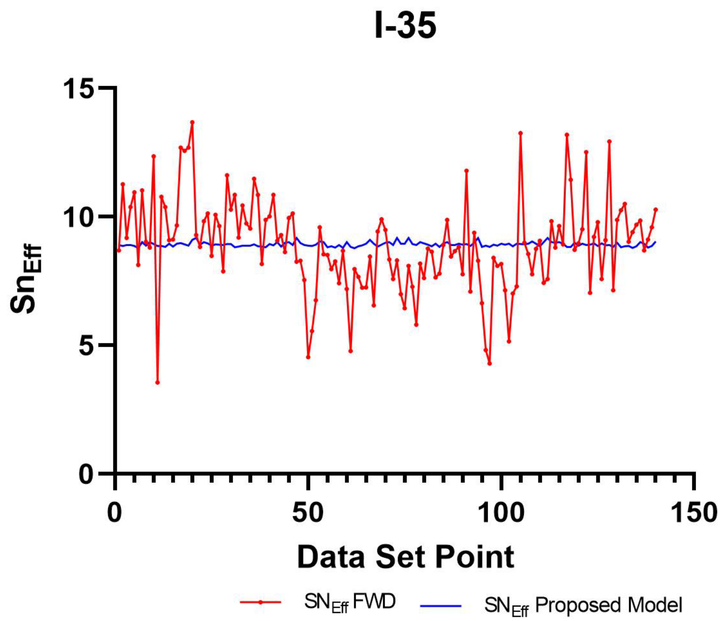


**Figure 3.26 Comparison of $SN_{eff}$ Values for the I-35 Section Predicted Using the Rhode Equation, FWD data, and Calibrated Model**

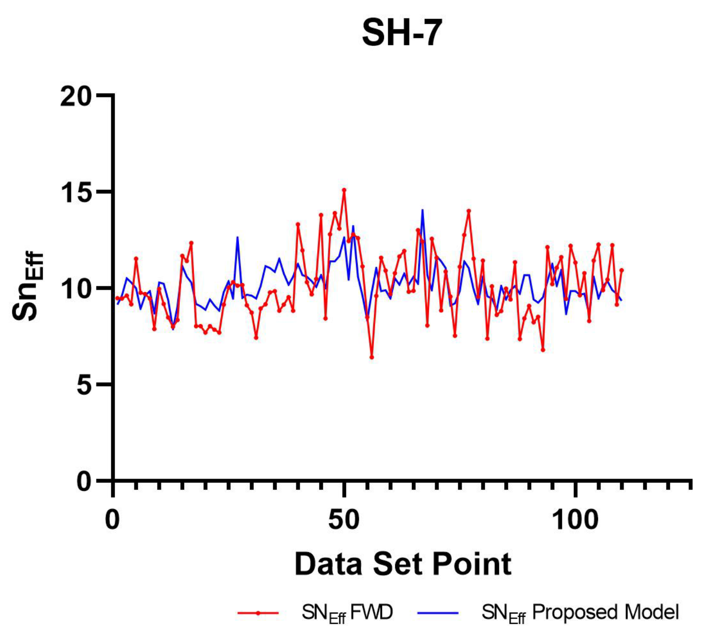


**Figure 3.27 Comparison of $SN_{eff}$ Values for the SH-7 Section Predicted Using the Rhode Equation, FWD Data, and Calibrated Model**

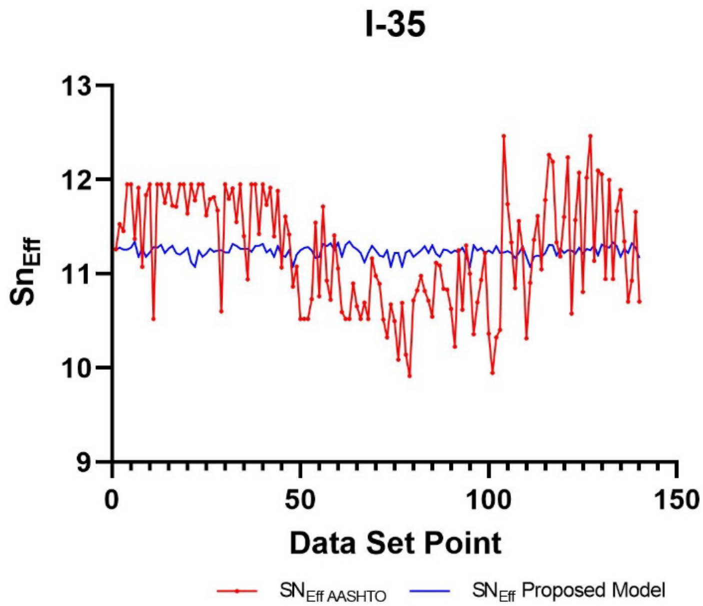


**Figure 3.28 Comparison of $SN_{eff}$ Obtained from the AASHTO Method and the TSD Data Using Calibrated Model for I-35**

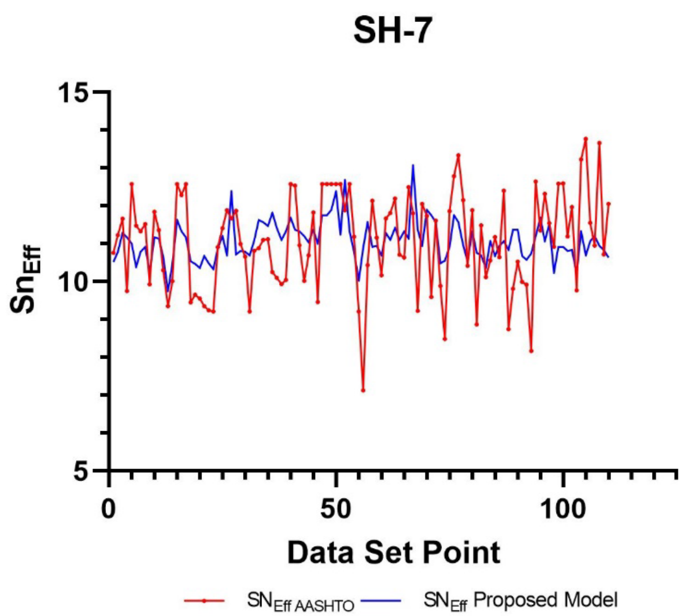


**Figure 3.29 Comparison of $SN_{eff}$ Obtained from the AASHTO Method and the TSD Data Using Calibrated Model for SH-7**

CHAPTER

# 4

# PREDICTION OF ELASTIC MODULI AND DEFLECTIONS FROM TRAFFIC SPEED DEFLECTOMETER (TSD) USING LINEAR REGRESSIONS AND RANDOM FOREST MODELS [3]

## ABSTRACT

Transportation agencies collect roadway structural and functional condition data to optimize their resources for pavement maintenance, repairs, and rehabilitations. Several tools and techniques are currently available for these evaluations. However, concerns over slow rate of data collection, possibility of traffic congestion and safety hazards for the road users have limited their use. In this study, pavement condition data collected using a relatively new tool, known as Traffic Speed Deflectometer (TSD), were compared with a commonly used tool, namely Falling Weight Deflectometer (FWD) or Fast Falling Weight Deflectometer (FFWD) data. Pavement condition data were collected from two selected sections, namely I-35 and SH-7 sections, in Oklahoma. Artificial Intelligence (AI)-based models, namely Random Forest (RF) and common Linear Regression (LR) models were developed and used to predict the back-calculated elastic moduli of different layers within the pavement structure. Also, the effectiveness of these models to predict back-calculated elastic moduli was investigated. Similarly,

[3] This chapter has been submitted to the International Journal of Pavement Engineering under the title "Prediction of Elastic Moduli and Deflections from Traffic Speed Deflectometer using Linear Regressions and Random Forest Models." The current version has been formatted for this dissertation.

RF- and LR-based models were developed and used to predict FWD deflections from the TSD data for deflections and basins. Temperature correction was addressed in using these models for comparison because of its influence on FWD deflections. Relative strengths of the RF and LR-based models were compared using Coefficient of Determination ($R^2$), Mean Absolute Error (MAE) and Root Mean Square Errors (RMSE) for any associated combinations of the studied parameters or variables. The random forest models showed very promising results for the training and testing sets compared to the LR models. Also, the predicted rut and roughness values from these models were compared and their influence on the models investigated.

**4.1 INTRODUCTION**

Transportation agencies invest billions of dollars in road infrastructure and its maintenance. Pavement management systems (PMS) assists with the effective and efficient management of the various activities involved in providing and maintaining pavements in an acceptable condition for the traveling public at the lowest possible cost (100). Typically, two levels are considered in a PMS, namely network-level and project-level. Activities at the network-level determine the best strategies for allocating pavement rehabilitation and maintenance funds across the entire network. For a project level PMS, activities are targeted toward the best strategies for the construction or rehabilitation of a particular roadway section. The pavement condition assessment plays an important role in classifying pavements based on their condition. Pavement roughness, rutting, faulting, and cracking are the common distresses used to evaluate the condition of the pavement at the network-level. Currently, the state Departments of Transportation (DOTs) rely on mapping cracks and distresses, deflection measurements from Falling Weight Deflectometer (FWD) and/or Fast Falling Weight Deflectometer (FFWD) testing, transfer of load at joints, characterization of soil, and in-situ testing to assess pavement condition at the project-level. Typically, the structural condition and capacity data are used at the project-level. However, some agencies are seeing benefits of including these indicators at the network-level (3).

Traffic Speed Deflectometer (TSD) can collect both surface and structural data at traffic speed pertaining to pavement conditions. Lately, this device is gaining popularity for pavement management at the network-level (15,101,102). Its capability to collect data faster, without traffic control and with less personnel in the field makes it attractive to DOTs However, there is a need to closely review the data obtained from the TSD and develop predicting tools or models to estimate elastic modulus of pavement layers – an important indicator of structural capacity of the pavement. In the present study, a broader set of TSD data were considered including deflections, basin parameters, rutting, roughness, and temperature to develop prediction models for elastic modulus and deflections and to compare them with FWD or FFWD data.

For the purpose of this study, data were collected from a state highway and an interstate pavement in Oklahoma. Specifically, a 14.5-mile section of Interstate 35 (I-35) and a 5-mile section of State Highway 7 (SH-7) were studied. The TSD data were collected by the Oklahoma Department of Transportation (ODOT) at these sections as part of a pooled fund study led by the Virginia Tech Transportation Institute (VTTI). The FWD data were collected as part of an ODOT Task Order to investigate sub-surface issues associated with the I-35 and SH-7 sections.

In addition, asphalt cores were extracted and used to determine the thicknesses and properties of materials of the studied sections. Deflection data and basin indices obtained from the FWD and TSD tests were compared, correlated and used to develop models to predict surface elastic moduli and deflections. Artificial Intelligence (AI)-based models, namely Random Forest (RF) model and Linear Regressions (LR) model, were used and compared to examine the effectiveness of the prediction models.

**4.2 BACKGROUND**

Since the 1980’s, FWD has been one of the most widely used devices for pavement condition assessment in the United States. In this test, deflection basin is measured under an impact load using geophones or force-balance seismometers. The size of the plate and impact load depend on the material being tested (asphalt, stabilized subgrade, compacted subgrade, etc.). Generally, an impact load is applied on a circular plate 12 in. (300 mm) in diameter and placed on the surface of the pavement. The load is normalized to 9 kips (40 kN), which is equal to half of equivalent single axle load (ESAL). Generally, transportation agencies rely on the deflection at the center of the plate to reflect the overall structural capacity of the pavement. Commonly, deflections under the center of the load ($D_0$) are considered the maximum deflection. Additionally, FWD or FFWD collects deflections at 12 in. (300mm), 24 in. (600mm), 36 in. (900mm), 48 in. (1200mm), 60 in. (1500mm), and 72 in. (1800mm) from the center of the plate. Transportation agencies generally use these deflections and pavement thicknesses to determine modulus of different layers, including subgrade soil, as an indicator of stiffness of the pavement structure. Figure 4.1 show the stress distribution and measured deflection bowl beneath the FWD plate.

The TSD is an instrumented truck that applies a rear axle load varying from 13 to 28 kips (58 kN to 125 kN). It commonly has seven Doppler laser sensors that are positioned at 0 in., 8 in. (200 mm), 12 in. (300 mm), 24 in. (600 mm), 36 in. (900 mm), 48 in. (1,200 mm), 60 in. (1,500 mm), and 72 in. (1,800 mm) in front of the loaded axle (i.e., traffic direction) and a single laser located outside the bowl that serves as the reference sensor (15). The TSD calculates the deflection slope based on the vertical pavement deflection velocity and the vehicle horizontal velocity of each laser sensor location. A deflection basin is defined from these data and used to represent the profile of the deflected pavement. Integrating the deflection slope generates the pavement deflection. The primary differences between the FWD and TSD measurements are the nature of the loading (impact load in FWD and moving half-axle load in TSD) and the measuring sensors (geophones for FWD and laser for TSD). Other factors that can also influence TSD data include frequency, load magnitude, damping, tire pressure, and truck dynamics (16). Previous studies have reported significant correlations between the FWD and TSD data for maximum deflection, surface curvature index (SCI), deflection slope index (DSI), and others (63,103–108). Also, TSD loading mechanism better represents the actual traffic loading a pavement is subjected to, analyzed for and/or designed for.

Over time, several studies have proposed deflection basin-related indices or deflection bowl parameters to analyze deflection data from deflectometers. These parameters tend to focus mainly on the deflection under the center of the load (maximum deflection) and differences in deflection among and between the sensors as an indicator of stiffness of different layers within the pavement structure, including the stiffness of the subgrade, and the remaining life. A summary of the most influential parameters, formulas, and structural indicators from measured deflections is provided in Equation 4.1 through 4.17.

Radius of Curvature (RoC) = $L^2/(2D_0[\left(\frac{D_0}{D_{200}}\right) - 1]$ Equation 4.1

where,

L=127 mm in the Dehlen curvature meter and 200 mm for the FWD

Base Layer Index (BLI) or Surface Curvature Index (SCI) = $D_0 - D_{300}$

Equation 4.2

Middle Layer Index (MLI) or Base Damage Index (BDI) = $D_{300} - D_{600}$

Equation 4.3

Lower Layer Index (LLI) or Base Curvature Index (BCI) = $D_{600} - D_{900}$

Equation 4.4

Spreadabilty (S) = $\frac{\left[\frac{D_0+D_{300}+D_{600}+D_{900}}{5}\right]100}{D_0}$ Equation 4.5

Area (A) = $\frac{6[D_0+2D_{300}+2D_{600}+D_{900}]}{D_0}$ Equation 4.6

Shape Factor F1 = $(D_0 - D_{600})/D_{300}$ Equation 4.7

Shape Factor F2 = $(D_{300} - D_{900})/D_{600}$ Equation 4.8

Shape Factor F3 = $= (D_{600} - D_{1200})/D_{900}$ Equation 4.9

Slope Deflection (SD) = $\tan^{-1}(D_0 - D_{600})/600$ Equation 4.10

Area Under Pavement Profile (AUPP) = $\frac{(5D_0-2D_{300}-2D_{600}-D_{900}}{2}$

Equation 4.11

Additional Area (A2) = $\frac{6(D_{300}+2D_{450}+D_{600})}{D_0}$ Equation 4.12

Additional Area (A3) = $\frac{6(D_{600}+2D_{900}+D_{1200})}{D_0}$ Equation 4.13

Area Index 1 (AI1) = $(D_0 + D_{300})/2D_0$ Equation 4.14

Area Index 2 (AI2) = $(D_{300} + D_{600})/2D_0$ Equation 4.15

Area Index 3 (AI3) = $(D_{600} + D_{900})/2D_0$ Equation 4.16

Area Index (AI4) = $(D_{900} + D_{1200})/2D_0$ Equation 4.17

The above-mentioned indices are indicators of the structural condition of the upper, middle, and lower layers (17). The DSI and SCI are used by the Virginia Department of Transportation to determine the pavement condition. The DSI is defined as the difference in deflections at 4 in. (100 mm) ($D_4$) and 12 in (300 mm) ($D_{12}$) from the center of the load, whereas SCI represents the difference in deflection between at 0 mm ($D_0$) and (15). Additional deflection parameters (see Equations (4.18) through (4.22) below) were proposed by Rada et al. (8) and are being used by the Federal Highway Administration (FHWA) for pavement condition assessment.

$R1r = \frac{r^2}{2Do\left(1-\frac{Dr}{Do}\right)}$ Equation 4.18

$R2r = \frac{r^2}{2Do(\frac{Do}{Dr}-1)}$ Equation 4.19

$SCI_r = D_0 - D_r$ Equation 4.20

$DSI_{s-r} = D_s - D_r$ Equation 4.21

$SD_r = \frac{\tan^{-1}(D_0-D_r)}{r}$ Equation 4.22

where,

r, s = distance from applied load in inches or mm. (s > r);

$D_x$ = deflection at distance x from the load; and

D = differential operator.

Another parameter known as the tensile strain at the bottom of the Asphalt Concrete (AC) layer is used as an indicator of the damage and remaining service life of the pavement. Based on the review of previous studies, $R1_{12}$, $R2_{18}$, $SCI_{12}$, $SD_{12}$, and TS (which is the ratio between the vertical particle velocity and the vehicle speed is analogous to deflection slope directly reported by the TSD) were found to have the best correlations with the maximum horizontal strains at the bottom of the AC layer (8).

It has been reported that the deflectometer measurements can be significantly influenced by the surrounding temperature (109). Currently, there are no proven methods to correct TSD measurements for temperature. One of the common methods to deflection correction based on surface temperature, proposed by AASHTO design guide, is based on the maximum deflection obtained from the FWD data. This method requires determining a correction factor based on surface temperature and AC thickness to normalize maximum deflections at a reference temperature of 68°F (20°C). Researchers have proposed methods to adjust strains at the bottom of the AC layer based on the temperature correction. It essentially measures the moduli ($E_f$) based on the strain ($\varepsilon$) at the time of the test and is represented as $E_f = c * \varepsilon^d$. Here, $c$ and $d$ are model coefficients. Rada et al. (8) proposed the values for coefficients $c$ and $d$. The temperature correction for $SCI_{12}$ could be performed using the approach developed by Nasimifar et al. (28). The approach is inspired by the Lukanen method for FWD measurements and is based on loading applied to a moving device on a viscoelastic medium (29). A similar approach was used by Katicha et.al (5). In these approaches, BELLS FHWA equation, as shown in Equation (4.23), was used to calculate the temperature at the mid-layer of the pavement (29,110). Also, temperature correction using a model known as VEA was proposed by Nasimifar et al. (28). The VEA model accounts for all the sensitive parameters including thicknesses, temperatures, moduli, and binder types. Asphalt properties, such as layer thickness and temperature were observed to be the most sensitive parameters for $SCI_{TSD}$. Equations (4.24) and (4.25) show the temperature adjustment factors for $SCI_{TSD}$. It is noted that Equation (4.24) is only applicable to locations within the United States. However, Equation (4.25) can be used for any location. Latitudes for specific binder Performance Grades (PGs) are included in the models proposed by Nasimifar et al. (111).

$$T_d = 2.9 + 0.935\, IR\, [log_{10}(d) - 1.25]\big[-0.487\, IR + 0.6266\, T_{1-day} + 3.29\ \sin(hr_{18} - 15.5)\big] + 0.037\, IR \sin\,(hr_{18} - 13.5) \qquad \text{Equation 4.23}$$

where,

$T_d$ = pavement temperature at depth, d, within the asphalt layer, °C;

$IR$ = surface temperature measured with the infrared temperature gauge, °C;

$d$ = depth at which the temperature is to be predicted, mm

$T_{1\text{-}day}$ = the average of the previous day's high and low air temperatures, °C; and

$hr_{18}$ = time of day in the 24-hour system but calculated using an 18-hour asphalt temperature rise and fall time as explained by Stubstad et al. (112)

$$\lambda = \frac{SCI_{Ref}}{SCI_T} = \frac{10^{-0.05014T_{Ref}+0.019049T_{Ref}\log(h_{AC})log\varphi}}{10^{-0.05014T+0.019049T\log(h_{AC})log\varphi}} \qquad \text{Equation 4.24}$$

$$\lambda = \frac{SCI_{Ref}}{SCI_T} = \frac{10^{-0.0521T_{Ref}+0.0322T_{Ref}\log(h_{AC})}}{10^{-0.0521T+0.0322T\log(h_{AC})}} \qquad \text{Equation 4.25}$$

where,

λ = Temperature adjustment factor;

$SCI_{Ref}$ = Adjusted $SCI_{TSD}$ at reference temperature;

$T_{Ref}$ = Reference temperature, °C;

$T$= Mid-depth AC layer temperature at time of measurement, °C;

$h_{AC}$= Asphalt layer thickness, mm; and

$\Phi$ = Latitude of location of measurement (within 30 to 50 degrees).

Lately, the use of Artificial Intelligence (AI) and other traditional methods has gained popularity due to their capability to predict and learn from data. Methods such as RF tree-based models, Support Vector Machine (SVM) models and Artificial Neural Network (ANN) models are being used in many fields of engineering. The RF is a machine learning algorithm proposed by Breiman (49). It is a non-parametric technique that uses a decision tree model. This method consists of a set of trees with a series of input vectors that form a forest in which each tree produces outputs and is generated by bootstrap samples. The average of all outputs from each formed tree is taken as the final output. Usually, input data are divided into sets: the training (bagging) set, and the testing (out-of-bag) set. Figure 4.2 show the region approach of a RF model. It show the output of recursive binary splitting on a two-dimensional example, a tree corresponds to the partition, and a perspective plot of the prediction surface corresponds to that tree (113). Pavement deterioration, effective structural number, deflection indices, surface conditioning, and other pavement metrics have been modeled using techniques such as machine learning, Gaussian Process Regression (GPR), M5P Model Tree (M5P), Multi Linear Regression Model (MLR), Quasi-Poisson, Artificial Neural Network (ANN), RF models and others (5,57,60,114,115).

## 4.3 DATA COLLECTION

Two different pavement sections were considered in this study. The I-35 section was 14.5 miles in length beginning at the Carter/Murray County line Mile Post 45 (34.376384, -97.144182) and extended north to Mile Post 59.5 (34.559871, -97.193138). The SH-7 section started 1-mile west of the intersection with I-35 (34.510042, -97.194876) and extended 5 miles west (34.521343, -97.284874) in Garvin County.

In this study, TSD and FWD data were collected, analyzed, and compared using both statistical and AI-based methods. Asphalt cores were extracted to determine layer thicknesses. The I-35 section consisted of a 20 in. AC layer over either a Continuous Reinforced Concrete Pavement (CRCP) layer or a Jointed Concrete Pavement (JCP) layer. The SH-7 section consisted of a 20 in. AC layer with fabric constructed over compacted subgrade.

During FWD testing, temperature, load, and deflection data were collected at 0, 12 in. (300 mm), 24 in. (600 mm), 36 in. (900 mm), 48 in. (1,200 mm), 60 in. (1,500 mm), and 72 in. (1,800 mm) from the center of the plate. For TSD, vertical pavement deflection velocities and the vehicle horizontal velocities were recorded at 0 in., 8 in. (200 mm), 12 in. (300 mm), 24 in. (600 mm), 36 in. (900 mm), 48 in. (1,200 mm), 60 in. (1,500 mm), and 72 in. (1,800 mm) from the center of the wheel. Deflections were calculated using the Area Under the Curve (AUTC) model by numerically integrating the deflection bowl. Also, loads, temperature, and distresses, namely rutting and roughness data, were collected during the TSD testing.

## 4.4 DATA ANALYSIS RESULTS AND DISCUSSIONS

### 4.4.1 International Roughness Index and Rutting Data from TSD

Figure 4.3 and Figure 4.4 show the average rutting and IRI values for both sections. A strong trend or relation between the IRI and rut values was observed for the westbound lane of the SH-7 section and the northbound lane of the I-35 section. Excessive rut was observed on the eastbound lane of the SH-7 section. The strongest correlation (r = 0.38) was observed for the westbound lane of SH-7, followed by the northbound lane of I-35 (r = 0.289). Both eastbound lane of SH-7 (r = -0.012) and southbound lane of I-35 (r = -0.333) showed negative correlations.

### 4.4.2 Deflection Measurements from TSD and FWD

Figure 4.6 show the maximum deflections for the northbound and southbound section of I-35 and westbound and eastbound section of SH-7 from obtained from the FWD and TSD testing. From Figure 4.5, the TSD deflections were found to be higher than the FWD deflections for both bounds of the SH-7 section and lower for both bounds of the I-35 section. Also, the TSD and FWD deflections after temperature correction ($\lambda$) at 68°F (20°C) are shown in Figure 4.5 and Figure 4.6. For this purpose, the surface temperatures of the pavements were recorded during testing. The average surface temperatures of 88, 97, 38 and 59 °F (32, 36, 3, and 15 °C) were recorded for the westbound lane of SH-7, eastbound lane of SH-7, northbound lane of I-35 and southbound lane of I-35, respectively, during FWD testing. The corresponding average surface temperatures (in the same order) of 86, 92, 102, and 103 °F (30, 33, 39, and 40 °C) were recorded during TSD testing. The BELLS method was then used to estimate the temperature at the mid-depth of the asphalt layer and to calculate the temperature correction factor. For the I-35 section, after temperature correction, the TSD deflections were found to be reduced whereas, the FWD deflections increased. The difference in the time of data collection could have played a role in this regard. The TSD data were collected in July while the FWD data were collected in December 2020. The surface and mid-depth temperature were much lower than the reference temperature for FWD. Comparatively, the surface and mid-depth temperatures were significantly higher than the reference temperature for TSD. Correction factors slightly higher than 1 were observed for FWD, and correction factors close to or below 1 were observed for TSD.

The average load for the FWD and TSD tests were recorded as 9,072 and 9,470 lbs. (40.35 and 42.12 kN), respectively. Higher loads were observed for TSD tests on the SH-7 section, in general, compared to those for the I-35 section. From Figure 4.5 and Figure 4.6, larger differences in deflections between TSD and FWD were observed for the I-35 section compared to the SH-7 section. The reasons for such differences may be associated with the pavement structure (concrete layer for the I-35 section).

#### 4.4.3 Back-calculation of Elastic Moduli from FWD and TSD

Elastic moduli for the surface layer were back-calculated from FWD deflections using Modulus 7.0 (latest version), a software developed by Texas Transportation Institution (TTI). This software fits a deflection bowl to a set of bowl shapes by optimizing layer stiffnesses. For comparison purposes, TSD data were also converted to Modulus 7.0 format to back-calculate elastic moduli. Figure 4.7 and Figure 4.8 show the comparison between back-calculated elastic moduli from the FWD and TSD data, respectively. The elastic moduli from the FWD and TSD tests exhibited a correlation of 0.27 and an $R^2$ of 0.08 for the eastbound lane of SH-7 section. Comparatively, for the westbound lane of the SH-7 section, the corresponding correlation was 0.62 and the $R^2$ was 0.38. In general, the elastic moduli from FWD and TSD tests showed a higher correlation ("r" = 0.5) and ($R^2$ = 0.3) for the SH-7 section compared to the I-35 section. The "r" and $R^2$ values were negative or close to zero for this section. The TSD data from the SH-7 section were much cleaner, with less outliers, than those from the I-35 section. The TSD data for composite pavements may have limitations both relative to trend and accuracy. In addition to aforementioned comparisons, an attempt was made in this study to develop models to predict back-calculated elastic moduli from the FWD tests using parameters derived from the TSD tests.

### 4.4.4 Correlations Between Different Parameters

Figure 4.9 show the Pearson Correlation Coefficient (r) for all the measured parameters from the FWD and TSD tests for the I-35 and SH-7 sections. The Pearson correlation measures the strength of the linearity between two variables. A positive correlation means that a variable tends to increase when the other variable increases, and a negative correlation means an opposite trend. However, a high negative correlation still means that there is a strong relationship. Figure 4.9 show the relationship between parameters collected by both devices. As shown in Figure 4.9, higher correlations were observed for deflections for the SH-7 section. Specifically, a higher correlation was observed between TSD ($D_0$) and FWD ($D_0$). As per rut and IRI, there is a positive correlation for both sections, with a stronger correlation for the I-35 section. From deflection perspective, the IRI values showed a stronger relationship with the TSD and FWD data for the deflections measured at the center of the load for the I-

35 section. Similarly, rut values showed much better correlations with deflections closer to the center of the load, especially for the SH-7 section.

Over twenty (20) basin indices, as described in Equations 4.1 to 4.22 were calculated from the TSD data. These parameters were compared with the TSD and FWD deflections, as shown in Figure 4.10 and Figure 4.11. Also, rut, temperature, IRI, and loading were compared to determine the potential input parameters for the prediction models to be used. Over forty (40) FWD and TSD parameters were compared. Figure 4.10 and Figure 4.11 summarize the correlation matrix between the measured and calculated parameters. It can be observed that the SH-7 section exhibited much stronger correlations between parameters compared to those for the I-35 section. The higher speed of data collection in the I-35 section and presence of a very stiff concrete layer underneath can lead to very small deflections in TSD testing compared to FWD testing. As a result, deflections were insignificant and/or not recordable by the TSD. Different TSD measurements and basin indices correlated better with the FWD deflections and elastic moduli calculated from the FWD data. Again, this may be linked to the different structural sections of the pavements (AC and composite). For elastic moduli, the AI and SCI basin parameters showed higher correlations for the SH-7 section than the I-35 section. Similar observations were made for the Shape factors (F) and IRI. For FWD maximum deflection $D_0$, AI and SCI basin parameters showed higher correlations for the SH-7 section than those for the I-35 section for both TSD ($D_0$) and BCI.

### 4.4.5 Random Forest and Linear Regression Modeling

#### *4.4.5.1 Prediction of Elastic Moduli*

Random forest and linear regression models were developed using Python software. Different combinations of variables or parameters were used to identify stronger correlation variables. The results are summarized in Figure 4.10 and Figure 4.11. In this study, TSD deflections and basin indices were used to develop a model to predict elastic modulus that were back-calculated using the FWD data. It was evident that both sections (SH-7 and I-35) needed to be analyzed separately because of significant differences in layer configurations and materials. About 80 percent of the data, selected randomly, in both sections were used to train (bagging) the model and 20 percent were used for testing (out-of-bag) the model. When a model matches the training data too closely and is overfit, it produces subpar results on new or untried data. In other words, the models or correlations are only high in accuracy for that specific set of data. About 1,012 assorted variable combinations were modeled and compared for the I-35 and SH-7 section using the Python code. Figure 4.12 show the $R^2$, MAE and RMSE errors in training and testing for the 10 best combinations of parameters for the SH-7 section. The best combination to train and validate the data using the RF and LR models includes AUPP and rut. This combination resulted in an R2 of 0.47, a MAE of 187 ksi and an RMSE of 236 ksi. It can be observed that the AUPP, rut and TSD ($D_0$) are the most significative parameters for the RF and LR models to predict elastic modulus of the SH-7 section. Figure 4.13 show a comparison between the predicted and back-calculated elastic moduli obtained from the FWD data using Modulus 7.0. It can be observed that the trend line for the testing set is closer to the equality line compared to the training set. However, the $R^2$ values differed significantly, as shown in Figure 4.12.

Figure 4.14 show the $R^2$, MAE and RMSE errors for training and testing sets for the 10 best combinations of parameters for the I-35 section. The best combination to train and validate the data using the RF and LR models includes TSD ($D_{48}$), IRI, and $DSI_{8-12}$. This combination had a $R^2$ of 0.42, a MAE of 273 ksi and an RMSE of 360 ksi. It can be observed that the TSD ($D_{48}$) and IRI are the most significant parameters for the RF and LR models to predict elastic moduli of the I-35 section. Figure 4.15 show the comparison between predicted and the back-calculated elastic moduli obtained from the FWD data using Modulus 7.0. As noted above, for the SH-7 section, the equality line for the testing set is closer compared to the training set. However, the $R^2$ values differed significantly, as shown in Figure 4.14,

Different variables correlated better to elastic moduli, and different assorted combinations showed higher accuracy than others. It can be observed that deflections near the center of the load TSD ($D_0$) and DSI are the most significant variables in both cases. Also, RF models were found to be a better model to predict elastic moduli compared to linear regressions. For both sections, the LR testing models didn't show much improvement from training sets.

#### *4.4.5.2 Prediction of Maximum FWD Deflections*

In this study, an attempt was made to predict the maximum deflections from the FWD tests using TSD parameters in the RF and LR models. Prediction of this deflection can be useful since several transportation agencies have thresholds limits for the FWD deflection, which is used to characterize pavement conditions. The methodology used for the prediction of elastic moduli was used to predict FWD ($D_0$). About 1,012 combinations of variables were tried and compared for the I-35 and SH-7 sections using the Python code. Figure 4.16 show the $R^2$, MAE and RMSE errors in training and testing for the 10 best combinations of parameters for the SH-7 section. The best combination to train and validate the data using the RF and LR models includes TSD ($D_0$), AUPP, $SCI_{18}$ and rut. This combination had an $R^2$ of 0.53, a MAE of 0.64 mils and an RMSE of 0.79 mils. It can be observed that the TSD ($D_0$) is the most significative parameter for the RF and LR models to predict FWD ($D_0$) for the SH-7 section. Figure 4.17 show a comparison between the actual and predicted FWD maximum deflections ($D_0$). In this case, the equality line is close to the trend line for both testing and training sets.

Figure 4.18 show the $R^2$, MAE and RMSE errors in training and testing for the 10 best combinations of parameters for the I-35 section. The best combination to train and validate the data using the RF and LR models includes TSD ($D_{12}$) and IRI. This combination had an R2 of 0.27, a MAE of 0.5 mils and a RMSE of 0.65 mils. It can be observed that IRI is the most significative parameter for the RF and LR models to predict FWD ($D_0$) for the -35 section. However, the $R^2$ value was significantly lower compared to that for the SH-7 section, which consisted of AC layers only. Figure 4.19 show a comparison between the actual and predicted FWD maximum deflections ($D_0$). The testing trend line matched the equality line, while the training set differed substantially. However, the training set showed higher $R^2$ values compared to those for the testing set.

## 4.5 CONCLUSIONS AND RECOMMENDATIONS

From the results and the discussions presented in the preceding sections, the following conclusions and recommendations can be drawn:

- Random forest models performed better than linear regression models for both training and testing sets. The RF models for the SH-7 section were observed to perform better compared to the I-35 section for the prediction of elastic moduli and FWD maximum deflection ($D_0$). The correlations between different TSD and FWD parameters were higher for the SH-7 section. The presence of a very stiff concrete layer (PCC and JCPC) in the I-35 sections likely resulted in very small and undetectable deflections in TSD testing.
- Maximum deflections from TSD ($D_0$) was found to be the most significant parameter in all the proposed models. Roughness and rut showed a similar trend. IRI was found to be an important variable for the I-35 section, whereas rut was found to be more important for the SH-7 section.
- Significant errors were observed while using TSD deflections directly in Modulus 7.0 to back calculate elastic moduli for composite pavements. The back-calculated elastic moduli from the TSD data did not compare well with the results obtained from the FWD deflections. Overall, better correlations were observed for the SH-7 section than for the I-35 section.

This study involved only two pavement sections, a state highway (SH-7) and in interstate (I-35). The findings of this study should be judged accordingly. It is recommended that future studies be performed to enrich these findings. In view of the emerging trend in using TSD by the transportation agencies, establishing correlations between FWD and TSD results are deemed helpful. The nature of loading (impact load FWD and vehicular load in TSD) needs to be addressed in future studies. Also, future studies should closely examine the use of TSD for composite pavements. Finally, selected coring and laboratory testing to validate pavement conditions derived from the TSD data are important and necessary.

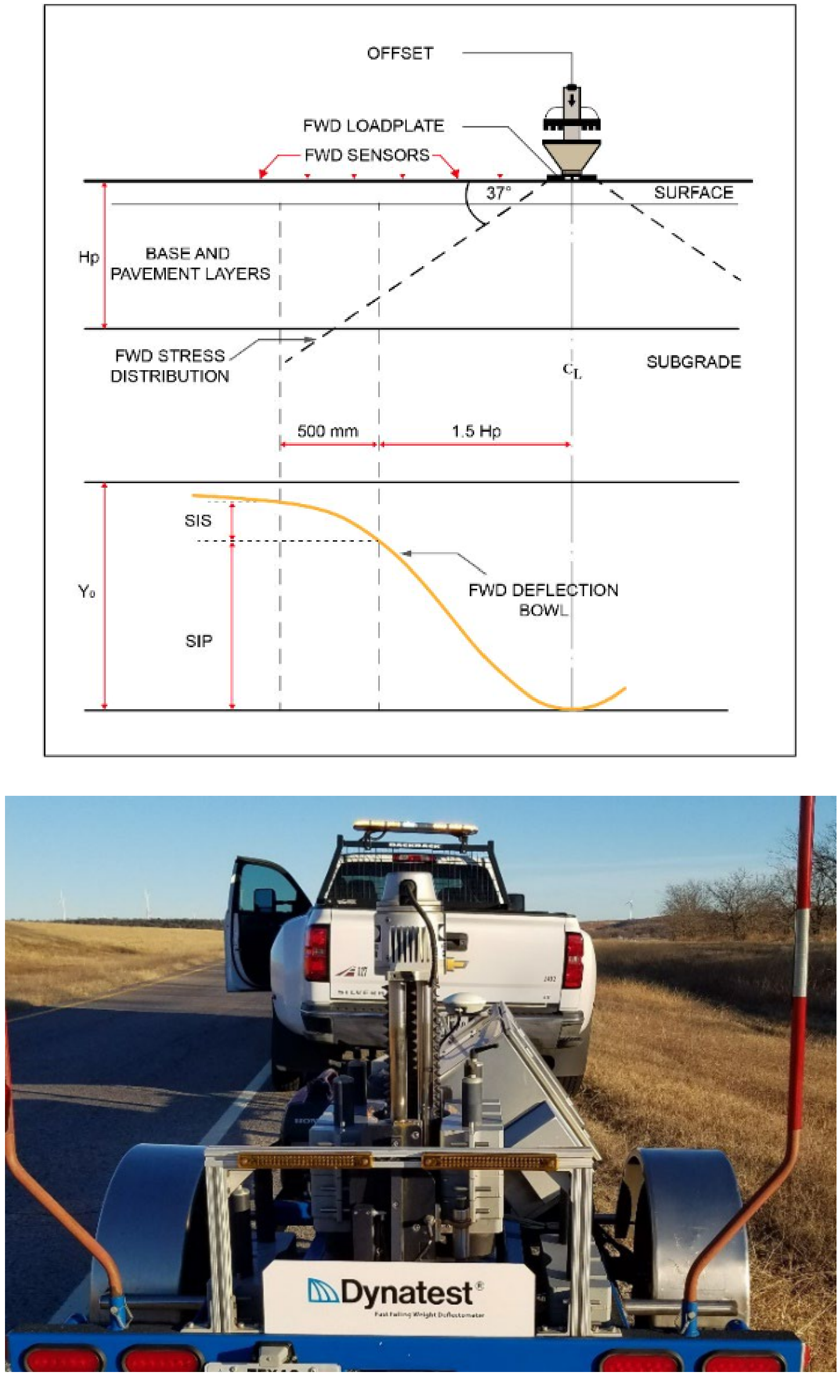


**Figure 4.1 Falling Weight Deflectometer Measurement Approach (116)**

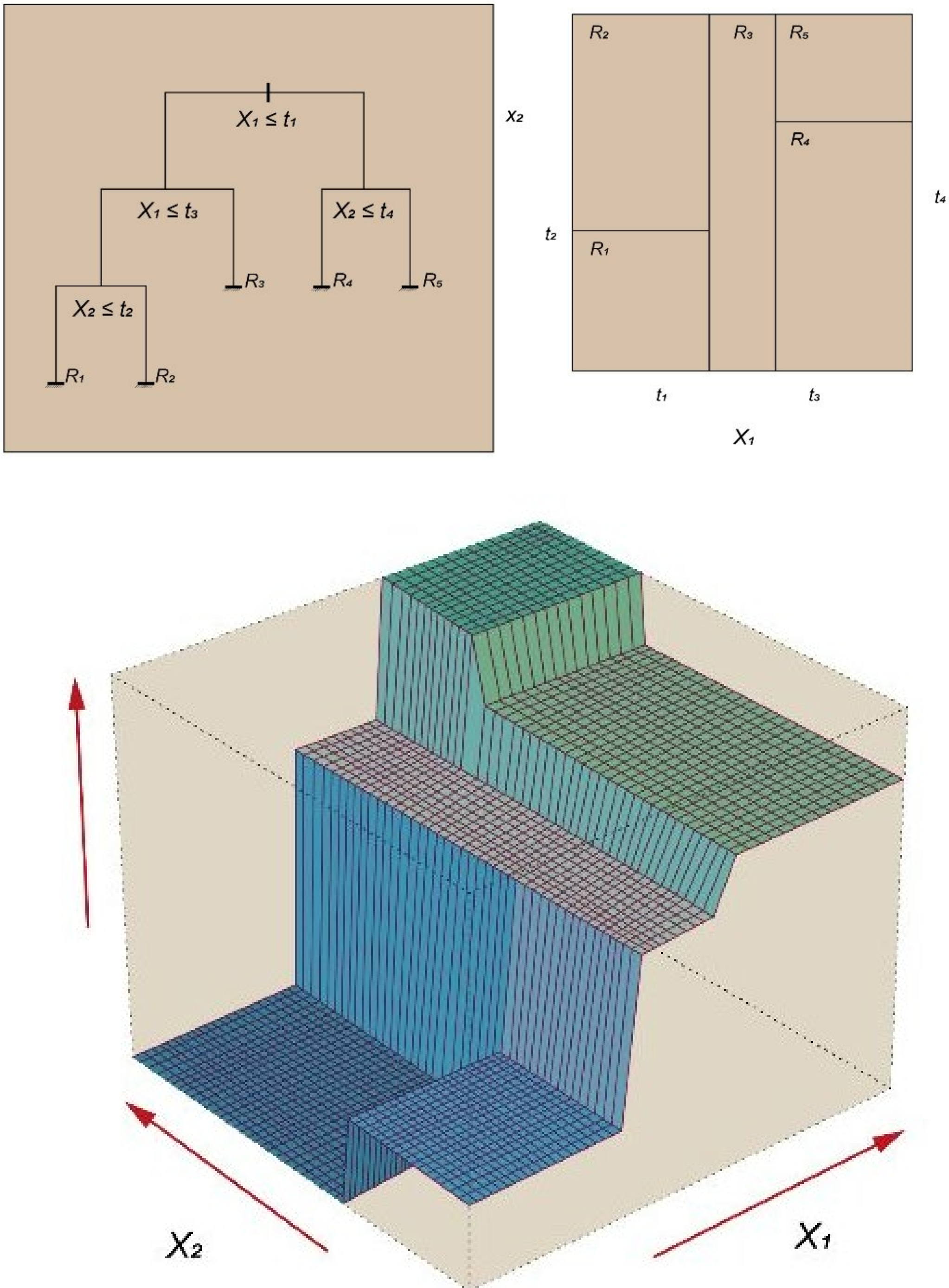


**Figure 4.2 Random Forest Model Approach (113)**

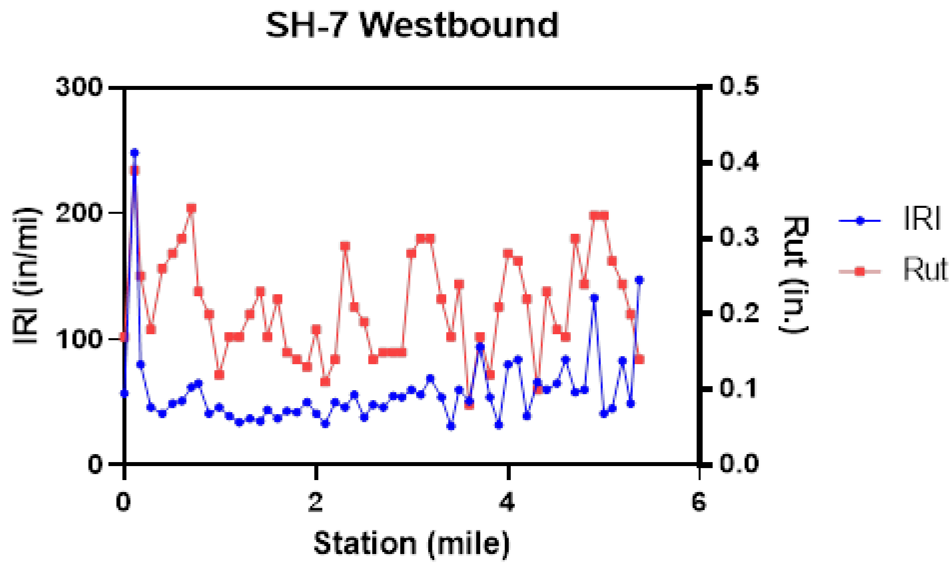


(a)

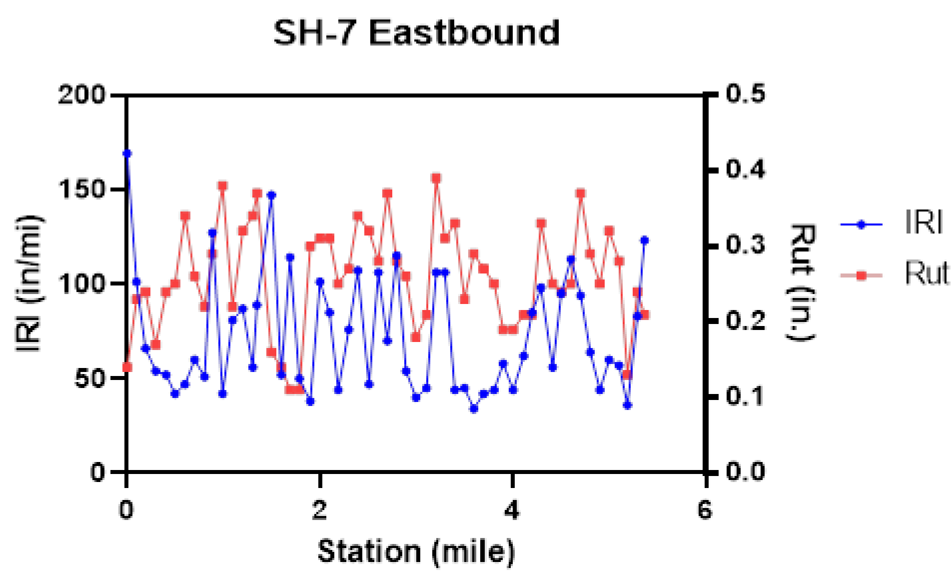


(b)

**Figure 4.3 TSD Roughness and Rut for SH-7**

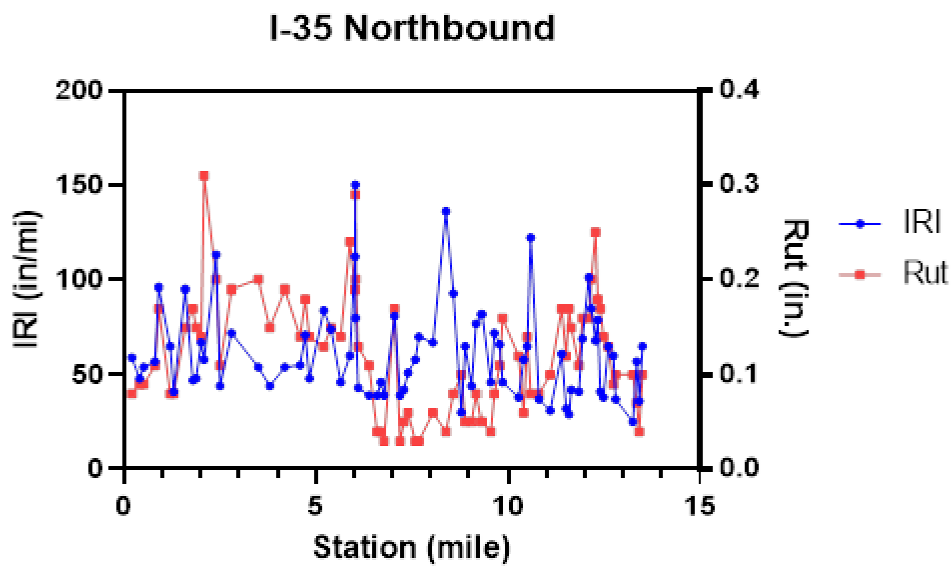


(a)

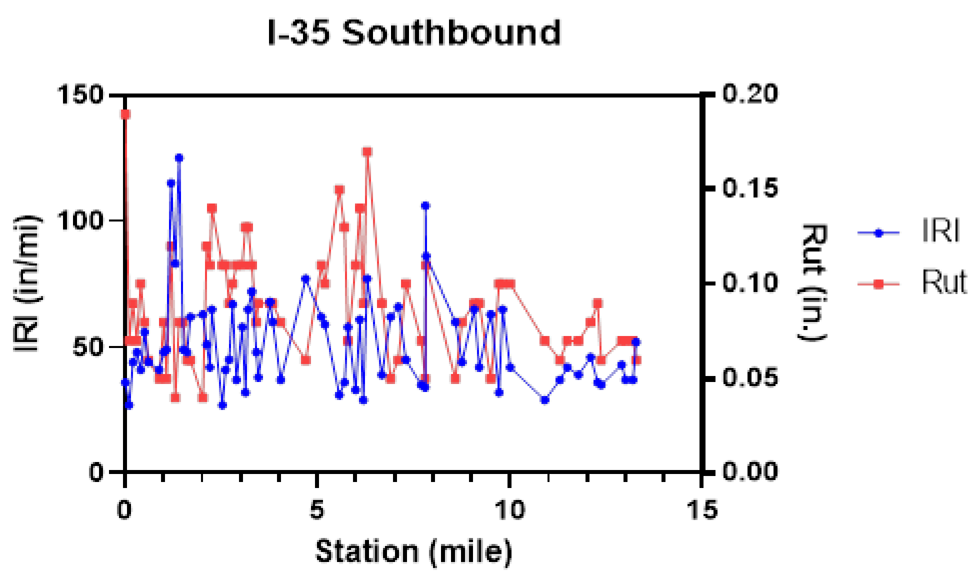


(b)

**Figure 4.4 TSD Roughness and Rut for I-35**

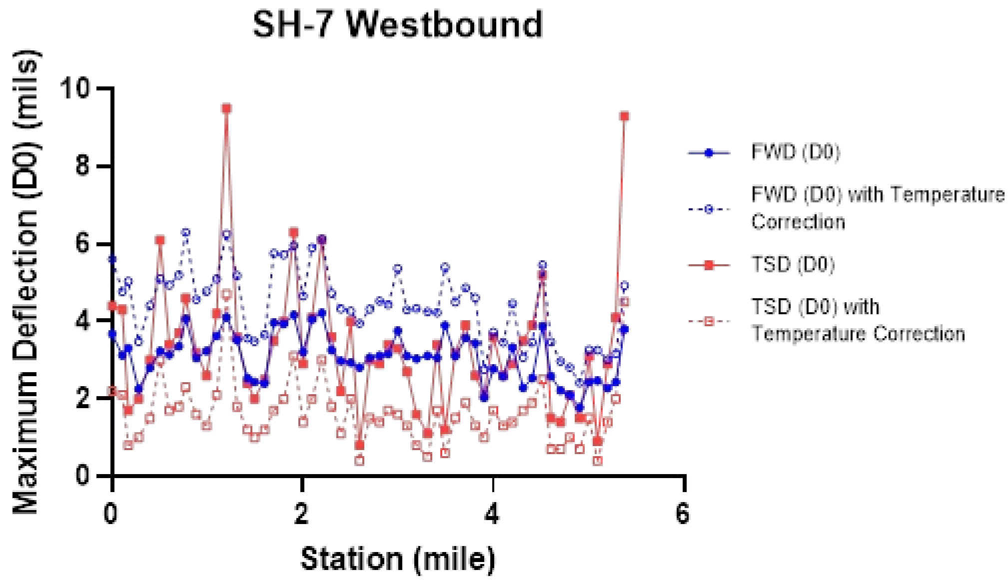


(a)

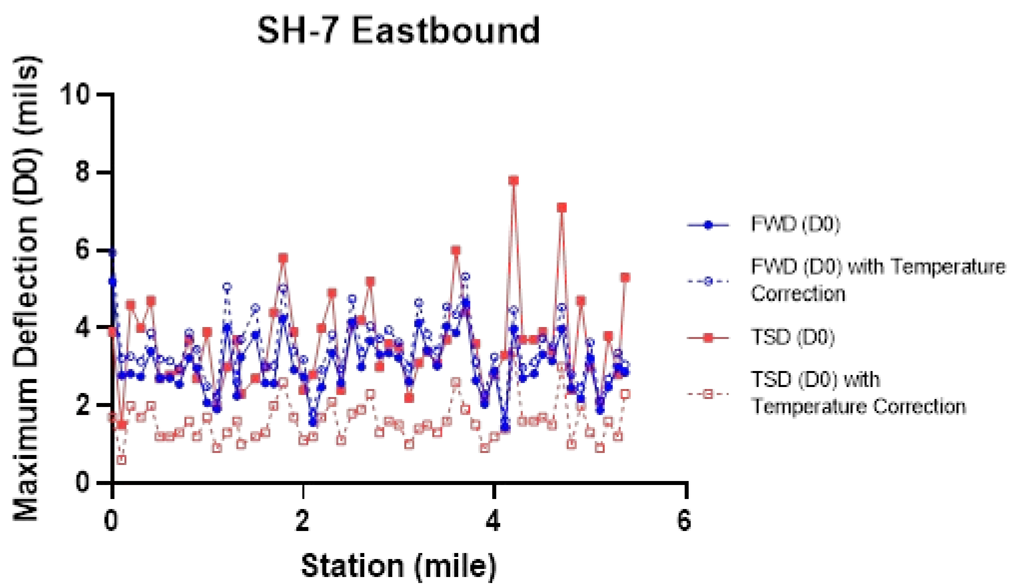


(b)

**Figure 4.5 FWD and TSD Maximum Deflections for SH-7**

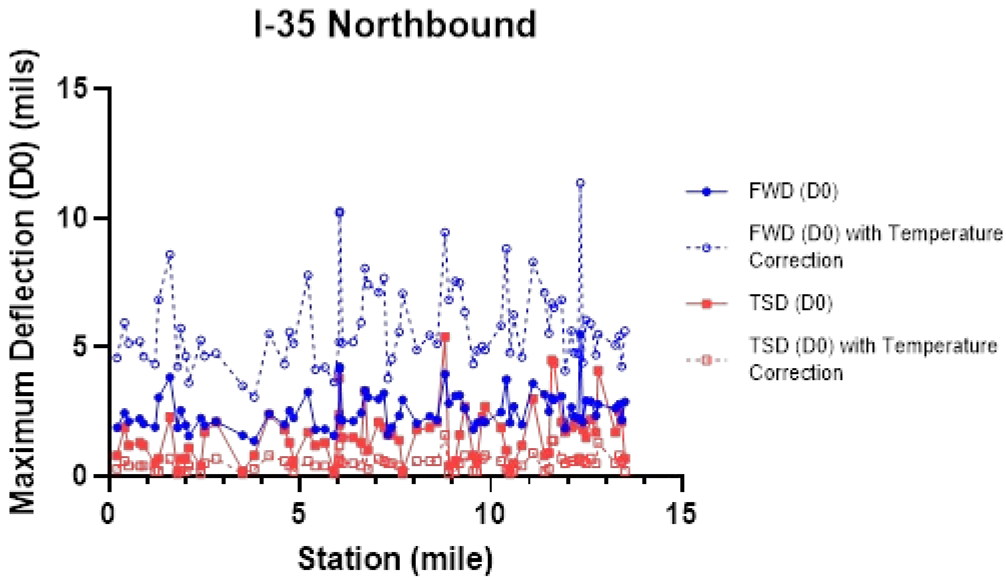


(a)

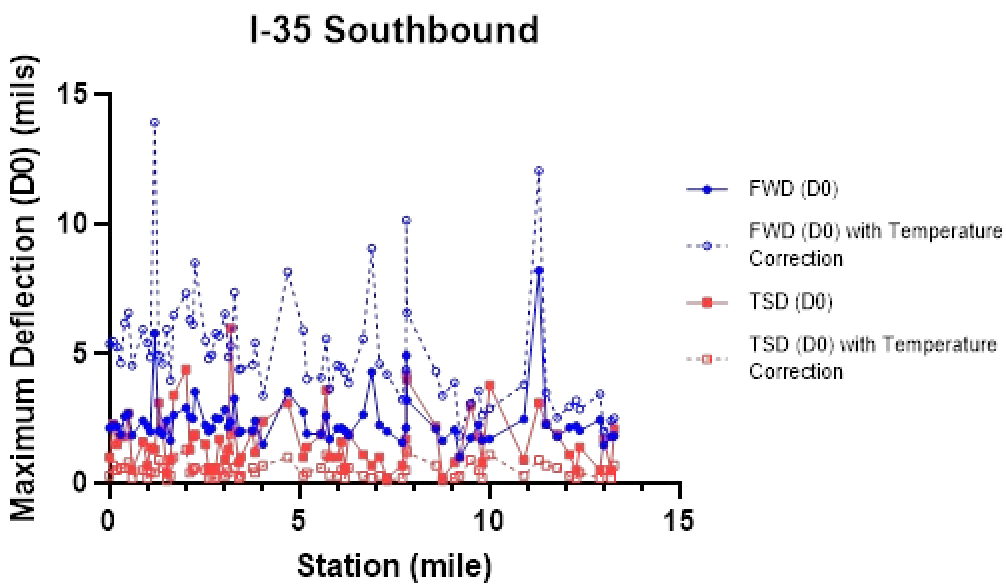


(b)

**Figure 4.6 FWD and TSD Maximum Deflections for I-35**

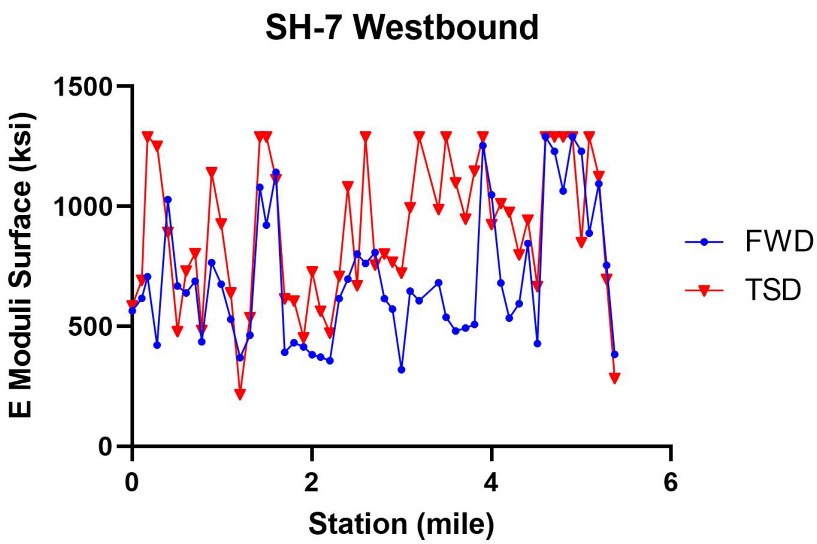


(a)

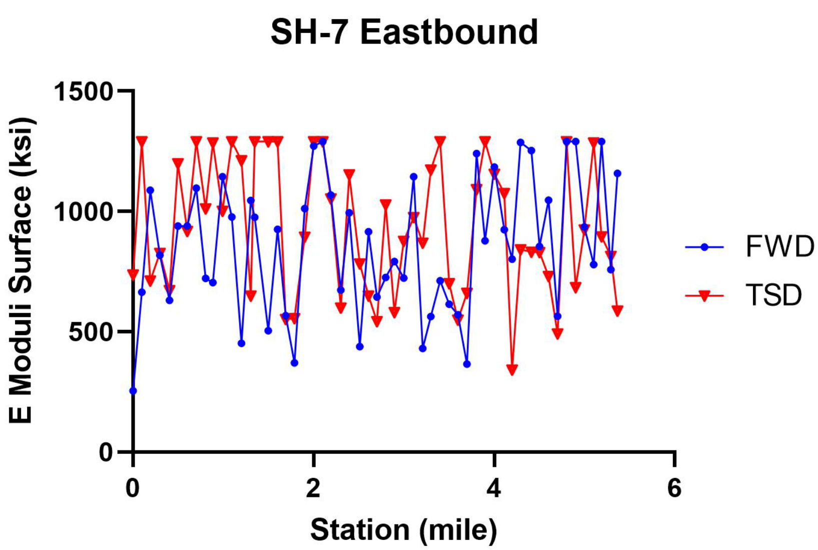


(b)

**Figure 4.7 TSD and FWD Back-calculated Elastic Moduli from Modulus 7.0 for SH-7**

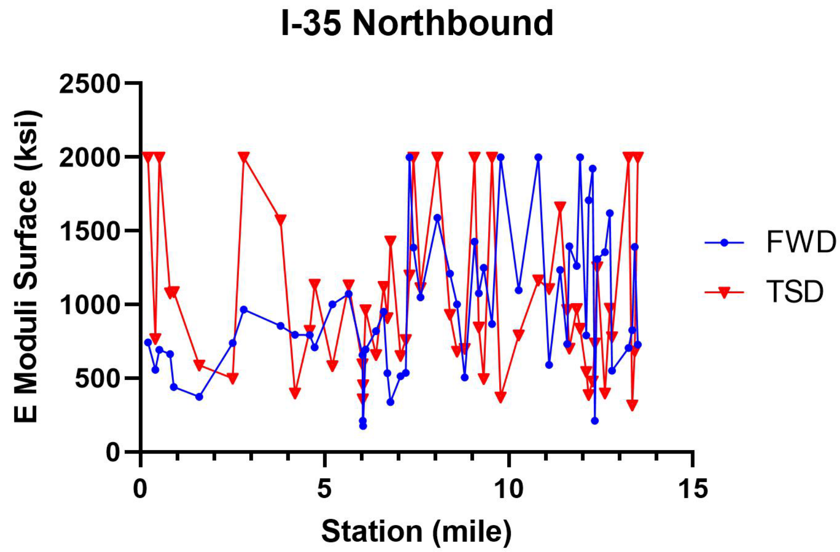


(a)

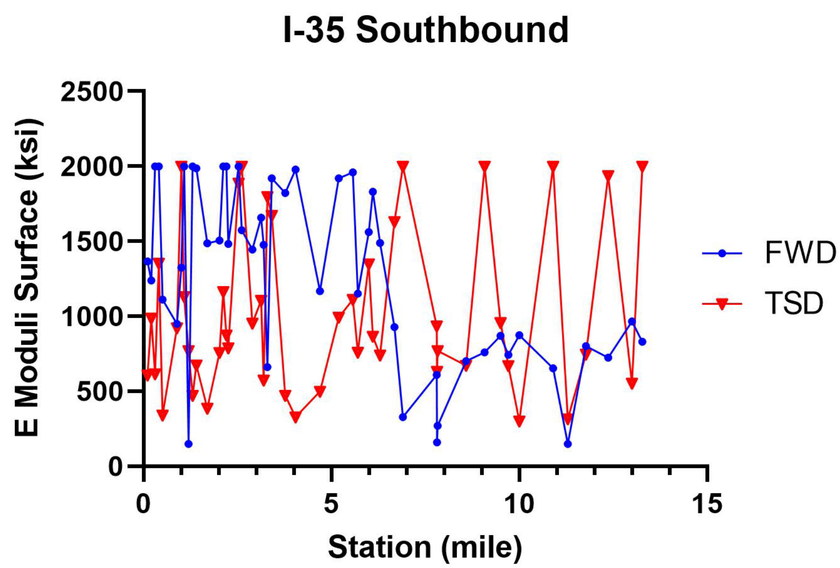


(b)

**Figure 4.8 TSD and FWD Back-calculated Elastic Moduli from Modulus 7.0 for I-35**

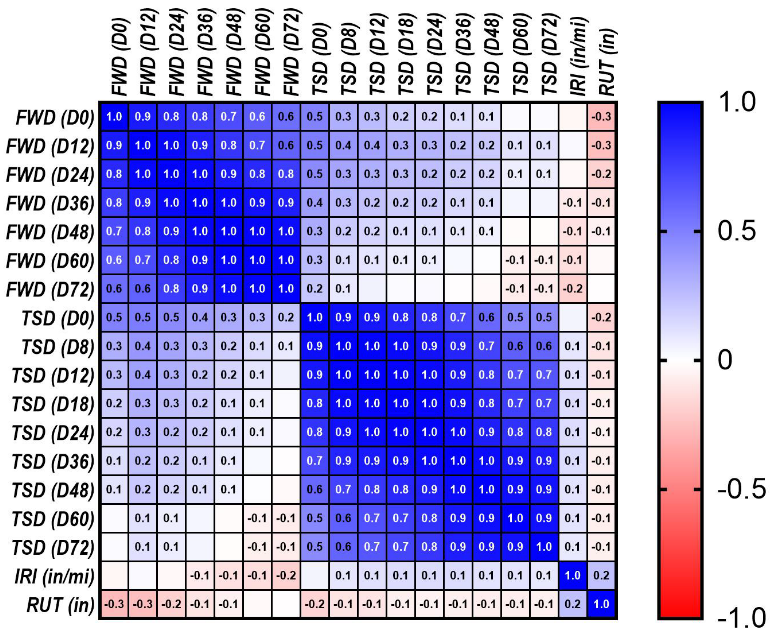


(a)

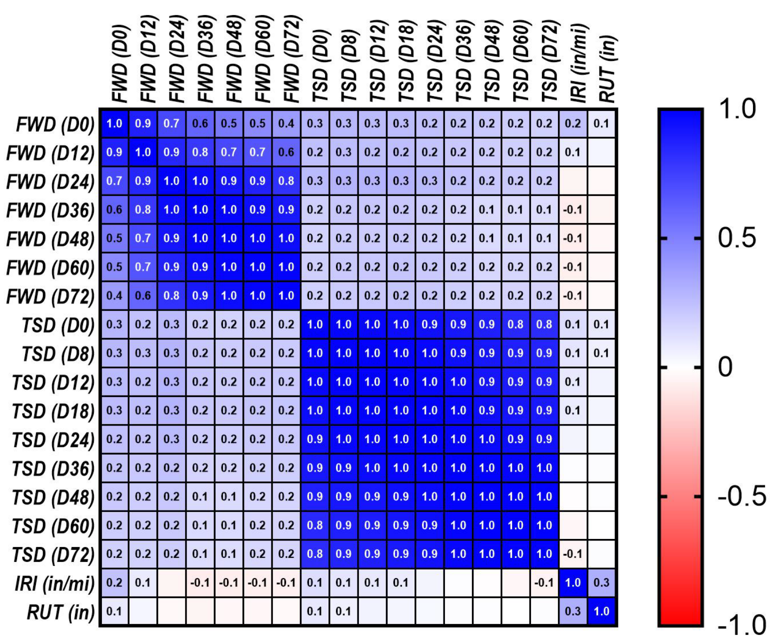


(b)

**Figure 4.9 Correlations Between FWD and TSD Parameters: (a) SH-7, and (b) I-35**

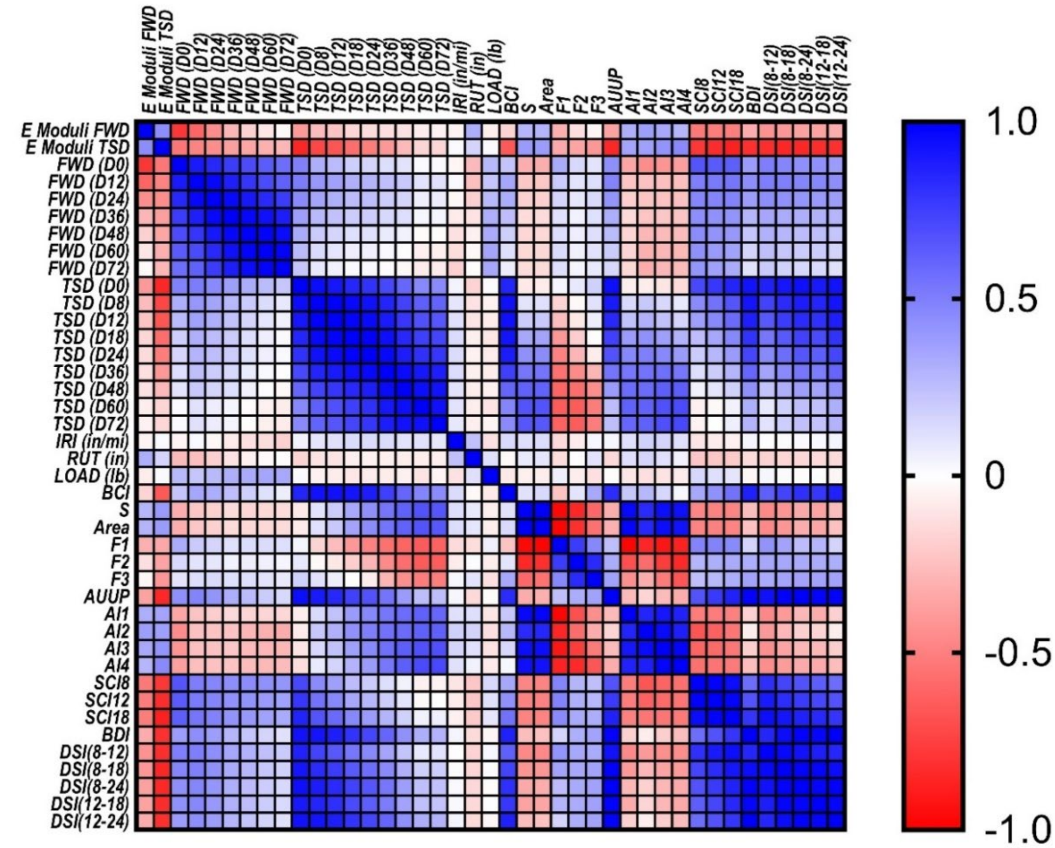


**Figure 4.10 FWD and TSD Basin Indices Correlation for SH-7**

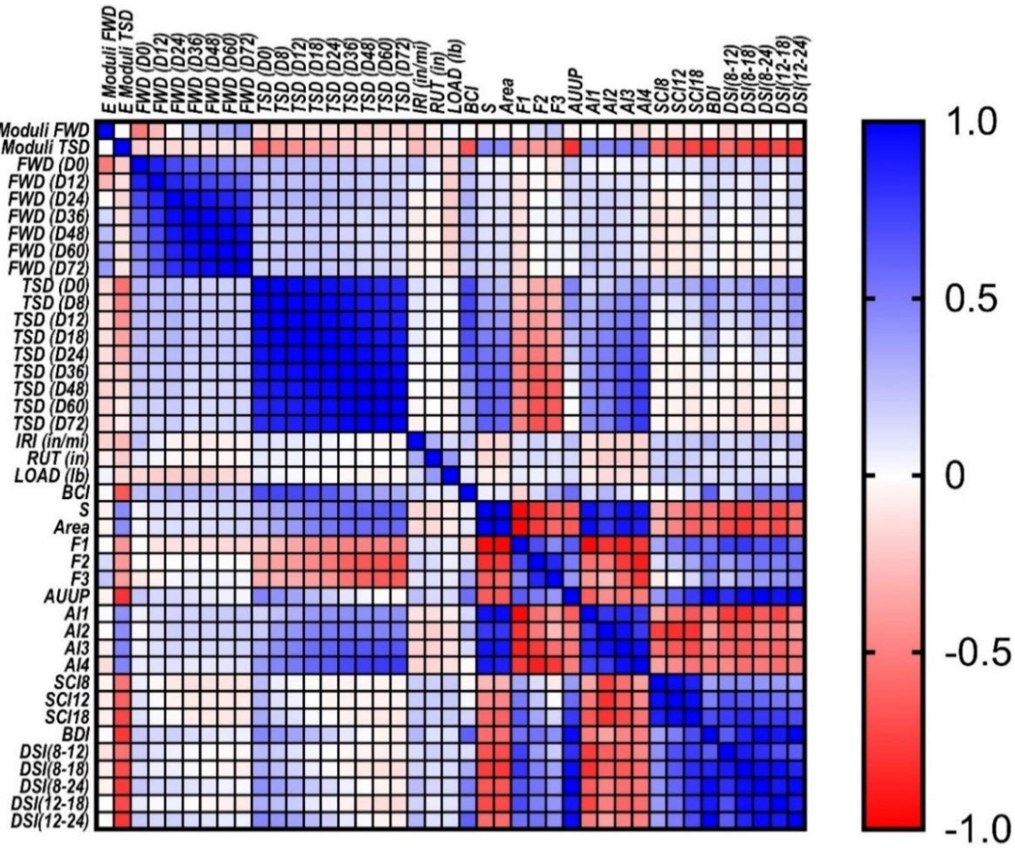


**Figure 4.11 FWD and TSD Basin Indices Correlation for I-35**

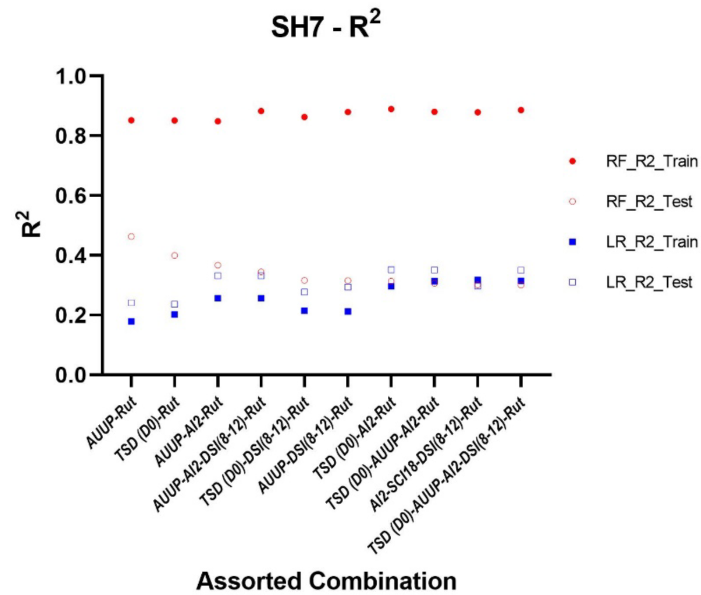


(a)

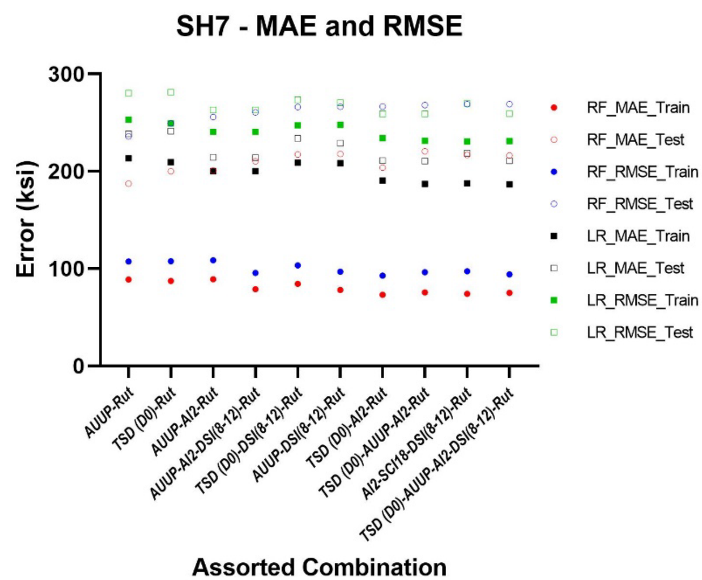


(b)

**Figure 4.12 Errors and Coefficients of Determination from Random Forest and Linear Regression Models for Prediction of Elastic Moduli of SH-7 (a) $R^2$ and, (b) MAE and RMSE**

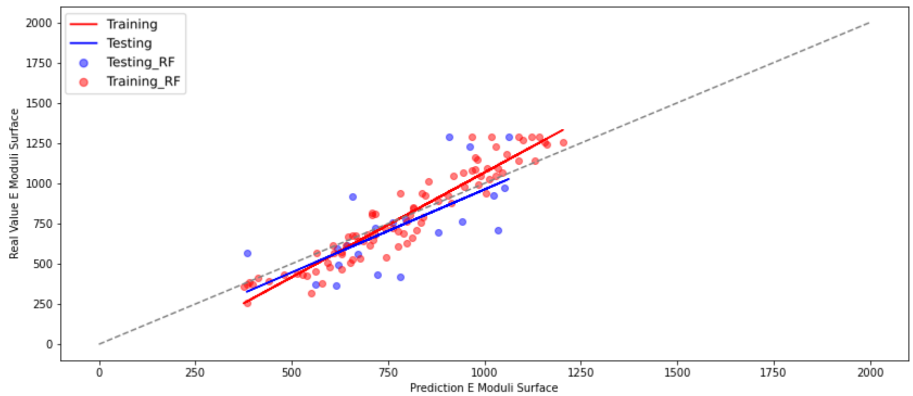


**Figure 4.13 Results of Training and Testing Sets for Prediction of Elastic Moduli of SH-7 Using Random Forest Model**

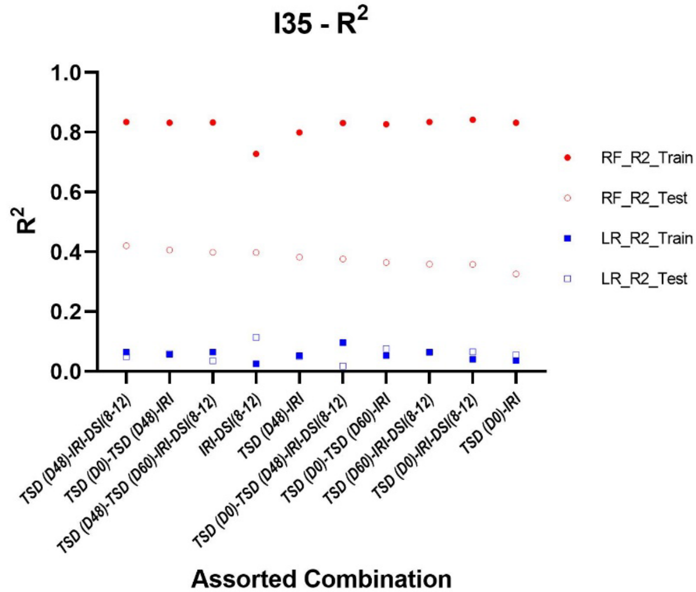


(a)

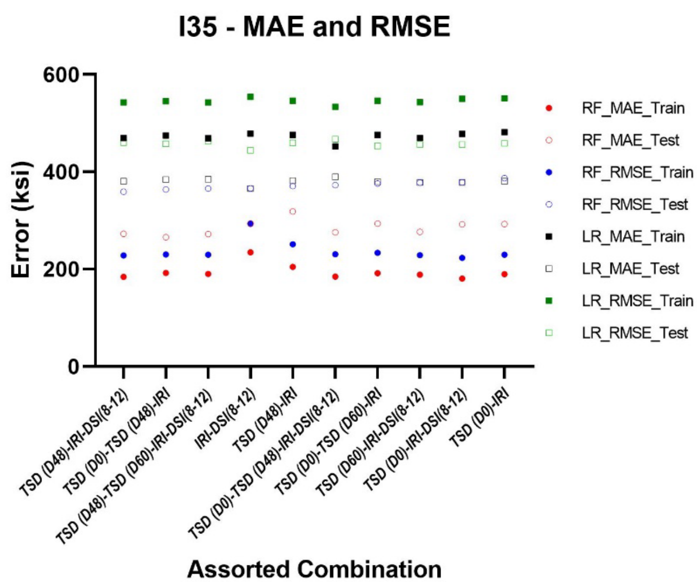


(b)

**Figure 4.14 Errors and Coefficients of Determination from Random Forest and Linear Regression Models for Prediction of Elastic Moduli of I-35 (a) $R^2$ and, (b) MAE and RMSE**

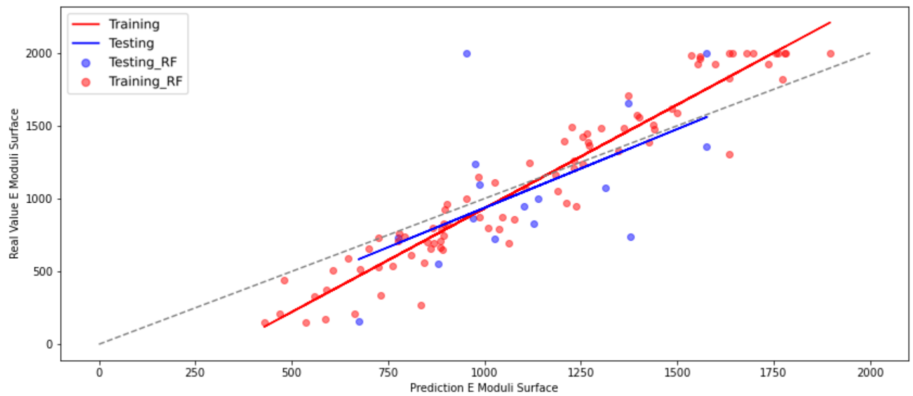


**Figure 4.15 Results of Training and Testing Sets for Prediction of Elastic Moduli of I-35 Using Random Forest Model**

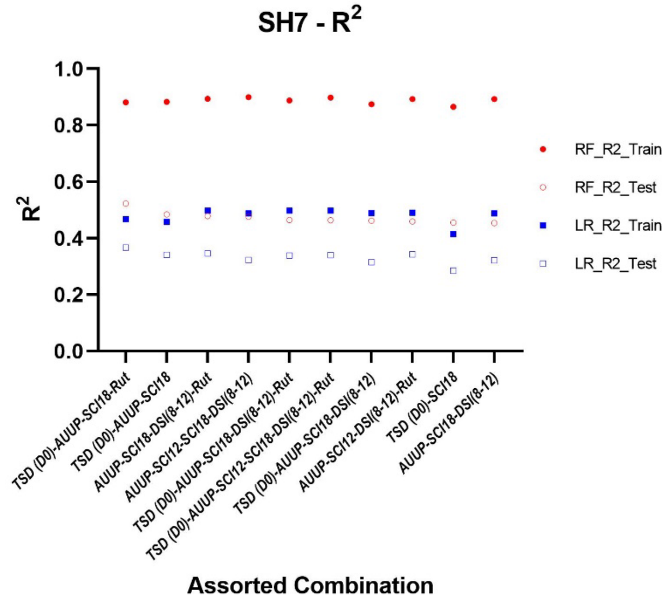


(a)

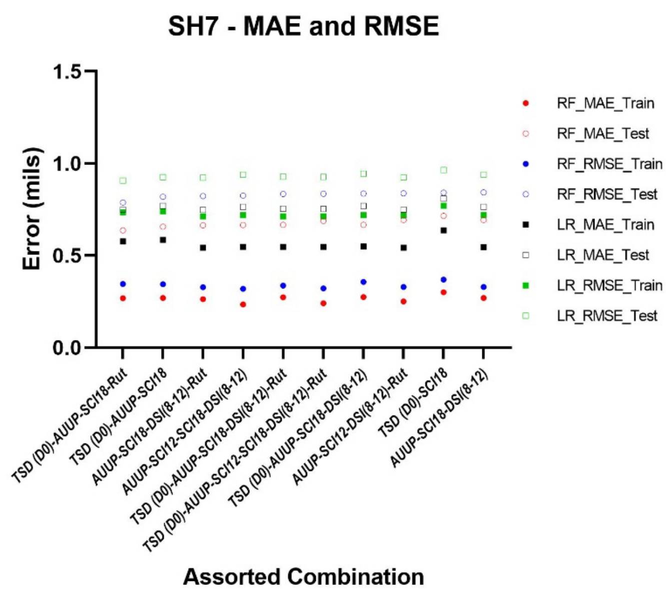


(b)

**Figure 4.16 Errors and Coefficients of Determination from Random Forest and Linear Regression Models for FWD Maximum Deflection ($D_0$) Prediction on SH-7 (a) $R^2$ and, (b) MAE and RMSE**

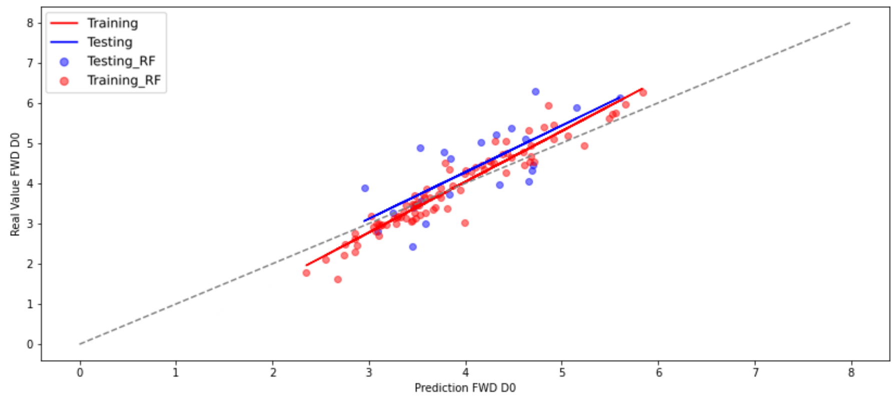


**Figure 4.17 Random Forest Results for Training and Testing sets for FWD Maximum Deflection ($D_0$) on SH-7**

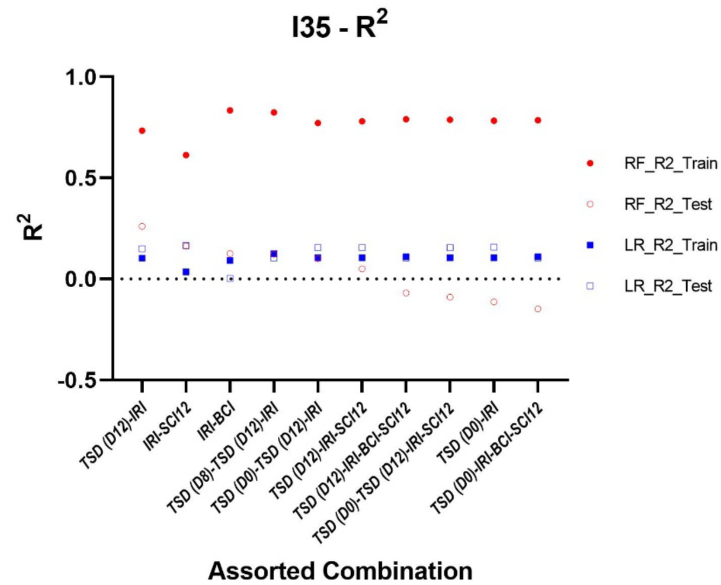


(a)

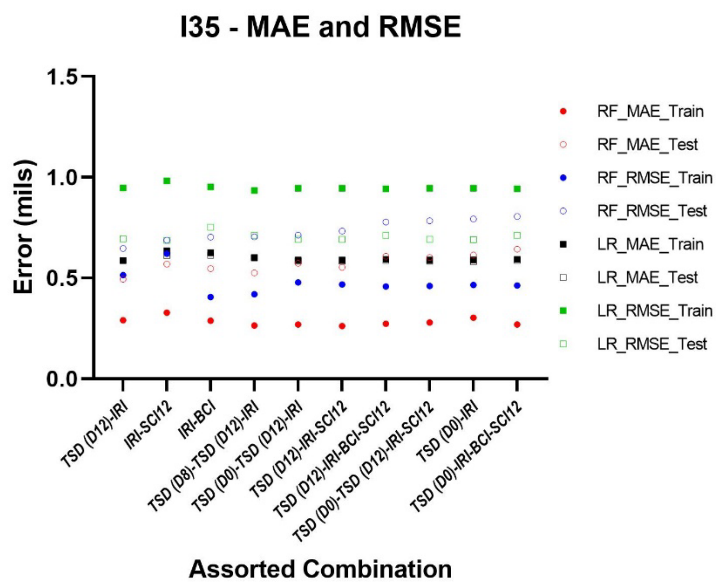


(b)

**Figure 4.18 Errors and Coefficients of Determination from Random Forest and Linear Regression Models for FWD Maximum Deflection ($D_0$) Prediction on I-35 (a) $R^2$ and, (b) MAE and RMSE**

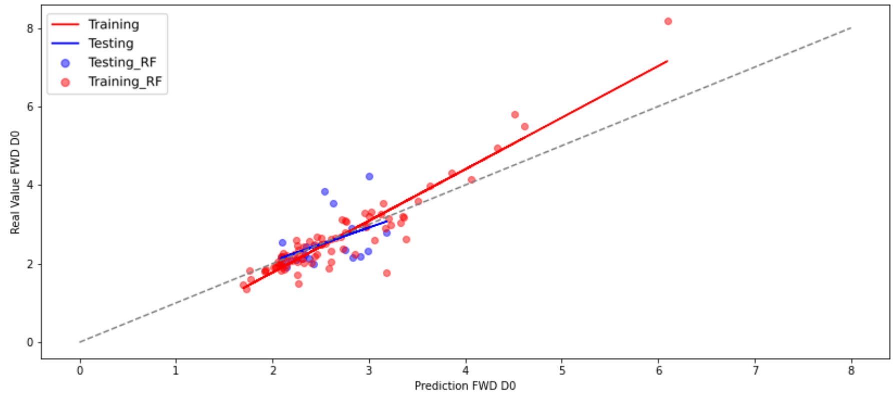


**Figure 4.19 Random Forest Results for Training and Testing Sets for FWD Maximum Deflection ($D_0$) on I-35**

CHAPTER

# 5

# CONCLUSIONS AND RECOMMENDATIONS

In this study, over forty (40) miles of pavements from two different sections (I-35 and SH-7) in Oklahoma were studied. Both destructive and nondestructive tests were conducted on the studied sections and the results were analyzed, compared, and calibrated to understand and rationalize the distresses observed, and to assess their structural conditions. The presence of different pavement structures (asphalt concrete pavement in the SH-7 section and composite pavements in the I-35 section) added to the challenges in establishing correlations, the analyzes conducted, and the conclusions drawn. Also, collected data were used to develop predictive models using regression and artificial intelligence-based methods and models. In Chapter 2, a forensic investigation was conducted over the studied sections to understand the distresses such as reflection cracking, edge cracking, rut, and longitudinal edge depressions. Field testing involving GPR, Pave3D 8k and FWD, and TSD were used to collect pavement data. Also, asphalt cores were extracted, and laboratory tests conducted to examine prevailing conditions and estimate remaining service life. Attempts were made to understand the strengths and weaknesses of TSD as a tool for pavement condition assessment, particularly for composite pavements. In Chapter 3, selected current models that are used to characterize pavements based on the measured strains and deflections were calibrated. To this end, the TSD and FWD data as well as KENLAYER modeling results were used for the calibration of parameters or coefficients used to estimate effective structural number and tensile strains at the bottom of the asphalt concrete. Both pavement types (asphalt concrete and composite) were considered in these calibrations. In Chapter 4, linear regression and random forest models were used to establish correlations among different distresses (rutting, roughness), structural condition indicators (elastic moduli), and parameters used in the TSD and FWD data (deflections, basin indices), as well as temperature, for both pavement types. Relative strengths of the predictive models were discussed in this chapter.

## 5.1 CONCLUSIONS

Conclusions for individual chapters were provided in the respective chapters. The overall conclusions are summarized below: Two different pavement types were visible in the I-35 segment under study on the GPR survey. The segment south of Mile Post 51.5 has Continuously Reinforced Concrete Pavement, while the area north of Mile Post 51.5 has Jointed Concrete Pavement. Severe reflective cracking was visible in the JCP section. On the CRCP segment, longitudinal edge cracking and edge failure were the main distresses. The main factor causing longitudinal edge failure is the existence of joints between the shoulder and lane inside the stripe paint.

i. Significant rut, cracking and longitudinal joint cracking were observed on the eastbound lane of SH-7. The GPR images and extracted asphalt cores revealed a very thick layer of HMA in this section. A loose or delaminated fabric layer not attached to the pavement below might have been responsible for causing shear failure and rut in the HMA layer. The GPR data exhibited an increase in moisture over the joint indicating infiltration of water through the longitudinal joint crack. The inside lanes of SH-7 were found to be in fairly good condition.

ii. Overall, good modulus (E) values were observed for the I-35 section and low modulus values were observed for the eastbound inside lane of the SH-7 section, where major depressions and ruts were observed.

iii. Laboratory performance tests were conducted on extracted cores. The I-FIT test and CT Index did not meet the minimum passing criteria for fatigue cracking. Also, very low cycles to failure were observed from the OT test. The results of the HWT tests indicated potential for rut failure of the SH-7 section.

iv. Specialized GPR used in this project, in collaboration with TTI/TAMU, collected data at highway speed. This can be a useful tool for selective data-driven coring of pavement, which is a destructive process.

v. FWD or FFWD when used in conjunction with TSD can be a useful tool for validating TSD results and identifying pavement conditions (project level application) confidently. Also, using pavement layer thicknesses from the GPR data at highway speed enhances the utility of TSD data for network-level application.

vi. Better correlations were observed between the TSD and Pave 3D 8k data. Both tools were able to identify good and acceptable roughness and rut thresholds.

vii. Tensile strains at the bottom of asphalt concrete layer obtained from the KENLAYER exhibited different trends for composite pavements, tension in the bottom of AC in composite pavements were not observed in all the studied sections. For non-composite pavements, tensile strains were observed at the bottom of asphalt concrete layer for all sections, as expected.

viii. Parameters or coefficient for effective structural number from TSD data were calibrated using FWD data. The Rhode method correlated better than the AASHTO method. Also, better correlations were observed for the SH-7 section, in general.

ix. Random forest models performed better than linear regression models for both training and testing sets. The RF models for the SH-7 section were observed to perform better compared to the I-35 section for the prediction of elastic moduli and FWD maximum deflection ($D_0$). The correlations between different TSD and FWD parameters were higher for the SH-7 section.

x. Significant errors were observed while using TSD deflections directly in Modulus 7.0 to back calculate elastic moduli for composite pavements. The back-calculated elastic moduli from the TSD data did not compare well with the results obtained from the FWD deflections. Overall, better correlations were observed for the SH-7 section than for the I-35 section.

xi. TSD is a very resourceful tool that can be applied to forensic engineering in pavements, and to characterize the conditions of pavements from a ride, rut, functional and structural perspective. Its versatility to collect data from cameras, sensors, lasers, radars, profilers, accelerometers, and others, makes TSD a complete tool for network and project level assessment of pavements.

## 5.2 RECOMMENDATIONS

The following is a summary of the important recommendations based on the findings reported in the preceding chapters.

i. It is recommended that an air coupled GPR be used in conjunction with TSD and/or Pave3D 8k for pavement evaluation at the network level.

ii. Pavement thickness data are imperative for a meaningful assessment of effective structural number and tensile strains at the bottom of asphalt concrete layer. Future studies are needed to incorporate pavement thicknesses and moisture conditions of subsurface layers using GPR and or other methods such as electromagnetic induction imaging.

iii. It is recommended that detailed studies be conducted using TSD in conjunction with other projects and network level data collection. Results from such studies will help determine the appropriate maintenance and rehabilitation measures. Also, a detailed analysis of the basin indices is imperative to determine threshold limits for pavement evaluation.

iv. In this study, destructive testing was only conducted in asphalt layers. It is important to conduct testing on concrete materials to better understand the behaviour of composite pavements and associated maintenance and rehabilitation measures.

v. AI-based methods and models show great promise for pavement evaluation, calibration, modeling, and prediction. It is recommended that these tools be further explored in future studies.

vi. It is recommended that additional TSD data available at the transportation agencies as well as future data be analyzed following the approached outlined in this dissertation as well as other rational approaches. This way, deflections, basin parameters and other data collected by the TSD can be used to determine the necessary threshold limits for implementation in PMS.

## REFERENCES

1. Peraka NSP, Biligiri KP. Pavement asset management systems and technologies: A review. Vol. 119, Automation in Construction. Elsevier B.V.; 2020.
2. AASHTO. AASHTO GUIDE FOR DESIGN OF PAVEMENT STRUCTURES. American Assosiation of State Highway and Transportation Official. 1993.
3. Flintsch GW, McGhee KK, National Research Council (U.S.). Transportation Research Board., National Cooperative Highway Research Program., American Association of State Highway and Transportation Officials., United States. Federal Highway Administration. Quality management of pavement condition data collection. Transportation Research Board; 2009. 144 p.
4. Muller W, Roberts J. Revised Approach to Assessing Traffic Speed Deflectometer Data and Field Validation of Deflection Bowl Predictions. International Journal of Pavement Engineering. 2013;
5. Katicha SW, Flintsch GW, Shrestha S, Diefenderfer B. Network Level Pavement Structural Testing With the Traffic Speed Deflectometer [Internet]. 2020. Available from: http://www.virginiadot.org/vtrc/main/online_reports/pdf/21-r4.pdf
6. Huang H. Pavement Analysys and Design. 2nd ed. Pearson; 2004.
7. Rhode G. Determining Pavement Structural Number from FWD Testing. Transp Res Rec. 1994;1448(0361–1981):61–8.
8. Rada G, Nazarian S, Visintine B, Siddharthan R, Thyagarajan S. Pavement Structural Evaluation at the Network Level: Final Report [Internet]. 2016. Available from: http://www.ntis.gov

9. Xu B, Ranjithan SR, Kim YR. New relationships between falling weight deflectometer deflections and asphalt pavement layer condition indicators. In: Transportation Research Record. 2002.

10. Maina JW, Yokota H, Mfinanga DA, Masuda S. Prediction of pavement deterioration based on FWD results. ASTM Special Technical Publication. 1999;(1375).

11. Lytton R. Backcalculation of Pavement Layer Properties. In: Nondestructive Testing of Pavements and Backcalculation of Moduli. 2008.

12. Foxworthy P, Darter M. ILLI-SLAB and FWD Deflection Basins for Characterization of Rigid Pavements. In: Nondestructive Testing of Pavements and Backcalculation of Moduli. 2008.

13. Newcomb DE. Development and Evaluation of Regression Methods to Interpret Dynamic Pavement Deflections. [Seattle, Washington]: Department of Civil Engineering, University of Washington; 1986.

14. Razali M, Mahmood NAC, Hashim KA, Mansor S, Zainuddin NI. The falling weight deflectometer (FWD) for characterization bonding state of subgrade. In: AIP Conference Proceedings. 2018.

15. Katicha S, Flintsch G. Demonstration of Network Level Pavement Structural Evaluation with Traffic Speed Deflectometer in Virginia. 2017.

16. Rada G, Nazarian S, Daleiden J, Yu T. Moving Pavement Deflection Testing Devices: State-of-the-Technology and Best Uses. In: Eighth International Conference on Managing Pavement Assets. 2011.

17. Schnoor H, Horak E. POSSIBLE METHOD OF DETERMINING STRUCTURAL NUMBER FOR FLEXIBLE PAVEMENTS WITH THE FALLING WEIGHT DEFLECTOMETER. 2012. 978–979 p.

18. Nasimifar M, Siddharthan R V., Thyagarajan S, Motamed R. Field and numerical evaluation of traffic speed surface deflection measurements to estimate load-induced fatigue response. J Test Eval. 2017;45(5).

19. Thyagarajan S, Sivaneswaran N, Petros K, Muhunthan B. Development of a simplified method for interpreting surface deflections for in-service flexible pavement evaluation. In: Int Conf on Managing Pavement Assets. Santiago, Chile; 2011.

20. Horak E. Aspects of deflection basin parameters used in a mechanistic rehabilitation design procedure for flexible pavements in South Africa. Ph.D. thesis, Dept. of Civil Engineering, Univ. of Pretoria, Pretoria, South Africa.; 1988.

21. Horak E. The use of surface deflection basin measurements in the mechanistic analysis of flexible pavements. In: Proc, 6th Int Conf Structural Design of Asphalt Pavements. Univ. of Michigan, Ann Arbor, MI.; 1987.

22. Nasimifar M, Thyagarajan S, Siddharthan R V., Sivaneswaran N. Robust deflection indices from traffic-speed deflectometer measurements to predict critical pavement responses for network-level pavement management system application. J Transp Eng. 2016 Mar 1;142(3).

23. Nasimifar M, Siddharthan R V., Rada GR, Nazarian S. Validation of dynamic simulation of slow-moving surface deflection measurements. Transp Res Rec. 2016;2589.

24. Nasimifar M, Siddharthan R V., Rada GR, Nazarian S. Dynamic analyses of traffic speed deflection devices. International Journal of Pavement Engineering. 2017;18(5).

25. Noureldin S, Zhu K, Harris D, Li S. Final Report FHWA/IN/JTRP-2004/35 NON-DESTRUCTIVE ESTIMATION OF PAVEMENT THICKNESS, STRUCTURAL NUMBER AND SUBGRADE RESILIENCE ALONG INDOT HIGHWAYS Non-Destructive Estimation of Pavement Thickness, Structural Number and Subgrade Resilience along INDOT Highways. 2005.

26. Nasimifar M, Thyagarajan S, Chaudhari S, Sivaneswaran N. Pavement Structural Capacity from Traffic Speed Deflectometer for Network Level Pavement Management System Application. Transp Res Rec. 2019;2673(2).

27. Nasimifar M, Thyagarajan S, Sivaneswaran N. Backcalculation of flexible pavement layer moduli from traffic speed deflectometer data. Transp Res Rec. 2017;2641.

28. Nasimifar M, Thyagarajan S, Sivaneswaran N. Computation of Pavement Vertical Surface Deflections from Traffic Speed Deflectometer Data: Evaluation of Current Methods. Journal of Transportation Engineering, Part B: Pavements. 2018 Mar;144(1).

29. Lukanen E, Stubstad R, Briggs R. Temperature Predictions and Adjustment Factors for Asphalt Pavement. McLean, Virginia; 2000.

30. Weligamage J, Piyatrapoomi N, Gunapala L. Traffic speed deflectometer: Queensland trial. Queensland Roads. 2010;(9).

31. Wix R, Whitehead D. INNOVATIONS IN PAVEMENT CONDITION MANAGEMENT IN NEW ZEALAND USING STRENGTH INFORMATION FROM TRAFFIC SPEED DEFLECTOMETER DATA. 2015.

32. William Fredrick Flora. Development of a structural index for pavement management: An exploratory analysis. [Internet]. 2009. Available from: http://www.purdue.edu/policies/pages/teach_res_outreach/c_22.html

33. Aleadelat W, Ksaibati K, Wright CHG, Saha P. Evaluation of pavement roughness using an android-based smartphone. Journal of Stomatology. 2018;144(3).

34. Chatterjee A. A METHODOLOGY FOR QUANTIFYING AND IMPROVING PAVEMENT CONDITION ESTIMATION AND FORECASTING BY INTEGRATING SMARTPHONE AND 3D LASER DATA. 2019.

35. Zang K, Shen J, Huang H, Wan M, Shi J. Assessing and mapping of road surface roughness based on GPS and accelerometer sensors on bicycle-mounted smartphones. Sensors (Switzerland). 2018;18(3).

36. Islam S, Buttlar WG, Aldunate RG, Vavrik WR. Measurement of pavement roughness using android-based smartphone application. Vol. 2457, Transportation Research Record. 2014.

37. Melorose J, Perroy R, Careas S. Investigation of the Implementation of a Probe-Vehicle Based Pavement Roughness Estimation System. Statewide Agricultural Land Use Baseline 2015. 2011;1(August).

38. Massahi A, Ali H, Koohifar F, Baqersad M. Implementing a Smartphone Application for Assessing the Raveling Performance of Asphalt Pavements. International Journal of Advance in Scientific Research and Engineering. 2018;

39. Chang G, Gilliland A, Rada G, Serigos P, Simpson A, Kouchaki S. Successful Practices for Quality Management of Pavement Surface Condition Data Collection and Analysis. 2020.

40. Wang KCP. Pavement Surface Evaluation beyond Cracking with Deep Learning. 2019 RPUG & Pavement Evaluation Conference; 2019.

41. Wang K. Multi-Object and Real-Time Processing of Pavement Surface Distresses with Sub-mm 3D Data in the AI Environment. 2020.

42. Wang KCP, Li QJ, Yang G, Zhan Y, Qiu Y. Network level pavement evaluation with 1 mm 3D survey system. Journal of Traffic and Transportation Engineering (English Edition). 2015;2(6).

43. Wang G, Wang KCP, Yang G, Liu Y, Li JQ, Peters W. Nondestructive Bridge Deck Evaluation Using Sub-mm 3D Laser Imaging Technology at Highway Speeds. Journal of Bridge Engineering. 2022 Jun;27(6).

44. Heitzman M, Maser K, Tran NH, Brown T, Bell H, Holland S, et al. Nondestructive Testing to Identify Delaminations Between HMA Layers. 2013.

45. Gucunski N, Imani A, Romero F, Nazarian S, Yuan D, Wiggenhauser H, et al. Nondestructive Testing to Identify Concrete Bridge Deck Deterioration. 2013.

46. Katicha S, Shrestha S, Flintsch G, Diefenderfer B. Network Level Pavement Structural Testing With the Traffic Speed Deflectometer. 2020.

47. Noureldin S, Zhu K, Harris D, Li S. Non-Destructive Estimation of Pavement Thickness, Structural Number, and Subgrade Resilience Along INDOT Highways. 2005.
48. ASTM. Standard Test Method for Determining the Thickness of Bound Pavement Layers Using Short-Pulse Radar. In: ASTM Test Standards. 2020.
49. L. Breiman. Consistency For a Simple Model of Random Forests. 2004.
50. Guo X, Hao P. Using a random forest model to predict the location of potential damage on asphalt pavement. Applied Sciences (Switzerland). 2021;11(21).
51. Gong H, Sun Y, Shu X, Huang B. Use of random forests regression for predicting IRI of asphalt pavements. Constr Build Mater. 2018;189.
52. Hu Y, Sun Z, Pei L, Li W, Li Y. Evaluation of pavement surface roughness performance under multi-features conditions based on optimized random forest. In: Proceedings - 2021 9th International Conference on Advanced Cloud and Big Data, CBD 2021. 2022.
53. Cui L, Qi Z, Chen Z, Meng F, Shi Y. Pavement distress detection using random decision forests. In: Lecture Notes in Computer Science (including subseries Lecture Notes in Artificial Intelligence and Lecture Notes in Bioinformatics). 2015.
54. Kou B, Cao J, Huang W, Ma T. The rutting model of semi-rigid asphalt pavement based on RIOHTRACK full-scale track. Mathematical Biosciences and Engineering. 2023;20(5).

55. Qiu X, Xu WY, Zhang ZH, Li NN, Hong HJ. Surface Temperature Prediction of Asphalt Pavement Based on GBDT. In: IOP Conference Series: Materials Science and Engineering. 2020.

56. Fawaz Alharbi. Comparison of random forest regression and multiple linear regression for predicting pavement roughness in dry climate countries. Journal of Engineering and Computer Sciences. 2021;

57. Karballaeezadeh N, Hosein Ghasemzadeh Tehrani, Danial Mohammadzadeh S., Shahaboddin Shamshirband. Estimation of flexible pavement structural capacity using machine learning techniques. In: Frontiers of Structural and Civil Engineering . 2020.

58. Yu T, Pei LI, Li W, Sun Z yun, Huyan J. Pavement Surface Condition Index Prediction Based on Random Forest Algorithm. Journal of Highway and Transportation Research and Development (English Edition). 2021;15(4).

59. Nazmus Ahmed. Predicting Pavement Structural Condition Using Machine Learning Methods. University of South Carolina ; 2021.

60. Jia X, Woods M, Gong H, Zhu D, Hu W, Huang B. Evaluation of influence of pavement data on measurement of deflection on asphalt surfaced pavements utilizing traffic speed deflection device. Constr Build Mater. 2021;270.

61. Rada GR, Jones DJ, Harvey JT, Senn KA, Thomas M. Guide for Conducting Forensic Investigations of Highway Pavements [Internet]. Washington, D.C.: Transportation Research Board; 2013. Available from: https://www.nap.edu/catalog/22507

62. Chen DH. Field and Lab Investigations of Prematurely Cracking Pavements. JOURNAL OF PERFORMANCE OF CONSTRUCTED FACILITIES. 2007;

63. Chai G, Manoharan S, Golding A, Kelly G, Chowdhury S. Evaluation of the Traffic Speed Deflectometer Data Using Simplified Deflection Model. In: Transportation Research Procedia. Elsevier B.V.; 2016. p. 3031–9.

64. Mezhoud S, Clastres P, Houari H, Belachia M. Forensic Investigation of Causes of Premature Longitudinal Cracking in a Newly Constructed Highway with a Composite Pavement System. Journal of Performance of Constructed Facilities. 2017 Apr;31(2).

65. Saarenketo T, Scullion T. Road evaluation with ground penetrating radar [Internet]. Vol. 43, Journal of Applied Geophysics. 2000. Available from: www.elsevier.nlrlocaterjappgeo

66. Scullion T. Ground Penetrating Radar (GPR) Technology Review and Evaluation Report. 2006.

67. Wenting Liu, Scullion Tom. PAVECHECK: INTEGRATING DEFLECTION AND GROUND PENETRATING RADAR DATA FOR PAVEMENT EVALUATION. Austin; 2006.

68. Krysiński L, Sudyka J. GPR abilities in investigation of the pavement transversal cracks. J Appl Geophy. 2013 Oct;97:27–36.

69. Fernandes FM, Fernandes A, Pais J. Assessment of the density and moisture content of asphalt mixtures of road pavements. Constr Build Mater. 2017 Nov 15;154:1216–25.

70. Wang KCP, Li JQ. 3D LASER IMAGING FOR ODOT INTERSTATE NETWORK AT TRUE 1-MM RESOLUTION. 2014.

71. Wang KCP, Chair D. Multi-Object and Real-Time Processing of Pavement Surface Distresses with Sub-mm 3D Data in the AI Environment. 2020.

72. Chang G, Gilliland A, Rada G, Serigos P, Simpson A, Kouchaki S. Successful Practices for Quality Management of Pavement Surface Condition Data Collection and Analysis. 2020.

73. Kassem E, Chowdhury A, Scullion T, Masad E. Application of ground-penetrating radar in measuring the density of asphalt pavements and its relationship to mechanical properties. International Journal of Pavement Engineering. 2016 Jul 2;17(6):503–16.

74. Hossain Z, Chowdhury NH, Braham A. Forensic Evaluation of Premature Pavement Failures in Arkansas. Journal of Performance of Constructed Facilities. 2018 Jun;32(3).

75. AASHTO. Standard Method of Test for Determining the Fracture Potential of Asphalt Mixtures Using the Illinois Flexibility Index Test (I-FIT). In: AASHTO Standards. AASHTO; 2020.

76. ODOT. Method of Test for Hamburg Rut Testing of Compacted Hot-Mix Asphalt (HMA). In: Oklahoma Department of Transportation Test Methods. 2014.

77. Braham A, Aschenbrener T, Hossain Z. Forensic Investigation of Ten Asphalt Interstate Pavements with Varying Performance in Arkansas. Journal of Transportation Engineering, Part B: Pavements. 2018 Jun;144(2):04018019.

78. TxDOT. Test Procedure for Overlay Test. In: Texas Department of Transportation Test Methods. 2008.

79. Zhou F, Scullion T. USER MANUAL FOR TXDOT'S NEW OVERLAY TESTER. Austin; 2004.

80. AASHTO. Standard Method of Test for Resistance of Compacted Asphalt Mixtures to Moisture-Induced Damage. In: AASHTO Test Standards. 2014.

81. Fujie Zhou. Development of an IDEAL Cracking Test for Asphalt Mix Design, Quality Control, and Quality Assurance. 2018.

82. ODOT. Transportation Asset Management Plan (2019-2028). 2018.

83. Liu Y, Yang G, Wang KCP, Wang G, Li J, Nantung T. Automatic detection of deteriorated inverted-T patching using 3D laser imaging system based on a true story indiana. Intelligent Transportation Infrastructure. 2022;1.

84. Musick N, Petz A. Public Spending on Transportation and Water Infrastructure, 1956 to 2017. 2018.

85. Irfan M, Khurshid MB, Bai Q, Labi S, Morin TL. Establishing optimal project-level strategies for pavement maintenance and rehabilitation - A framework and case study. Vol. 44, Engineering Optimization. 2012. p. 565–89.

86. Abaza KA. Optimum Flexible Pavement Life-Cycle Analysis Model. J Transp Eng. 2002;

87. He S, Salem O, Salman B. Decision Support Framework for Project-Level Pavement Maintenance and Rehabilitation through Integrating Life Cycle Cost Analysis and Life Cycle Assessment. Journal of Transportation Engineering, Part B: Pavements. 2021 Mar;147(1):04020083.

88. Mohamed AS, Xiao F, Hettiarachchi C. Project Level Management Decisions in Construction and Rehabilitation of Flexible Pavements. Vol. 133, Automation in Construction. Elsevier B.V.; 2022.

89. Shrestha S. Network Level Decision-Making Using Pavement Structural Condition Information from the Traffic Speed Deflectometer. 2022.

90. WARRIP. An Evaluation of the Traffic Speed Deflectometer for Main Roads Western Australia. 2017.

91. Flintsch GW, Ferne B, Diefenderfer B, Katicha S, Bryce J, Nell S. Evaluation of traffic-speed deflectometers. Transp Res Rec. 2012;2304.

92. GEOSOLVE Ltda. Traffic Speed Deflectometer The Application of TSD Data in New Zealand for Asset Management and Design Report prepared for: NZTA The Application of TSD Data in New Zealand for Asset Management and Design [Internet]. 2016. Available from: http://rimsnz.yolasite.com/resources/Documents/RIMS_BoK_Documents/3.4i.%20BoK%2011_001%20Collection%20Pavement%20Structural%20Parameters%20Part%20I%20.pdf

93. Talebsafa M, Romanoschi SA, Papagiannakis AT, Popescu C. Evaluation of Strains at the Bottom of the Asphalt Base Layer of a Semi-Rigid Pavement Under a Class 6 Vehicle. MATEC Web of Conferences. 2019;271:08008.

94. Ranadive MS, Tapase AB. Parameter sensitive analysis of flexible pavement. International Journal of Pavement Research and Technology. 2016 Nov 1;9(6):466–72.

95. Bilodeau JP, Doré G. Estimation of tensile strains at the bottom of asphalt concrete layers under wheel loading using deflection basins from falling weight deflectometer tests. Canadian Journal of Civil Engineering. 2012 Jul;39(7):771–8.

96. Saleh M. A mechanistic empirical approach for the evaluation of the structural capacity and remaining service life of flexible pavements at the network level. Canadian Journal of Civil Engineering. 2016;43(8):749–58.

97. Elseifi MA, Uddin PEZ, Zihan A. Assessment of the Traffic Speed Deflectometer in Louisiana for Pavement Structural Evaluation [Internet]. 2018. Available from: www.ltrc.lsu.edu

98. Wenting Liu A, Scullion T. MODULUS 6.0 FOR WINDOWS: USER'S MANUAL. 2001.

99. Gopalakrishnan K. Backcalculation of Non-Linear Pavement Moduli Using Finite-Element Based Neuro-Genetic Hybrid Optimization. The Open Civil Engineering Journal. 2009 Jun 18;3(1):83–92.

100. American Association of State Highway and Transportation Officials (AASHTO). Guidelines on Pavement Management, AASHTO Joint Task Force on Pavements. 1985.

101. Uddin Z, Zihan A. Evaluation of Traffic Speed Deflectometer for Pavement Structural Evaluation in Louisiana [Internet]. 2019. Available from: https://digitalcommons.lsu.edu/gradschool_theses

102. Baoshan Huan, Miaomiao Zhang, Hongren Gong, Pawel Polaczyk. Evaluation of Traffic Speed Deflectometer for Collecting Network-Level Pavement

Structural Data in Tennessee [Internet]. 2022. Available from: http://www.tn.gov/.

103. Katicha SW, Flintsch GW, Ferne B, Bryce J. Limits of agreement method for comparing TSD and FWD measurements. International Journal of Pavement Engineering. 2014 Jul 3;15(6):532–41.

104. Muller WB. A comparison of TSD, FWD and GPR field measurements. In 2015. Available from: www.ndt.net/?id=18286

105. Elseifi MA, Zihan ZUA, Icenogle P. A Mechanistic Approach to Utilize Traffic Speed Deflectometer (TSD) Measurements into Backcalculation Analysis [Internet]. 2019. Available from: www.ltrc.lsu.edu

106. Katicha SW, Flintsch GW, Ferne B, Bryce J. Limits of agreement method for comparing TSD and FWD measurements. International Journal of Pavement Engineering. 2014;15(6).

107. Shrestha S, Katicha SW, Flintsch GW, Diefenderfer BK. Implementing Traffic Speed Deflection Measurements for Network Level Pavement Management in Virginia. Journal of Transportation Engineering, Part B: Pavements. 2022 Jun;148(2).

108. Saremi SG. Practical Models For Interpreting Traffic Speed Deflectometer Data.

109. Chen DH, Bilyeu J, Lin HH, Murphy M. Temperature correction on falling weight deflectometer measurements. Transp Res Rec. 2000;(1716):30–9.

110. Fernando EG, Liu W, Ryu D. DEVELOPMENT OF A PROCEDURE FOR TEMPERATURE CORRECTION OF BACKCALCULATED AC MODULUS

5. Report Date Title: Evaluate the Use of FWD Data in Determining Seasonal Variations in Pavement Structural Strength Unclassified. 2001.

111. Nasimifar M, Chaudhari S, Thyagarajan S, Sivaneswaran N. Temperature adjustment of Surface Curvature Index from Traffic Speed Deflectometer measurements. International Journal of Pavement Engineering. 2020;21(11).

112. Stubstad RN, E. O. Lukanen, C. A. Richter, S. Baltzer. Calculation of AC Layer Temperatures from FWD Field Data. In: of the 5th International Conference on the Bearing Capacity of Roads and Airfields. Trondheim, Norway; 1998.

113. James G, Witten D, Hastie T, Tibshirani R. An Introduction to Statistical Learning with Applications in R. 2nd Edition. 2021.

114. Abohamer H, Elseifi MA, Zihan ZUA, Wu Z, Kebede N, Zhang Z. Development of an artificial neural network-based procedure for the verification of traffic speed deflectometer measurements. In: Transportation Research Record. 2021.

115. Lee J, Jan ZM, Verma B. A Novel Neural Network Based Method for Analysis of Pavement Deflection Data. In: 2019 IEEE Symposium Series on Computational Intelligence, SSCI 2019. 2019.

116. Zhang Z, Claros G, Manuel L, Damnjanovic I. EVALUATION OF THE PAVEMENT STRUCTURAL CONDITION AT NETWORK LEVEL USING FALLING WEIGHT DEFLECTOMETER (FWD) DATA. Transp Res Rec. 2003;